Progress in Materials Science 107 (2020) 100591

Contents lists available at ScienceDirect

Progress in Materials Science

journal homepage: www.elsevier.com/locate/pmatsci

X-ray photoelectron spectroscopy: Towards reliable binding energy referencing

G. Greczynski*, L. Hultman

Thin Film Physics Division, Department of Physics, Chemistry, and Biology (IFM), Linköping University, SE-581 83 Linköping, Sweden

ARTICLE INFO

Keywords:
XPS
Surface chemistry
Adventitious carbon
Binding energy reference
C 1s peak

ABSTRACT

With more than 9000 papers published annually, X-ray photoelectron spectroscopy (XPS) is an indispensable technique in modern surface and materials science for the determination of chemical bonding. The accuracy of chemical-state determination relies, however, on a trustworthy calibration of the binding energy (BE) scale, which is a nontrivial task due to the lack of an internal BE reference. One approach, proposed in the early days of XPS, employs the C 1s spectra of an adventitious carbon layer, which is present on all surfaces exposed to air. Despite accumulating criticism, pointing to the unknown origin and composition of the adventitious carbon, this is by far the most commonly used method today for all types of samples, not necessarily electrically insulating. Alarmingly, as revealed by our survey of recent XPS literature, the calibration procedure based on the C 1s peak of adventitious carbon is highly arbitrary, which results in incorrect spectral interpretation, contradictory results, and generates a large spread in reported BE values for elements even present in the same chemical state. The purpose of this review is to critically evaluate the *status quo* of XPS with a historical perspective, provide the technique's operating principles, resolve myths associated with C 1s referencing, and offer a comprehensive account of recent findings. Owing to the huge volume of XPS literature produced each year, the consequences of improper referencing are dramatic. Our intention is to promote awareness within a growing XPS community as to the problems reported over the last six decades and present a guide with best practice for using the C 1s BE referencing method.

1. Introduction

X-ray photoelectron spectroscopy (XPS) is by far the most commonly used technique in areas of materials science, chemistry, and chemical engineering to assess surface chemistry, bonding structure, and composition of surfaces and interfaces. As summarized in Fig. 1 the number of papers where XPS was employed has increased more than 15 times during last 30 years, resulting in that only during the last year more than 9000 published papers used XPS [1]. A 5-year derivative of number of XPS-related publications exhibits a continuous increase with a clear disruption following the 2008 crisis in global economy, and for the last four years was highest ever.

The strength of the XPS technique relies on that the chemical environment of an atom has a pronounced effect on the assessed binding energies (BEs) of core-level electrons, the effect commonly referred to as the *chemical shift* [2]. This allows for determination of bonding structure and the changes thereof as a function of processing parameters or surface treatments. The information about existing bonds is typically extracted by comparing measured BE values to literature data bases [3].

* Corresponding author.
E-mail address: grzegorz.greczynski@liu.se (G. Greczynski).

https://doi.org/10.1016/j.pmatsci.2019.100591
Received 11 June 2018; Received in revised form 29 April 2019; Accepted 24 July 2019
Available online 30 July 2019

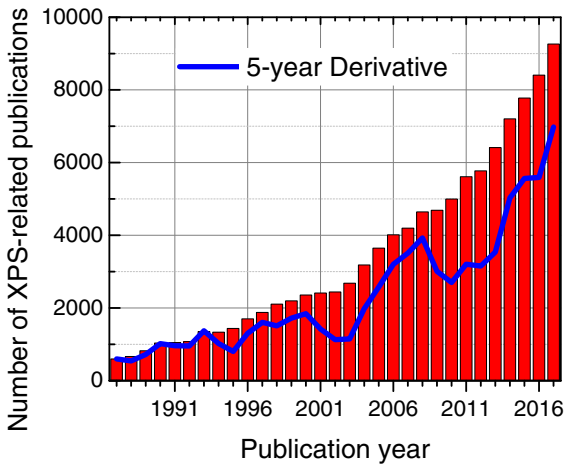

Fig. 1. Number of publications per year where XPS was used based on a Scopus data base search performed in June 2018 for the term "XPS". The blue curve indicates a 5-year derivative.

The first necessary condition to make an accurate determination of the BEs from the XPS spectrum is that the energy scale of the spectrometer is correctly calibrated. Numerous procedures for relative BE calibration have been presented over the years, starting with a seminal book by Siegbahn and co-workers [4]. At present, due to extensive efforts by the Seah group, the calibration procedure relying on the use of primary signals from metal foils previously *in situ* cleaned with Ar ion beams to remove surface contaminants, is incorporated in an ISO standard [5]. After such a calibration step, the Fermi edge of metallic samples that remain in good electrical contact to the spectrometer should coincide with the "0 eV" of the BE scale, as both bodies share a common Fermi level (FL), which becomes a natural reference level. All BE values determined in such way are thus given with respect to the FL.

The second condition, not as explicit as the first one and for this reason often overlooked, is that the FL of the spectrometer and that of the sample to be analyzed are aligned. This can only take place if there is a sufficient charge density in the sample so that once brought in contact with the instrument, charge transfer across the interface leads to FL alignment. If, for any reason (like low conductivity or bad contact) this condition is not fulfilled, the FL of the sample is decoupled from that of the spectrometer leading to incorrect BE values. This is a serious problem for semiconductors and insulators, where the lack of density-of-states (DOS) at the FL prevents direct verification whether FL alignment at the sample/spectrometer interface takes place or not. An additional complication arises from the fact that, during the measurement, negative charge has to be refilled at a sufficiently high rate to maintain charge neutrality at the surface. If this is not the case, then positive charge accumulates leading to so-called *sample charging* and shift of all core-level peaks towards higher BE values, as the electrons leaving the surface are attracted by the positive potential. Since the steady-state charge state is not known *a priori*, there are no straightforward means to compensate for this effect.

Various approaches have been proposed to cope with this situation all relying on the same concept of measuring the BE of a well-defined peak and applying a corresponding linear correction to the BE scale. The most prominent reference employs the C 1s peak from the surface contamination layer, the so-called *adventitious carbon* (AdC), and was proposed already back in 60s to be used as a BE reference (in this context often called *charging reference*) [4].

1.1. The culprit: Adventitious carbon referencing

Today, the BE scale referencing based on the C 1s peak of AdC is part of both ASTM and ISO standards [6,7]. Perhaps the main reason for the great popularity of this referencing technique is the fact that AdC is present on essentially all air-exposed surfaces. Our literature survey performed on a selected fraction of the enormous XPS library, restricted to the top-cited papers on magnetron-sputtered thin films published between 2010 and 2017, reveals that in the vast majority of cases the C 1s peak originating from AdC was used for BE referencing [8]. Alarmingly, the technique was applied irrespective of whether samples were electrically conducting or not. Thus, the essential question of FL alignment at the sample/instrument interface was completely neglected.

Moreover, the literature displays a great deal of confusion as to: (i) the chemical identity of AdC, (ii) the binding energy values assigned to the C 1s peak of AdC, and (iii) the referencing procedure itself. To exemplify the gravity of the situation, we can mention that to calibrate the BE scale, the C—C/C—H peak is quite arbitrarily set at any value in the range 284.0–285.6 eV, which contradicts the very notion of a BE reference. This is highly disturbing, given that improper calibration of the binding energy scale likely results in misinterpretation of chemical bonding unless there is an accidental match.

A most disturbing consequence of the BE referencing problems outlined above is the fact that the reported binding energies for primary core-levels of constituent elements in many technologically-relevant materials exhibit an unacceptably large spread, which often exceeds the magnitude of related chemical shifts [9]. This is illustrated in Fig. 2 where the difference between the lowest and the highest binding energy ΔBE, according to the NIST XPS data base [10], is plotted for primary metal peaks of commonly-studied metals, oxides, nitrides, carbides, sulfides, chlorides, and fluorides. Each colored bar in the figure corresponds to one materials

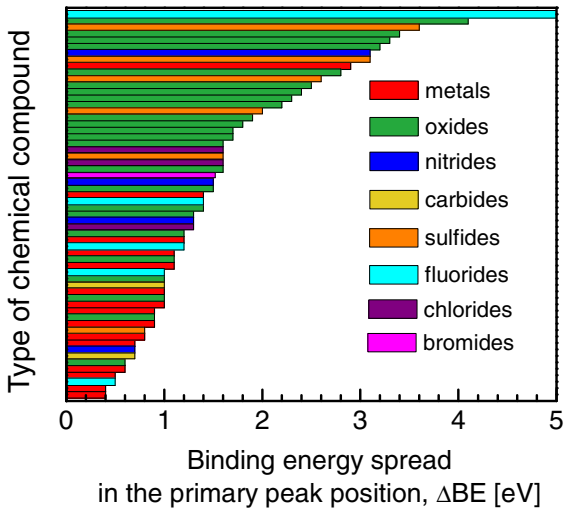

Fig. 2. The difference between the lowest and the highest binding energy plotted for primary metal peaks of commonly-studied metals, oxides, nitrides, carbides, sulfides, chlorides, and fluorides. Data are collected from the NIST XPS data base [10]. Each colored bar in the figure corresponds to one materials system.

system. ΔBE ranges from 0.4 eV for Al 2p and Ta 4f of corresponding metal samples to 8.5 eV for the Si 2p peak of SiF_4. The best consistency between different labs is obtained for metals, $0.4 \leq \Delta BE \leq 1.4$ eV (with the exception of Fe for which $\Delta BE = 2.9$ eV), which is justified by the fact that they are highly conducting, hence the risk of erroneous measurement due to surface charging is minimized. In addition, most metals exhibit a high density of states at the Fermi level (often referred to as the "Fermi level cut-off"), which together with intense and narrow core-level peaks, allows for better calibration of the BE scale. Nevertheless, for the majority of metallic samples $\Delta BE \sim 1$ eV, which is of the order of a typical difference between chemically shifted peak positions, hence, far from satisfactory. The fact that the electric conductivity plays a crucial role for the accuracy of BE measurement is responsible for large ΔBE values noted for oxides, which range from 0.6 eV for the Cu $2p_{3/2}$ peak of Cu_2O to 4.1 eV for the V 2p peak from V_2O_3. For the vast majority of oxides, $\Delta BE > 1.6$ eV. Other compounds included in this comparison fare not better: $0.7 \leq \Delta BE \leq 3.1$ eV for nitrides, $0.8 \leq \Delta BE \leq 3.6$ eV for sulfides, and $0.5 \leq \Delta BE \leq 8.5$ eV for fluorides, to mention only these material groups, which are well-represented in Fig. 2. A direct consequence of such large variations in reported core-level BEs is incorrect bonding assignment, an arbitrary spectral interpretation, and, in the end, contradictory and often unreliable results. This is especially so for compounds where the chemical shifts are relatively small, of the order of 1 eV or less. In such case, the risk of data misinterpretation is particularly high, which presents a formidable stumbling block in case of XPS spectral deconvolution particularly nowadays for the often encountered multicomponent material samples, with multiple chemical states of the same element.

There may be numerous reasons for the disconcerting situation introduced in Fig. 2, including sputter-damage effects that often result in large changes in the peak positions [11,12], or the fact that no cross-peak correlations are considered while extracting chemical information from XPS spectra [13]. However, uncertainties associated with proper referencing of the BE scale and the common use of adventitious carbon for this purpose, with all other associated issues, appears to be the main source of problems. It is therefore the main ambition of the present paper to comprehensively review the use of C 1s peak of AdC for XPS BE referencing, with the aim to make all XPS practitioners aware of related issues and limitations and, eventually, contribute to the improved accuracy of BE determination.

In order to make this review self-comprehensive, we start in Section 2 with a brief overview of XPS covering basic aspects of the technique. Emphasis is devoted to discussion of chemical shifts, spectral modelling, and sample charging. In Section 3 we discuss all issues related to BE referencing, including energy diagrams, calibration of the BE scale and a brief description of BE referencing procedures other than that based on AdC. Section 4 is specifically devoted to the review of existing literature on C 1s referencing. The origin of the AdC and BE of the C 1s peak are treated first, after which we present an account of criticism that accumulated over the years, followed by a presentation of the *status quo* based on the literature survey. The most recent findings from extensive studies involving more than hundred samples performed in our XPS Lab in the years 2016–2018 are presented in Section 5. Thus, we reexamine the nature of AdC species, shifts in the BE of the C 1s peak together with consequences for BE scale correction, and the effect of sample *work function* and *vacuum level* (VL) alignment. Sections 6 and 7 provide conclusions and outlook, including our suggestion for experimental protocols devoted to using the C 1s BE referencing method.

2. Basics of X-ray photoelectron spectroscopy

We begin with a brief overview of the XPS technique covering the aspects which are most relevant to XPS practitioners concerned with the energy referencing issues. For more in-depth information, the reader is referred to numerous textbooks [14–16] and excellent review articles [17–19].

2.1. Operational principles

The physical phenomenon behind XPS and other kinds of photoelectron spectroscopy is the emission of electrons from surfaces irradiated by light. It is the so-called photoelectric effect, discovered by Hertz in the end of the XIX century [20]. Studies that followed revealed a number of puzzling observations that were in conflict to the classical theory of radiation [21]. For example, Maxwell's theory predicted that the electron energy should increase with increasing light intensity, which was not observed experimentally. Instead, it was noticed that the energy of emitted electrons increases with the frequency of the incident light. To add to the confusion, for each surface there is a threshold light frequency below which the effect does not take place no matter how intense the light is. The dilemma was resolved by Einstein in one of his *Annus Mirabilis* papers [22], where it was proposed that "the energy of light is distributed discontinuously in space". He described light as being composed of energy quanta (later named photons), each with the energy $h\nu$, where h is Planck's constant and ν stands for the light frequency. The process of electron emission from the solid is thus in simple terms viewed as the absorption of photons. Within this framework, the emission takes place only if the energy acquired by the electron in a solid exceeds the minimum energy necessary for it to leave the surface (equal to the work function ϕ). If $h\nu < \phi$, the electron is unable to escape and any increase in the photon flux only multiplies the number of low-energy electrons within the solid, but cannot create a single electron with energy high enough to be released from the surface. Thus, the energy of the emitted electrons is governed by the incident photon energy and is independent of the intensity of the incoming light. As electrons absorb over the entire photon energy, the conservation of energy requires that their kinetic energy is equal to $h\nu - W$, where W is the work required to escape the solid and apart from ϕ comprises also the electron binding energy E_B. In 1914 Rutherford established that kinetic energy of emitted electrons is equal to $h\nu - E_B$, [23,24] and, at that time, it became clear that the photoelectron energy contains information about the solid it was emitted from, although it took another half a century before the first XPS spectrometers were introduced.

2.2. Selected instrumental aspects

The schematic setup for XPS experiments is shown in Fig. 3. During analysis the sample is irradiated by photons of known energy, which gives rise to the photoelectric effect. A fraction of electrons generated close to the surface leaves the sample into vacuum and enters the analyzer slit of the spectrometer, which is capable of measuring the electron current (corresponding to number of electrons per unit time) as a function of their energy. Such intensity *vs.* energy plots are referred to as XPS spectra. A typical example is shown in Fig. 4, where the wide energy range spectrum recorded from a CrAlN thin film sample with a native oxide layer is shown.

The most common X-ray sources employ characteristic Kα lines from Al and Mg anodes, which are superimposed onto continuous Bremsstrahlung background radiation extending from 0 eV up to the incident electron energy (typically in the range 10–15 keV). The primary lines have energies of 1253.6 and 1486.6 eV, respectively, and are thus high enough to access core-level electrons from the vast majority of elements. In both cases, the Kα lines are in fact $K\alpha_1$- $K\alpha_2$ doublets with the 1:2 intensity ratio separated by a few tenths of eV, which has a detrimental effect on the energy resolution. For example, in the case of an Al anode, both lines have a natural width of 0.5 eV and appear at 1486.70 ($K\alpha_1$) and 1486.27 ($K\alpha_2$) eV, resulting in the composite line width of approximately 0.85 eV. An additional complication is the presence of other characteristic lines ($K\alpha_3$ through $K\alpha_6$, as well as Kβ), weaker than the primary Kα lines (< 10% of the intensity) and relatively close in terms of energy (8–70 eV higher energy) [25,26]. So-called *ghost lines* can also appear in an XPS spectrum recorded with non-monochromatized X-rays. These are artefacts from the Cu Kα radiation from the exposed Cu base of an overused anode or the O Kα light produced by an oxidized anode, and can be recognized by measuring the relative energy shift with respect to the Kα lines from the main source [27].

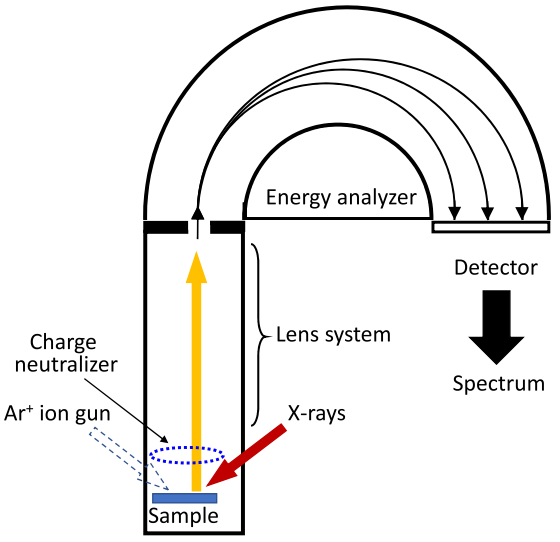

Fig. 3. The schematic view of the photoelectron spectrometer with a hemispherical electron energy analyzer.

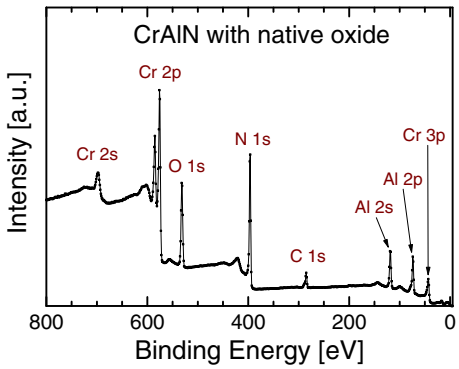

Fig. 4. A wide energy range XPS spectrum recorded from a CrAlN thin film sample with native oxide layer. [Author's original work.]

An excellent cure to the issues listed above is to use monochromatized X-ray sources, first demonstrated by Siegbahn and coworkers [28]. As illustrated in Fig. 5, an X-ray source, a monochromator crystal and a sample are placed on the circumference of the Rowland circle. The X-rays are focused on the sample by using a properly bent quartz crystal or a whole array of crystals. The energy dispersion of the monochromator is then inversely proportional to the diameter of the Rowland circle (typically in the range 0.5–1.0 m). In such a case, the first-order Bragg diffraction of Al Kα X-rays by the set of $10\bar{1}0$ planes of a quartz crystal (or crystal array) is used to reduce the energy spread of the incident radiation to only 0.26 eV.

A comparison between core-level spectra recorded with and without a monochromator is included in Fig. 6 for the Ag 3d lines measured with (a) non-monochromatized Mg Kα, and (b) monochromatic Al Kα radiation. Clearly, in the latter case $K\alpha_3$ and $K\alpha_4$ satellites are eliminated and the background level lowered (no Bremsstrahlung radiation), together resulting in higher signal-to-noise ratio. In addition, the full-width-at-half-maximum (FWHM) of the Ag $3d_{5/2}$ peak is reduced from 0.9 to 0.5 eV, which also allows one to resolve closely-spaced doublets such as Si 2p (energy split ΔE of 0.57 eV) or Al 2p (ΔE = 0.40 eV). The negative aspect of the monochromatized source is the higher risk of surface charge buildup when analyzing poorly conducting samples as the high flux of low-energy electrons excited by the Bremsstrahlung radiation is absent.

Two concepts are used for the sample illumination by X-rays in modern XPS instruments with monochromatized sources. In the first case, the X-ray beam is focused into a small spot (probe) of a few μm in diameter which allows for spatially-resolved analyses or, in case this is not needed, the beam is rastered over the sample area to be analyzed. However, the necessity of focusing X-rays to a small spot implies a shorter radius for the Rowland circle, which has a negative impact on the X-ray dispersion and, hence, the energy resolution. The alternative approach uses a relatively broad X-ray beam of 1–2 mm (at the sample plane) such that the sample is essentially flooded with X-rays and the area to be analyzed is defined by a pair of apertures in the analyzer optics.

The heart of the spectrometer is the electron energy analyzer. The most common type is the electrostatic hemispherical analyzer consisting of two concentric hemispheres (see Fig. 7) [29,30]. To improve the energy resolution, electrons emitted from the sample are typically retarded before they enter the hemispherical analyzer. For an electron arriving with an energy E_i, the entrance slit is biased negatively at V_i such that $E_i - eV_i = E_0$ is maintained constant. E_0, referred to as the *pass energy*, is the energy of the electron travelling from the analyzer entrance to the exit slit along the equipotential plane defined by $R_0 = (R_{in} + R_{out})/2$, in which R_{in} and R_{out} are the inner and outer hemisphere radii, respectively. The voltages on the inner and outer hemispheres, V_{in} and V_{out}, are then linked

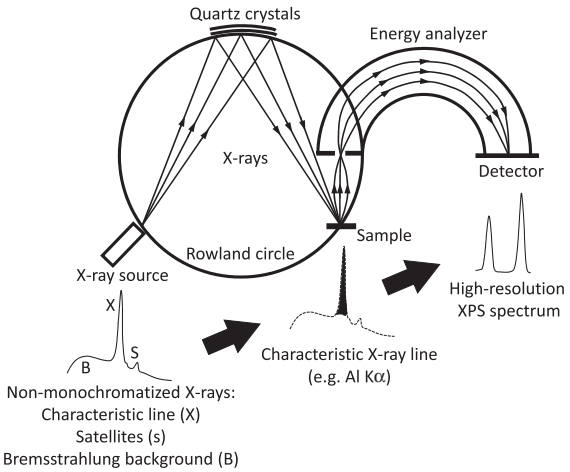

Fig. 5. Schematic illustration of the principle behind X-ray monochromatization: X-ray source, a monochromator crystal and sample are placed on the circumference of the Rowland circle. [Inspired by Fig. 2.7 in Ref. [14].]

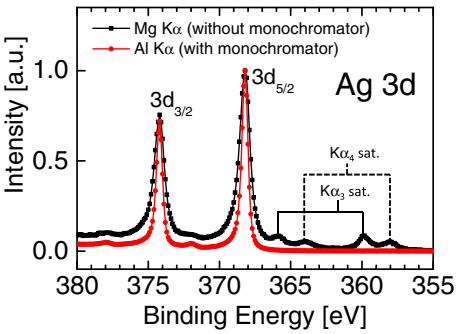

Fig. 6. Ag 3d core-level spectra recorded with (a) non-monochromatized Mg Kα, and (b) monochromatic Al Kα radiation [data courtesy of Dr. Adam Roberts at Kratos Analytical, UK].

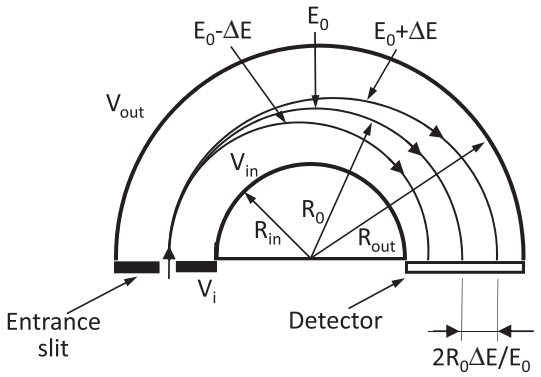

Fig. 7. The schematic illustration of the principle behind energy-resolving power of the hemispherical analyzer. [Inspired by Fig. 7(a) in Chapter 5 of Ref. [16].]

to R_{in}, R_{out}, and E_0 through the relationship [31]

$$e(V_{out} - V_{in}) = E_0\left(\frac{R_{out}}{R_{in}} - \frac{R_{in}}{R_{out}}\right). \tag{1}$$

In the process of spectrum acquisition, V_i, V_{out}, and V_{in} are scanned to probe the electrons within a kinetic energy range interesting to the user, who also selects the E_0 value, which determines the absolute energy resolution ΔE. Since $\Delta E/E_0 =$ constant (of the order of few %, depending on the construction details of the spectrometer), the lower pass energy the better the energy resolution.

The energy-resolving power of the analyzer is illustrated in Fig. 7. Electrons entering with energies higher (lower) than E_0 hit the detector plane closer to the outer (inner) hemisphere, where they are collected at different sections of the parallel multichannel detector, allowing for the reconstruction of the intensity *vs.* energy profile. Fig. 8(a) and (b) show as-measured and normalized Ag $3d_{5/2}$ narrow-range spectra recorded from a sputter-cleaned Ag foil with different E_0 values ranging from 5 to 160 eV. The advantage of higher energy resolution at lower pass energy is very clear, the FWHM of the Ag $3d_{5/2}$ peak decreases from 1.66 eV with $E_0 = 160$ eV to only 0.44 eV with $E_0 = 5$ eV. The improvement comes, however, at the steep price of lowered signal intensity (lower

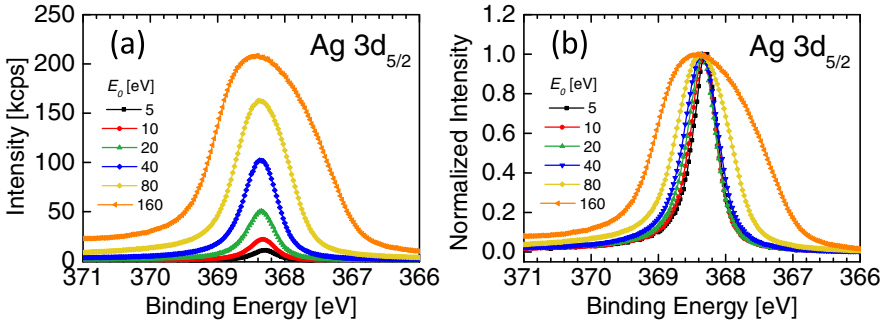

Fig. 8. Ag $3d_{5/2}$ narrow-range spectra recorded from sputter-cleaned Ag foil with different values of pass energy E_0 ranging from 5 to 160 eV: (a) as-measured, and (b) normalized to the highest intensity. [Author's original work.]

E_0 means lower electron current through the analyzer), which decreases more than 20 times in the same pass energy range.

More detail treatment of instrumental issues can be found in Refs. [14,16].

2.3. Spectral interpretation

As illustrated in Fig. 4 XPS spectra have the form of intensity *vs*. binding energy plots and it is a customary to present them with the BE values decreasing from left to right. Peaks correspond to the fraction of core-level electrons (ejected upon interaction with incident photons) that did not collide on their way to the surface, hence preserved their original energy. All other inelastically scattered electrons contribute to the background on the high BE side of the core-level line they originate from (best visible in Fig. 4 for the strongest Cr 2p and N 1s core-levels), giving rise to the peculiar appearance of the wide-energy range (survey) XPS spectra with a characteristic step-like background shape. The practical consequence of the background which increases with increasing BE is an associated decrease in the signal-to-noise ratio which implies longer acquisition times for core-level lines appearing higher up on the binding energy scale.

As the inelastic electron mean free path λ for electrons with kinetic energies of several hundreds of eV is typically of the order of 10–25 Å [32], XPS is often referred to as a surface-sensitive technique [33]. The commonly used term *probing depth* (or *information depth*), corresponds to the thickness of the top surface layer, which accounts for 95% of the total signal intensity. In the absence of elastic scattering of the photoelectrons, one assumes an exponential decay of the signal intensity I_0 with depth x:

$$I = I_0 e^{-x/\lambda cos\theta} \tag{2}$$

in which θ is the electron emission angle referred to the surface normal. It is easy to show that the effective probing depth is equal to $3 \times \lambda$.

The core-level binding energy E_B in XPS is directly calculated from the measured kinetic energy E_{kin} of detected photoelectrons from Einstein's relation

$$E_B = h\nu - E_{kin} \tag{3}$$

where $h\nu$ is the energy of the incident photons. This equation is only valid for gas-phase measurements. In the case of solid samples, other aspects like the sample and spectrometer work functions have to be considered, as discussed more in Section 3.1.

The concept of electron binding energy is central to XPS measurements of core-level spectra and therefore it is highly relevant to understand it properly. Contrary to the widespread notion, specific BE values obtained from XPS do not correspond to any individual energy associated with electrons occupying a given core-level. As a matter of fact, in the ground state of an atom, electrons do not have any distinct energies, but share simultaneously the total energy of the system. Therefore, one should rather think of a BE corresponding to a core-level C1 as the difference between the energy of an atom in the ground state and that of a positive ion with a core-hole state left after the photoionization event has taken place by emitting an electron from C1. In this respect, XPS probes the final state, while the properties of the initial state (before photoionization) are actually not accessed directly. Hence, the XPS spectrum maps the final states, i.e., energy differences between the ground state of the sample and the numerous final (or ionized) states.

The XPS notation for core-level signals is of the form "X nl_j", where X denotes the element, n is the principal quantum number (n = 1, 2, 3, …), while l is the angular quantum number denoted as s, p, d, f corresponding to l = 0, 1, 2…, $n-1$. j in "X nl_j" stands for the total angular momentum quantum number equal to the sum of the angular and the spin projection ($s = \pm 1/2$) quantum numbers $j = l + s$. For example, Zr $3d_{5/2}$ corresponds to electrons from a Zr atom with n = 3, l = 2, and s = ½. All core-level signals with $l \geq 1$ have a form of spin-split doublets: $p_{3/2}$-$p_{1/2}$, $d_{5/2}$-$d_{3/2}$, $f_{7/2}$-$f_{5/2}$ with the respective theoretical area ratios of 2:1, 3:2, and 4:3, determined by the degeneracy of each electronic level ($2j + 1$). The BE splitting between these two components, ΔBE, varies from a fraction of eV to several eV and depends on the average radius of the involved orbital. In general terms, ΔBE increases with atomic number for a given subshell (constant n, l) and decreases as l increases for a given shell (n constant). To add to the complexity, both

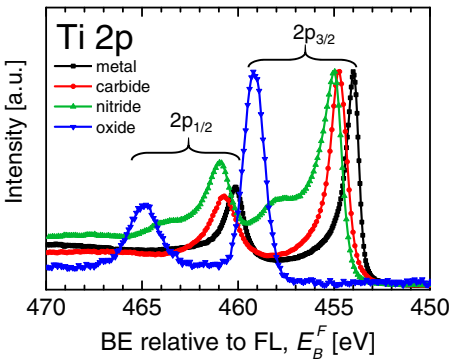

Fig. 9. Ti 2p spectra recorded from Ti, TiC, TiN, and TiO_2 thin film surfaces previously sputter-etched with a 0.5 keV Ar^+ ion beam incident at an angle of 70° from the surface normal. [Author's original work.]

the area ratio and the BE splitting are not constant for a given element and show some variation with, e.g., chemical environment. This is illustrated in Fig. 9 where the Ti 2p spectra recorded from Ti, TiC, TiN, and TiO_2 surfaces are shown. Clearly, the overall spectrum appearance depends strongly on the element to which Ti is bonded. The BE of the Ti $2p_{3/2}$ peak varies from 454.0 eV for the metal to 454.7, 455.0, and 459.2 eV for carbide, nitride, and oxide, respectively. The spectra acquired from Ti and TiC show a certain degree of asymmetry on the high BE side, which is not present in the case of the Ti 2p signal from the TiO_2 sample. In addition, the spectrum obtained from TiN exhibits a pair of satellites shifted from the primary peaks by ca. 2.7 eV towards higher BE (see Section 2.6). Furthermore, the BE separation between the spin-split components, $2p_{3/2}$ and $2p_{1/2}$, shows some dependency on the chemical state of the Ti atoms and amounts to 6.1 eV for Ti and TiC, 6.0 eV for TiN, and 5.7 eV for TiO_2.

XPS is moreover referred to as a finger-print technique, as each element has a unique set of associated core-level peaks that allow for unambiguous identification. For elemental analysis, a wide range, so-called *survey* spectrum is typically recorded with the BE range extending from 0 to >1000 eV (cf. Fig. 4) in order to obtain signatures from all species present in the sample. Peak overlap is not uncommon. Hence it is advisable to check whether all core-level lines from the element under consideration are in fact present in the survey spectrum. The energy resolution is of minor importance here since the survey scans are performed at high pass energy to take advantage of the higher count rate with the positive impact on the detection limit. The latter depends on the relative sensitivity factors (RSFs), which are experimentally-derived and tabulated for major core-level signals. In general, the practically attainable detection limits are in the range of 0.1 to 1 at%.[34] Lower values can be achieved with prolonged scanning, as the detection limit is inversely proportional to the square root of the number of scans.

Following the survey, in the second step one takes a closer look at the primary core-level signals from elements of interest by performing narrow-region high-energy-resolution scans. In this case, a low pass energy is used, and often one has to compromise between FWHM and the total acquisition time (cf. Fig. 8).

In cases where multiple narrow regions are defined, it is advisable to perform scanning in a one-by-one sweep fashion rather than to complete multiple scanning of one region before starting the next one. This procedure eliminates potential drifts of the spectra intensity with time, which is especially relevant if the data are intended for quantification (see Section 2.4).

The measured widths of the core-level peaks vary greatly. For example, the FWHM of the Ag $3d_{5/2}$ line recorded in our laboratory under ultimate conditions of pass energy on the Axis Ultra DLD instrument of Kratos Analytical can be as low as 0.45 eV, while the FWHM of the Au 4 s peak exceeds 8 eV. The main factors that determine peaks FWHM are: (i) the natural width of the core-hole state ΔE_N given by the uncertainty principle $\Delta E_N = h/\tau = 4.1 \times 10^{-15}/\tau$ [eV], in which τ is the core-hole life-time, (ii) the dispersion of the photon source ΔE_P (down to 0.26 eV for monochromatized Al Kα radiation, see Section 2.2), and (iii) the analyzer resolution ΔE_A (<0.1 eV under optimized conditions). The resulting FWHM is then given by $\sqrt{\Delta E_N^2 + \Delta E_P^2 + \Delta E_A^2}$.

Besides the primary core-level peaks of the type discussed above, XPS spectra may, and often do, contain other features caused by a whole range of phenomena including Auger electron emission, multiplet splitting, shake-up and shake-off events, or plasmonic excitations. Each of these features contains a great deal of information about the studied material. Examples of the most commonly occurring ones are shown in Fig. 10.

Auger peaks are commonly observed in photoelectron spectra (cf. Fig. 10(b)). In the process of Auger-electron emission, the inner-shell core hole left after the photoionization event is refilled by an electron from an outer shell of the same atom and the resulting excess energy (equal to the energy difference between the inner and the outer shell) is transferred to another shallow outer-shell electron, which then becomes ejected. There are usually numerous possibilities for filling the core hole resulting in a rather complex Auger peak pattern. In the example shown in Fig. 10(b) the core hole created in the K electronic shell of an Mg atom is filled with an electron from shell L_1 and the escaping electron originates from shell L_{23}. Thus, the corresponding Auger peak is denoted as KL_1L_{23}. As the kinetic energy of Auger electrons is solely determined by the electronic structure of the emitting atom, the position of Auger peaks on the BE scale depends on the energy of the exciting radiation, which makes them easily distinguishable from photoelectron peaks.

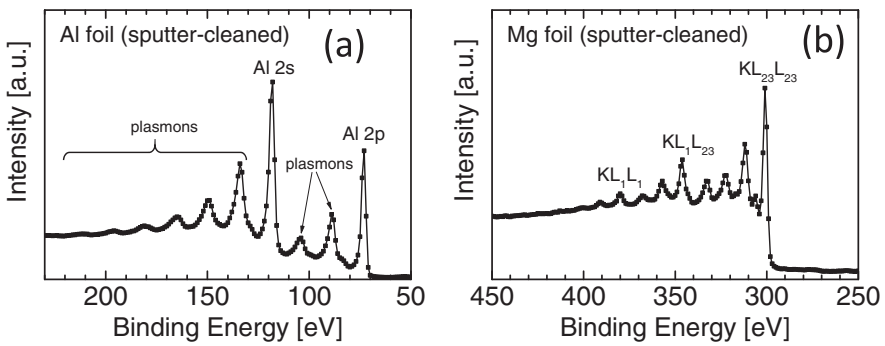

Fig. 10. Examples of (a) plasmon losses observed in the spectrum recorded from Al foil, and (b) Auger transitions detected in the spectrum of Mg thin film sample. In both cases samples were sputter-etched with a 0.5 keV Ar^+ ion beam incident at an angle of 70° from the surface normal. [Author's original work.]

2.4. Quantitative analysis

An essential part of XPS analysis is the evaluation of elemental composition in the surface region. The most common way to do that is an empirical approach based on the measured areas under the main core-level lines of all elements present in the sample. For a homogenous sample containing n elements the molar concentration x_i of element i is then given by [35]

$$x_i = \frac{A_i/s_i}{\sum_{j=1}^{n}(A_j/s_j)} \tag{4}$$

in which A_i is the area under the corresponding core-level peak, and s_i is the relative sensitivity factor (RSF). The latter is an experimentally-determined value, which is specific for each core-level peak (typically normalized to one specific signal like C 1s or F 1s) and apart from basic components like the photoionization cross-section and electron inelastic mean free path is also affected by the instrument-related factors like the transmission function of the spectrometer [36]. For this reason, the best results are obtained if the RSFs are specifically determined on the same instrument as used for quantification and under the same experimental conditions (pass energy, anode power, aperture size, etc.). If this is not possible, standard sets of RSFs are also available [37,38], however, a negative impact on the accuracy of extracted sample stoichiometry can be expected. Special precautions should be taken while determining RSF using multielement samples, since the removal of surface oxides and contaminants by means of Ar^+ ion etch causes a number of side effects that may significantly alter the surface composition [12].

Apart from problems associated with RSF determination, large source of errors associated with Eq. (4) is related to the reliable measurement of peak areas (or peak intensities). Although this is an extensive subject, from the XPS practitioner perspective it breaks into two aspects: (i) spectra acquisition procedure and (ii) background subtraction. In order to record the core-level spectra in the most suitable way for quantitative analysis, it is required that the impact of all potential signal instabilities over time necessary to collect all spectra (often many hours), either related to the instrument operation or to sample itself, is minimized. This is best realized by performing the same number of scans over each core-level signal, irrespective of the signal strength, and setting up the acquisition sequence in such way that all BE regions of interest are scanned simultaneously rather than sequentially. Such procedure ensures that potential instabilities will have similar effect on all core-levels signals.

The XPS background analysis has been thoroughly studied [39–42] and the subject is well covered in many textbooks [43]. From the practitioner point of view, the essential point to bear in mind is that the particular choice of background function has a direct effect on the peak areas (and hence the extracted concentrations). The simplest background type comprises a line drawn between the data points on the high and low BE sides of the peak. Although very convenient, the linear background lacks theoretical grounds, and, more importantly for the sake of accurate quantification, makes the peak area dependent on the arbitrary selection of end points. Linear background can be sufficient for wide-band gap materials (e.g. polymers) [44] in which case the photoelectron energy losses associated with the presence of valence electrons occur several eV away from the no-loss line. As a result, the background intensities on the low and high BE sides of the peak are very similar, hence, the error due to the arbitrary selection of background end points is minimized. In contrast, for other classes of materials the uncertainty related to the selection of background end points may be significant. One good example is the Fe $2p_{3/2}$ spectrum shown in Fig. 11(a). In this case the arbitrary selection of end points affects the area under the peak by 14%.

More advanced, and also more popular, is the Shirley background [45]. In this case the background intensity at the binding energy E_b is proportional to the total peak area in the energy range defined by E_b and the end point on the low BE side of the peak. The basic assumption is that the number of inelastically scattered electrons contributing to the background increase is directly proportional to the total photoelectron flux. Clearly, also in this case the arbitrary choice of the end points affects the end result.

A third type of function from the conventional toolset available on essentially all modern instruments is the Tougaard background [46,47]. In clear distinction from the two other approaches discussed above, this method relies on the quantitative description of the inelastic scattering phenomena that give rise to the background. Moreover, it provides area estimates that are largely independent of the choice of end points on the lower and higher BE sides of the peak. All three background types discussed above are compared in Fig. 11(b) and (c), for peaks characterized by low (C 1s from polymer sample) and high (Au $4p_{3/2}$ from metallic sample) background increase. While in the former case the background choice has a negligible effect on the peak area estimate (all three functions essentially overlap), the Au $4p_{3/2}$ peak area varies by as much as 12% depending upon which function is selected. The reliability of all three background types for peak area determination in the case of polycrystalline metals and metallic alloys has been evaluated by Tougaard et al. [48]. In that paper, the authors compared the peak-intensity ratios obtained with different backgrounds to the theoretical predictions based on calculated photoionization cross sections. They concluded that Tougaard background provides highest consistency and validity of all background-subtraction methods tested.

Another related issue, equally problematic for all background functions, is the treatment of spin-split doublets with closely spaced components, like the pair of Au 4d peaks in Fig. 11(d). In this case, a single Shirley background extending over both components yields an area which is 23% larger than that obtained with two separate Shirley backgrounds. This example presents a serious dilemma to the XPS user, since there are no clear guidelines available as to which alternative should be selected.

It has to be emphasized that Eq. (4) only applies to samples that are homogeneous within the analyzed volume, i.e., within the first 50–100 Å from the surface. In all other cases, knowledge of the depth distribution is necessary in order to extract meaningful results [49,50]. This is the largest obstacle in practical XPS studies and, if neglected, typically is the main source of errors. As a matter of fact, due to the nature of the method, extremely different elemental depth distribution functions can produce an identical signal intensity [51]. One approach to circumvent this problem has been proposed by Tougaard et al. who developed a formalism for

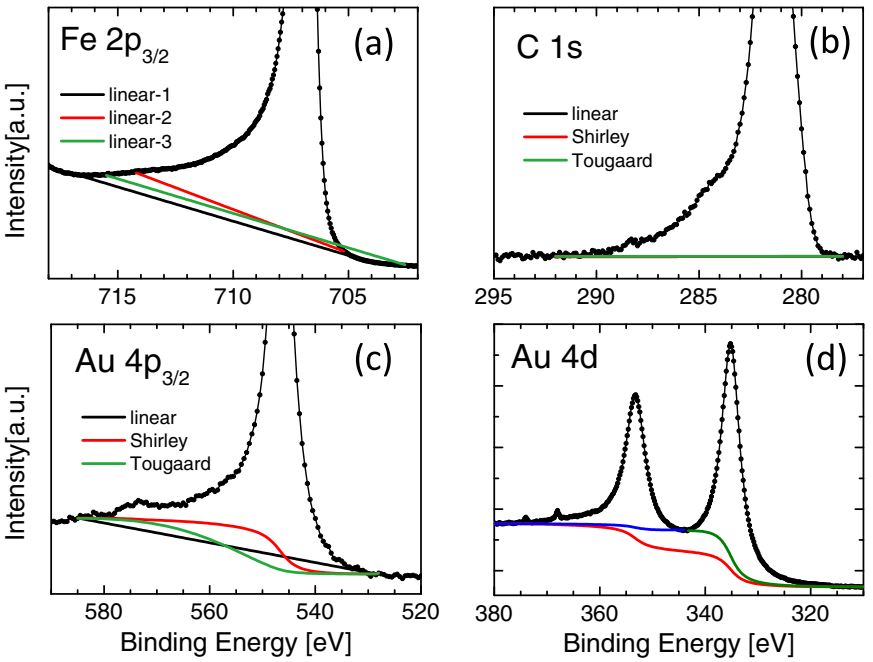

Fig. 11. (a) Fe $2p_{3/2}$ core-level spectrum with three linear backgrounds characterized by different end points, (b) C 1s spectrum from polymer sample fitted with linear, Shirley, and Tougaard background functions (all three functions overlap), (c) Au $4p_{3/2}$ spectrum from metallic film fitted with linear, Shirley, and Tougaard background functions, and (d) Au 4d doublet with a single Shirley background extending over both peaks as well as with two separate Shirley functions, one for each spectral component. [Author's original work.]

quantitative XPS based on the analysis of the peak shape together with the high BE side background [52,53]. The advantage of this method is that it allows for a non-destructive *in situ* studies of the surface composition during various types of treatments (e.g. annealing, adsorption, etc.).

The positive side of the strong influence of elemental depth distribution on the XPS signal intensity is that it can be utilized to measure thickness of thin (< 100 Å) continuous overlayers like, e.g., the case of native oxides on metals. Strohmeier et al. shown that if elastic scattering of the photoelectrons is ingored, the thickness d of a uniform oxide overlayer with a volume atom density N_o formed on top of the metal film with a volume atom density N_m can be related to the measured intensity ratio of oxide and metal peaksI_o/I_m as:[54,55]

$$d = \lambda_o cos\theta ln\left(\frac{N_m \lambda_m}{N_o \lambda_o}\frac{I_o}{I_m} + 1\right) \tag{5}$$

in which λ_m and λ_o are inelastic electron mean free paths in metal and oxide, respectively. As in majority of cases the metal and oxide peaks are either separated in terms of BE or can be resolved by constructing peak models (see Section 2.6), Eq. (5) provides means to assess oxide thickness *in situ* in a non-destructive way. The reliability of the method is enhanced by the fact that signals from the same element present in two different chemical states are analyzed which eliminates the uncertainty related to the determination of photoionization cross-sections. In addition, the errors due to instrumental factors like the transmission function of the spectrometer are not of concern as electrons excited from metal and oxide core-levels have a similar kinetic energy.

Eq. (5) is often simplified to

$$d = \lambda cos\theta ln\left(\frac{N_m}{N_o}\frac{I_o}{I_m} + 1\right) \tag{6}$$

upon further assumption that the electron mean free paths in metal and the oxide layer are similar $\lambda_m = \lambda_o = \lambda$. To further enhance the accuracy one can then utilize the dependence on the electron emission angle θ by recording the spectra as a function of sample tilt angle with respect to the analyzer axis. The plot of $ln\left(\frac{N_m}{N_o}\frac{I_o}{I_m} + 1\right)$ as a function of $1/cos\theta$ allows one to determine the overlayer thickness from the slope d/λ.

An important aspect of quantification rather unique to XPS is that apart from finding the elemental composition, the technique provides information on the relative amounts of a given element present in different chemical states. As in this type of analysis only one element type is involved, much better accuracy can be obtained provided that the chemically shifted spectra components are well separated in energy (see for example C 1s spectra of trifluoroacetate in Fig. 12).

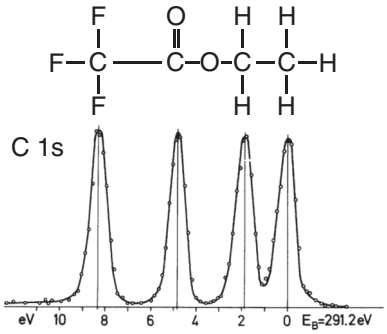

Fig. 12. Chemical structure of ethyl trifluoroacetate (top), and corresponding C 1s core-level spectrum adopted from Ref. [63] (bottom).

2.5. Chemical shifts

Undoubtedly, the main reason for the enormous popularity and success of XPS in modern materials science is its ability to address the bonding state of analyzed elements. This is due to the phenomena known as *chemical shift* discovered in 1957 by the group of Kai Siegbahn, who was later awarded a Nobel Prize in Physics (1981) for this ground-breaking achievement. The first observation of chemical shift was made for Cu atoms present in metallic and oxidized states [2]. Photoelectron spectra recorded from oxidized copper resulted in the Cu 1s line being shifted by 4 eV with respect to the corresponding signal obtained from metallic Cu. Although the discussion of the result was well-motivated and correct, it was established later that the chemical shift is in fact only 1 eV, and, hence, the excess shift in the original experiments was dominated by the charging of the Cu oxide sample [56]. More spectacular evidence, free from charging artefacts, which brought international attention to this emerging field, was the report on the S 2p peak split in the photoelectron spectrum of sodium thiosulfate $Na_2S_2O_3$ [57,58]. Unlike the case for Cu, where chemical shifts were detected for separate metal and oxide samples, two distinctly different valence states of S atoms in the same molecule (6+ and 2−) resulted in the first chemically-split core-level spectrum with two components separated by 6.7 eV, i.e., large enough to be resolved at that time. As a matter of fact, the full-width-at-the-half-maximum of the S 2p line from sublimated sulfur reported in Ref. [58] was 6.5 eV, primarily due to the natural line width of the Cu Kα radiation used as the excitation source. As the corresponding spectrum of pure sulfur published in the same paper exhibited only one peak (the $2p_{3/2}$-$2p_{1/2}$ spin-spin doublet could not be resolved at that time), the potential influence of instrumental factors could be eliminated. After that, chemical shifts were demonstrated for C atoms in 1,2,4,5-benzenetetracarboxylic acid [59], and a whole series of N-containing organic molecules [60], which laid grounds for chemical analysis by electron spectroscopy (ESCA), here referred to as XPS [61].

It is imperative to consider the reason for the apparent BE differences between photoelectrons originating from the same core-level in atoms with different chemical environment. For the purpose of this review, we will adopt the best-suited case of the “ESCA molecule” [62], i.e., ethyl trifluoroacetate with four C atoms in different bonding configurations. For this molecule, the valence charge density on the carbon site, highest in the case of the CH_3 unit, gradually decreases while going to C−O, O−C=O, and the C-F_3 carbons. As the molecule is perfectly suited for demonstration of a chemical shift, we note that Siegbahn's group synthesized the compound and put its spectrum on the cover of their seminal book [4].

The C 1s spectrum of ethyl trifluoroacetate, shown in Fig. 12 [63], is composed of four distinct peaks of equal intensity, hence there is a one-to-one correspondence to the C atoms in the chemical structure drawn above the spectrum. Clearly, XPS spectra are highly sensitive to the difference in chemical environment of each C atom, hence to the differences in the valence charge density, as it is valence electrons that participate in the formation of chemical bonds. A key question concerns the reason why the core-level electrons, that have nothing to do with bond formation are also affected? This is a central point to the correct understanding of the chemical shift. Still, it is a rather common misinterpretation that differences in the valence-charge density have a direct effect on the binding energy of core-level electrons. However, as we indicated in the previous section, electrons do not possess distinct energies, but rather share simultaneously the total energy of the whole system. Therefore, to be correct, rather than to say that the BE of the C 1s electron from an atom bonded to three F atoms is higher than that of C atoms bonded to H, one should speak in terms of the total energy before and after the photoionization event: it costs more energy to create a core hole localized on the C atom in CF_3 than on that in the CH_3 unit. The physical reason is that the negative valence charge density is significantly reduced on C atoms in the former configuration due to fluorine's high electronegativity, resulting in poorer screening of the core hole left after photoionization. Hence, a photoelectron leaving this site experiences stronger Coulomb attraction and, in consequence, arrives at the detector with lower kinetic energy than corresponding electrons originating from a C atom in the CH_3 unit. This phenomenon gives rise to the apparent split of more than 8 eV between the C 1s signal from the two sites, with C−O and O−C=O carbons being intermediate cases.

In everyday XPS practice, chemical shifts are rarely this large, which puts very strict requirements on the proper BE referencing in order to avoid false assignments.

2.6. Creating peak models

In order to extract specific information from the XPS core-level spectra, deconvolution into several component peaks is often

attempted. This is a procedure that requires rigorous treatment, which unfortunately is rarely the case, and, as a result, the XPS literature is filled with examples of overinterpreted or simply poorly fitted XPS spectra [64]. Minimization of the residuals in the fitting process should not be the dominating criterion during the deconvolution. In addition, peak assignment based on an XPS data base alone is unreliable due to the large spread in BE values reported for the same chemical species (see examples in Section 1.1). For these reasons, we formulate below guidelines which enhance the quality of the extracted chemical information:

(1) Before attempting spectral deconvolution, the clear purpose of a peak model should be formulated. A lot of information can be extracted from XPS spectra without advanced fitting procedures, hence one should always consider if the deconvolution process is indeed necessary.
(2) The proposed peak model should be comprehensive. In the vast majority of cases, the analyzed samples contain more than just one element. It is not sufficient to deconvolute spectra from one element, while completely neglecting all other primary core-level signals.
(3) The presented peak models for all core-level spectra should show qualitative self-consistency. That is, the presence of component *A1* in the deconvoluted spectrum of element *A* assigned to A_mB_n formation requires that the corresponding *B1* component peak is present in the core-level signal of element *B*.
(4) Quantitative self-consistency is also required. That is, the elemental concentrations extracted from *A1* and *B1* peak areas should reflect the compound stoichiometry *m*/*n*. For the latter condition, complementary sample compositional analysis (not relying on the same XPS spectra) should be used.
(5) The number of component peaks should be kept to the minimum necessary to obtain a decent fit. There should be a clear physical interpretation for each component peak. The artificial increase of the number of component peaks certainly helps to improve fit quality, however, the result could be fortuitous.
(6) Constraints that take into account underlying physics (e.g., BE splitting and peak-area ratios between spin-split components), and self-consistency of multiple data sets (constant peak position, BE separation, area ratio, FWHM, mathematical function, etc.) should be used.

The main advantage of the XPS spectral deconvolution performed according to the above-specified criteria is that the peak model does not rely on direct comparisons to reference binding energy values that in many cases exhibit alarmingly large spreads making the peak assignment ambiguous (see Section 1.1) [13]. Instead, all constraints imposed across all core-level spectra, that require both qualitative and quantitative self-consistency between component peaks belonging to the same chemical species, ensure that the extracted chemical information is correct.

One example of such self-consistent XPS peak modelling where the above criteria have been implemented is shown in Figs. 13–15 [13], which contain Ti 2p, N 1s, and O 1s core-level spectra recorded from a series of TiN thin films grown by dc magnetron sputtering and oxidized to different extents by varying the venting temperature T_v of the vacuum chamber before removing the deposited samples.

Deconvolution of this very complex set of core-level spectra obtained from air-exposed TiN surfaces, requires a step-by-step procedure starting with the simplest case of the native TiN surface, serving here as a reference, with only two Ti $2p_{3/2}$ components (main TiN peak and the satellite, TiN-sat, see Fig. 13(a)). The line shapes, $2p_{3/2}$-$2p_{1/2}$ BE splitting, and the $2p_{3/2}/2p_{1/2}$ area ratio obtained for pairs of TiN and TiN-sat peaks are then propagated to the more complex models containing up to four contributions (see the Ti 2p spectra corresponding to T_v in the range 29–430 °C). In addition, the BE difference between the TiN and TiN-sat peaks and the relative TiN/TiN-sat peak areas are fixed at values determined from the reference TiN sample. These constraints are necessary to enforce mathematical least squares solutions that are physically founded. An additional global constraint to the model is that the particular line shape representing a given chemical state is the same for all samples containing the compound of interest. The fitting parameters include the Ti $2p_{3/2}$ peak area, FWHM, and peak position. More technical details of the fitting procedure can be found in Ref. [13].

In the Ti 2p spectrum of native TiN surfaces, free from oxygen contamination, the Ti 2p spin-orbit split $2p_{3/2}$ and $2p_{1/2}$ components appear at 455.03 and 460.97 eV, respectively, while the satellite features (TiN-sat) [65–67] are shifted by 3.0 eV towards higher BE with respect to the primary peaks. A satisfactory fit requires asymmetric functions for the main components, which can be explained by energy loses due to simultaneous excitations of valence electrons, as the density of states near and at the Fermi level is high. TiN-sat peaks are well-represented by Voigt functions with a 95% Lorentzian fraction. The corresponding N 1s spectrum (cf. Fig. 14(a)), is dominated by a main peak centered at 397.34 eV and assigned to TiN. The low-intensity feature (~ 2% of the total N 1s peak area) to the high BE side of the main peak, at 399.35 eV, is assigned to the satellite. The N/Ti ratio due to TiN contributions (including satellites) is 1.02, in very good agreement to the bulk value of 1 ± 0.01 obtained from Rutherford backscattering (RBS).

Input from the Ti 2p and N 1s spectra deconvolution presented above serves to create more complex peak models for a series of TiN films exposed to atmosphere at temperatures ranging from 29 to 430 °C (see Fig. 13(b)–(d) and 14(b)–(d)). For completeness, peak models for corresponding O 1s spectra are also included in Fig. 15(a)–(c). The number of new component peaks added to the model in order to obtain a high-quality fit is kept to a minimum. Contrary to common practice, the assignment of new spectral contributions is not based solely on the comparison to the reference BE values, which differ greatly. Instead, quantitative self-consistency between Ti 2p, N 1s, and O 1s component peaks is one of the main criteria that justifies the quality of the fit.

The concentration of additional chemical species formed during air exposure of samples, here exemplified by TiO_2 and TiO_xN_y, clearly depends on the sample temperature. Peak assignment is predominantly based on the presence of corresponding components in all three core-level spectra Ti 2p, N 1s, and O 1s. More importantly, the peak-area ratio between TiO_2 contributions in the Ti 2p and O

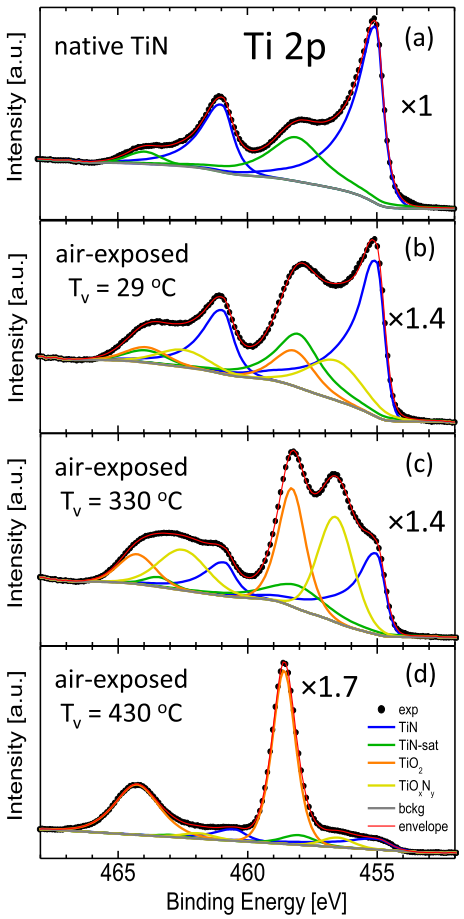

Fig. 13. Ti 2p XPS spectra obtained from polycrystalline TiN films: (a) capped *in situ* with 15-Å-thick Al layer to protect the surface from oxidation, (b)–(d) uncapped and exposed to atmosphere at different venting temperatures T_v ranging from 29 to 430 °C [adapted from Ref. [13]].

1s spectra results in the elemental concentration ratio O/Ti = 2.00 ± 0.03, for all T_v values, assuring that not only qualitative, but also quantitative cross-peak self-consistency of the model is reached. The formation of TiO_xN_y is concluded based on the observed Ti 2p – N 1s cross-peak correlation, which strongly indicates that, in addition to oxygen, the new compound contains both Ti and N. This observation excludes the potential assignment of this particular spectral feature in Ti 2p spectra to Ti_2O_3 which, according to literature, could give rise to peaks in a similar BE range.

The example discussed above illustrates how the additional restrictions introduced during the XPS peak modelling process in the form of qualitative and quantitative self-consistency between component peaks belonging to the same chemical species, enhance reliability of the extracted chemical information. A peak assignment which is solely based on comparisons to the reference binding energy values that exhibit large spread is likely ambiguous.

2.7. Examples of artefacts

2.7.1. Sputter damage

The majority of samples intended for XPS analysis has been exposed to air prior to inserting them into the spectrometer. Ar^+ ion etching is typically used to remove oxygen and other adventitious surface contamination prior to analysis. In such processing, the sample is irradiated with a 200–4000 eV Ar^+ ion beam, which is rastered over the surface to be analyzed. However, the etching process can lead to a number of artefacts including preferential elemental sputter ejection, recoil implantation, structural disorder, and perhaps the most problematic of all, changes in the surface chemistry [12], all of which make compositional and chemical analyses extremely challenging [68–71]. In the XPS literature any phrase with 'challenging' should be read as an euphemism.

To estimate the degree to which all of the above effects contribute to the XPS core-level spectrum, we can compare the thickness of the surface layer affected by the ion beam with typical XPS probing depths. A good estimate of the former is the recoil projected range that can be obtained using a Monte Carlo TRIM (Transport of Ions in Matter) [72] program included in the SRIM (Stopping power and Range of Ions in Matter) software package [73]. Fig. 16 shows the distributions of N and Ti recoils resulting from Ar^+ irradiation of a TiN surface. Two cases are considered: (a) high energy E_{Ar^+} = 4 keV Ar^+ ion flux incident along the surface normal

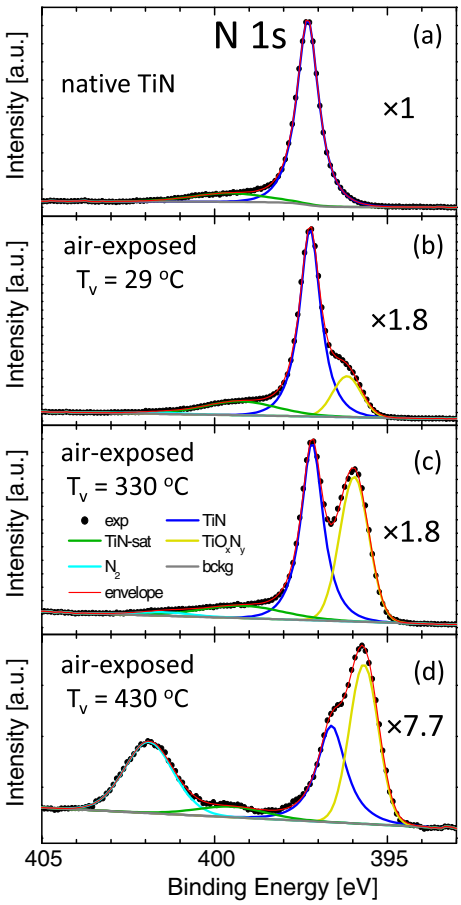

Fig. 14. N 1s XPS spectra obtained from polycrystalline TiN films: (a) capped *in situ* with 15-Å-thick Al layer to protect the surface from oxidation, (b)–(d) uncapped and exposed to atmosphere at different venting temperatures T_v ranging from 29 to 430 °C [adapted from Ref. [13]].

($\psi = 0°$), and (b) low energy $E_{Ar^+} = 500$ eV Ar^+ ions incident at an angle $\psi = 70°$ from the surface normal. Clearly, both ion energy and the ion incidence angle have a huge impact on the thickness of the ion-beam modified TiN layer, which ranges from >100 Å in the former case to ~20 Å obtained under the latter conditions. If we now consider that the inelastic mean free path for the Ti 2p electrons excited with Al Kα radiation ($E_{kin} = 1032$ eV) is 20 Å [32], the contribution to the core-level spectrum due to the Ar^+-modified top layer is 90% for high-energy ions ($\psi = 0°$) and 40% for low-energy Ar^+ ($\psi = 70°$). Thus, even for the mildest set of etching conditions, the surface cleaning step has a pronounced effect on the XPS results.

This situation is illustrated in Fig. 17 where the Ti 2p spectra recorded from TiN surface after Ar^+ sputter-cleaning with four sets of ion energy and incidence angle (E_{Ar^+}/ψ) conditions are shown [74]. The Ti 2p core-level spectra consist of a spin-orbit split doublet with Ti $2p_{3/2}$ and Ti $2p_{1/2}$ components at 455.2 and 461.1 eV, respectively. Both Ti 2p peaks exhibit satellite features on the high binding-energy side, shifted ~2.7 eV above the primary peaks. To facilitate comparison, the intensities of the Ti 2p spectra are normalized to those of the highest intensity features for each spectrum. The relative intensities of the satellite peaks (see inset in Fig. 17) are highest after etching with $E_{Ar^+} = 0.5$ keV and $\psi = 70°$; they decrease in intensity upon increasing E_{Ar^+} to 4 keV (at $\psi = 70°$); and decrease even further as ψ is lowered to 45° and 0°, while maintaining E_{Ar^+} at 4 keV. The reduction in the satellite peak intensity due to ion etching is accompanied by increasing background levels on the high BE side, both indicative of surface damage. In addition, the XPS-determined N/Ti ratio decreases from 0.74 ± 0.03 with $E_{Ar^+} = 0.5$ keV and $\psi = 70°$, to 0.72 ± 0.03, 0.70 ± 0.03, and 0.68 ± 0.03 with $E_{Ar^+} = 4$ keV and $\psi = 70°$, 45°, and 0°, respectively, indicating preferential N loss, in agreement with previous reports [75].

To circumvent the negative effects of Ar^+ ion etch, different approaches have been proposed including the application of capping layers which are later removed in vacuum [76–78] or made thin enough to be transparent to the electrons originating from the sample [74]. Another alternative is the *in situ* ultra-high vacuum (UHV) anneal, which has been demonstrated to effectively remove surface oxides from air-exposed transition-metal nitride films due to recrystallization [79]. The use of *in situ* XPS, glove box facilities, or portable vacuum chambers, to avoid air exposure is also in practice. More recently, the use of C_{60}^+ or Ar^+ cluster ion beams has been demonstrated to result in a significant reduction or even complete elimination of the surface damage for certain materials [80–82].

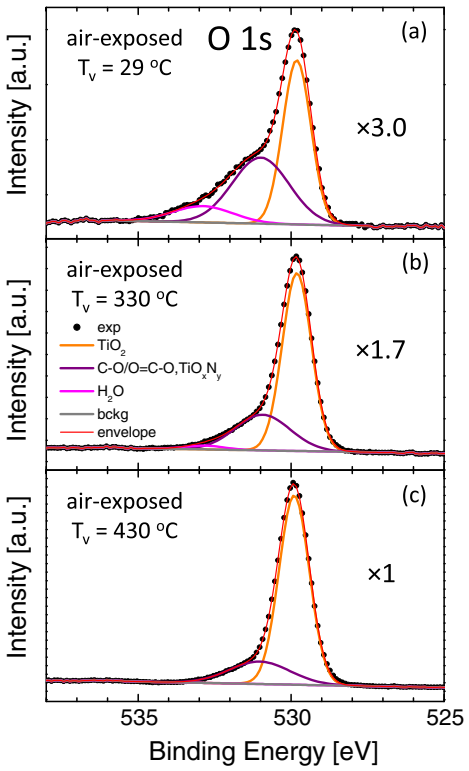

Fig. 15. O 1s XPS spectra obtained from polycrystalline TiN films: (a) capped *in situ* with 15-Å-thick Al layer to protect the surface from oxidation, (b)–(d) uncapped and exposed to atmosphere at different venting temperatures T_v ranging from 29 to 430 °C [adapted from Ref. [13]].

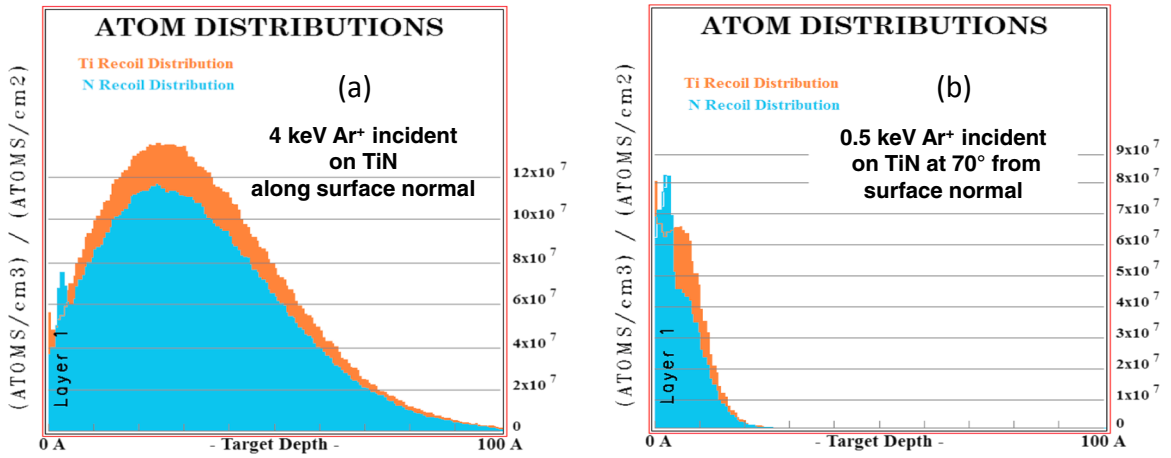

Fig. 16. Distributions of N and Ti recoils resulting from the Ar^+ irradiation of the TiN surface simulated with the TRIM software. Two cases are considered: (a) high energy $E_{Ar^+} = 4$ keV Ar^+ ion flux incident along surface normal ($\psi = 0°$), and (b) low energy $E_{Ar^+} = 500$ eV Ar^+ ions incident at an angle $\psi = 70°$ from the surface normal. [Author's original work.]

2.7.2. Sample charging

While the XPS measurement itself is not necessarily destructive to the sample, it relies on the photoelectric effect which leads to continuous loss of electrons (called in this context *photoelectrons*) from the surface region. If the photoelectrons are not replenished at a high-enough rate, charge neutrality is lost and the surface acquires a positive potential, which decreases the kinetic energy of escaping photoelectrons, and results in the shift of all core-level peaks towards higher BE. The latter can range from just tenths of an eV, in which case it may go unnoticed, to several hundred eV for insulators, where essentially no photoelectrons leave the surface. Under such circumstances, the FL of the spectrometer and that of the sample are no longer aligned, implying that the natural reference level is lost. This situation is commonly referred to as *charging* [83].

The factors that determine the steady-state equilibrium of the surface potential are: (i) electrical conductivity, (ii) photo-induced

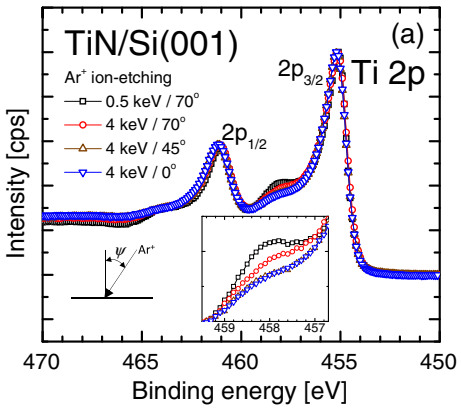

Fig. 17. Ti 2p spectra recorded from TiN surface after Ar^+ sputter-cleaning with four sets of ion energy and incidence angle (E_{Ar}+/ψ) conditions [adapted from Ref. [74]].

surface conductivity, (iii) X-ray flux, (iv) the photoelectric cross-section, (v) the photoelectron mean free paths, and (vi) the flux and energy distribution of electrons incident on the surface from the vacuum chamber [84,85]. Hence, one way to verify that sample charging indeed takes place, and to avoid confusion with alternative explanations of core-level shifts (see Section 2.3), is to monitor the BE changes as a function of X-ray power.

As the charging state of a specimen is not known *a priori,* the phenomenon often leads to problems with correct BE referencing. Except for metallic samples, where the natural "0 eV" on the BE is set by the FL cut-off, other specimens lacking an internal BE reference represent a serious challenge, which in consequence leads to reported BE values for the same chemical state exhibiting a large spread (see Fig. 2).

The situation is further complicated for non-homogenous samples in which case effects like differential charging [86], where regions with different conductivity are present, lead to peak broadening [87]. Ironically, charging is worse for today's most common monochromatic sources than for conventional unmonochromatized X-rays, since the photoinduced conductivity is lower due to the absence of the Bremsstrahlung background radiation.

There are means to compensate for the positive charge build up by the use of electron flood guns. The principle of operation is demonstrated in Fig. 18 adopted from Ref. [86] for devices used in Kratos instruments. The spectrometers are equipped with magnetic lenses, which are primarily used to enhance the electron collection efficiency, but also play a crucial role once used together with the filament serving as a source of low-energy electrons (electron flood gun). The magnetic field lines of the snorkel lens define the path of photoelectrons ejected from the sample on their way to the analyzer entrance slit. Simultaneously, they also define the path for electrons originating from the filament towards the sample surface in order to compensate for charge loss. The electrons generated at this filament drift horizontally into the lens aperture, are 'captured' by the field lines and spiral towards the sample surface in the analyzed area.

The primary function of charge-compensation devices is to allow for spectra acquisition from non-conducting samples. They do not represent, however, a solution to the energy-reference problem, as under- or over-compensation typically takes place, hence the surface potential remains unknown.

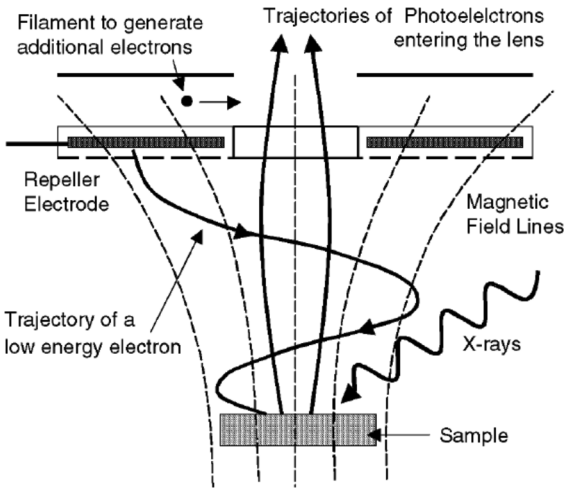

Fig. 18. Schematic adapted from Ref. [86] illustrating the principle of charge neutralization based on the use of low-energy electron source.

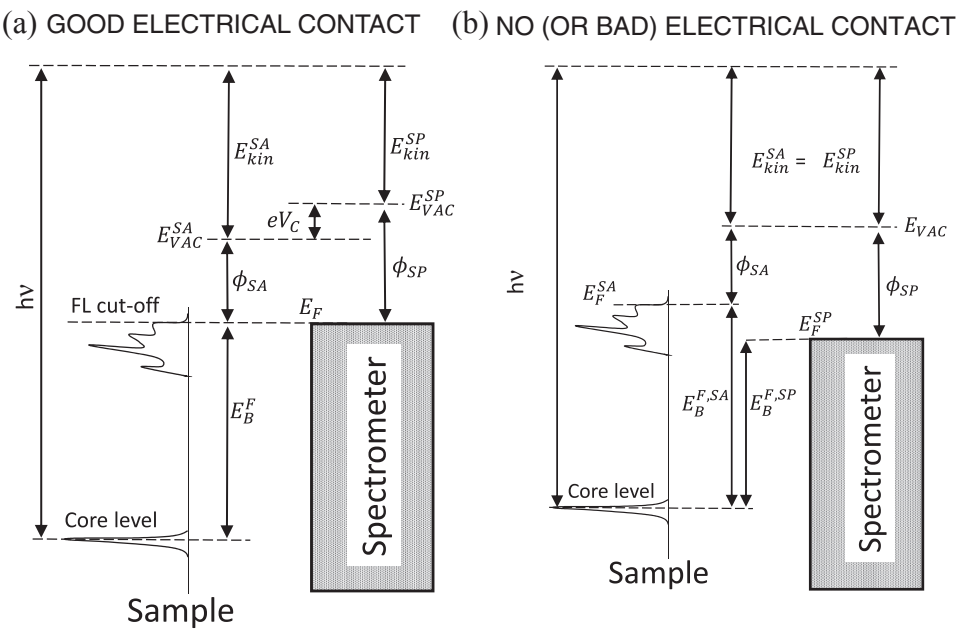

Fig. 19. Energy level diagram for (a) sample in good electrical contact, and (b) sample in poor or in no contact to the spectrometer.

3. Binding energy reference problem in XPS

3.1. Energy diagram and reference levels

The Einstein relation $E_B = h\nu - E_{kin}$ mentioned in Section 2.3 is applicable only for gas phase measurements, where the electron energy is naturally referenced to the *vacuum level* corresponding to the energy of a free electron at rest and infinitely far away from the considered system [88,89]. For solid samples, which are the subject of the present paper, the situation is more complicated due to the fact that photoelectrons escaping from the sample have to overcome the potential barrier at the surface, the so-called *work function* ϕ_{SA}, which corresponds to the energy difference between the *Fermi level* and the VL. In consequence, the FL appears as a more rational and convenient reference level and the electron binding energy is then denoted as E_B^F. Hence, as schematically shown in Fig. 19(a) the kinetic energy of a photoelectron after leaving the sample E_{kin}^{SA} is given by

$$E_{kin}^{SA} = h\nu - E_B^F - \phi_{SA} \tag{7}$$

and is, in general, different from the kinetic energy measured at the detector E_{kin}^{SP}. A common FL (denoted for consistency as E_F in Fig. 19(a)) is thus established across the interface as a result of negative charge transfer from the sample to the spectrometer characterized by the work function ϕ_{SP} if $\phi_{SP} > \phi_{SA}$, or from spectrometer to the sample (if $\phi_{SA} > \phi_{SP}$). This situation results in a contact potential difference V_C, which has to be accounted for while considering an electron travelling towards the entrance slit of the energy analyzer. Its initial kinetic energy E_{kin}^{SA} becomes either reduced ($\phi_{SP} > \phi_{SA}$) or increased ($\phi_{SA} > \phi_{SP}$), to the value E_{kin}^{SP} which is measured at the detector side (see Fig. 19(a)).

Since:

$$E_{kin}^{SA} + \phi_{SA} = E_{kin}^{SP} + \phi_{SP} \tag{8}$$

one can rewrite Eq. (7) in a more convenient form:

$$E_B^F = h\nu - E_{kin}^{SP} - \phi_{SP} \tag{9}$$

which is independent of the sample work function. The spectrometer work function is an experimental constant, which is established during the calibration procedure. Thus, photoelectrons originating from a given core-level always appear at the detector with the same kinetic energy, independent of the sample work function. An important implication is that any change in ϕ_{SA} does not affect the position of core-level XPS peaks with respect to the Fermi level E_B^F. They will be, however, shifted with respect to the VL. It is thus important for these limitations of the XPS technique to be understood if there are any modifications of the surface dipoles, which are masked by the nature of the method. In such cases complementary experiments, e.g., work function measurements from the secondary electron cut-off, have to be performed.

The above considerations only apply under the assumption that the *sample and spectrometer are in good electrical contact* and there are enough charges to establish a common FL. If, for any reason, these requirements are not fulfilled, the energy diagram can be modified as schematically represented in Fig. 19(b). Instead of FL alignment, the sample and spectrometer share a common VL. More

importantly, since the FL of the sample E_F^{SA} is different from that of the spectrometer E_F^{SP}, the BEs for core-level peaks referenced to the spectrometer "0 eV" level are off by the difference between sample and spectrometer work functions $\phi_{SP} - \phi_{SA}$. Hence, in contrast to the case of good electrical contact and FL alignment, any change in sample work function affects the core-level BE. On a related note, there is no contact potential difference, hence $E_{kin}^{SA} = E_{kin}^{SP}$.

The situation depicted in Fig. 19(b) is in general not considered as one tends to divide all XPS samples into two categories: (a) good conductors exhibiting FL alignment, or (b) poor conductors (insulators) that suffer from the charging phenomena (see Section 2.7.2). In fact, the former can only be verified for samples that possess significant DOS at the FL (Fermi level cut-off), which allows for a direct assessment of the E_F^{SA} position with respect to E_F^{SP} (established during calibration, see Section 3.2). In all other cases, the FL alignment is *assumed* to take place if the obtained results do not deviate substantially from the literature or tabulated data, which is a matter of subjective judgement. The qualification to the second category (samples prone to charging) is typically made based on the comparison of recorded BEs to tabulated values, if the charging is not so dramatic that no spectra can be obtained. Interestingly, the case of bad (or no) electrical contact at the sample/spectrometer interface can be easily detected only if $\phi_{SP} > \phi_{SA}$ and the sample possesses a well-defined FL cut-off (cf. Fig. 19(b)), as this situation results in a non-zero DOS above the FL of the spectrometer E_F^{SP}. If $\phi_{SP} < \phi_{SA}$ and/or if no FL cut-off exists, a lack of proper electrical contact to the spectrometer will remain unrevealed.

3.2. Calibration of the binding energy scale

The accurate determination of BEs from an XPS spectrum requires proper calibration of the energy scale. The procedure, nowadays an ISO standard [5], relies on measuring the positions of Au $4f_{7/2}$, Cu $2p_{3/2}$, and Ag $3d_{5/2}$ core-level peaks from metal foils, previously sputter-cleaned in order to remove surface contaminants [90]. Comparison to standardized values allows one to verify the necessary compensation and linearity of the BE scale. Details of how the BE scale is corrected depend on the instrument and are typically supplied by the manufacturer. The whole procedure is ideally done prior to a sample analysis and repeated on a regular basis to correct for errors that accumulate with time. In addition to core-levels, one may also use the lowest BE portion of valence-band spectra for Cu, Ag, and Au in the vicinity of the FL where the density of states exhibits a well-defined cut-off at a position corresponding to the Fermi energy, which defines the natural "0 eV" on the BE scale. While other metals could be used for this test, they typically require consideration of the DOS in the vicinity of the FL.

For the sake of this review article, it is very important to make a clear distinction between BE scale calibration as described above and *charge referencing*. The latter procedure is necessary for non-conducting samples, which tend to acquire positive potential during measurement (see Section 2.7.2) that directly lowers the photoelectron kinetic energy and, hence, leads to the apparent shift of measured BEs towards higher values. Often, the charge built up at the surface is so severe that one has to replenish the negative charge loss (e.g., by using an electron flood gun). While this procedure allows for spectral acquisition, it does not guarantee that the surface is electrically neutral, i.e., under or over-compensation is most often the case. It is thus necessary to find a means for estimating the amount by which core-level peaks are shifted from their neutral positions, so that the spectra can be corrected "by hand" after the measurement is completed. For this purpose, one can use a well-known standard that is part of the sample being measured. Different approaches have been tried over the years, where the most common ones employ the C 1s line of AdC as it is present on all samples in one form or another.

The distinction between BE-scale calibration performed prior to XPS analyses using standardized samples and a charge-calibration procedure based on carbon contamination accumulated on the sample of interest has typically not been elaborated on back in the early days of XPS, where both methods were considered more or less equivalent [91]. This is perhaps the reason why there is still a great deal of confusion among XPS practitioners when it comes to the BE scale calibration as we discuss in more detail in Section 4.

3.3. Alternative approaches to binding energy referencing for non-conducting samples

3.3.1. Noble metal decoration

To solve the problem of a missing BE reference in the case of non-conducting samples, often a small amount of Au (or other noble metal) is deposited *in situ* directly onto the sample [92–96]. Hnatowich et al. [92] showed that such prepared metal deposits come into electrical equilibrium with the surface of an insulating sample and can thus be used to monitor the charging state by comparing the measured BEs of noble metal peaks to those from metal samples in contact with the spectrometer. Apart from complications arising from the need for a deposition source, additional problems are introduced because the BE of Au atoms depends on the size of Au clusters [97,98]. Hence, a continuous film is required, which for many materials with significant surface roughness may imply severe damping of XPS signals from the sample and impractically long spectra acquisition times.

A somewhat more advanced approach, referred to as "biased referencing", was suggested in 1976 by Stephenson et al. [99]. In this case a gold dot is deposited onto an insulating surface that is subsequently exposed to an electron flux at a potential of 10 V to allow Fermi level alignment between the insulator and the gold dot and, hence, obtain a reliable reference level. The method was thoroughly tested by Edgell et al. [100] who investigated three different scenarios employing metal dots evaporated onto Cu and silica substrates: (1) in good electrical contact to each other and to the spectrometer; (2) electrically isolated from each other, and not in contact with the spectrometer; (3) not in contact with the spectrometer, but in contact with each other. By measuring positions of primary core-levels signals as a function of bias while exposed to a flood gun, the authors concluded that the bias referencing method works rather well, however, extracted BEs depend on the work function of the involved materials. An additional limitation is that the measured binding energies of metals either deposited on the surface of, or embedded in, the insulators depend upon whether the metals are in ohmic contact with each other or not. A very interesting observation was also made, that the surface potential may vary

in course of a single XPS measurement due to electric field penetration from the analyzer entrance grids [100]. As the retarding potential is scanned during spectra acquisition, electrons with significantly different BE experience different surface potential. This may show up as a BE difference between two lines of the same element, e.g., Au $4f_{7/2}$ and Au $3d_{5/2}$ of Au dots evaporated onto an insulating sample, is different from that obtained for metallic Au samples.

3.3.2. Intentionally deposited organic layers [101,85]

An original solution for BE referencing was proposed by Vesely et al. [102]. The authors added an additional term ϕ to Eq. (9) to account for possible sample charging

$$E_B^F = h\nu - E_{kin}^{SP} - (\phi_{SP}+\phi) \tag{10}$$

and measured the sum $\phi_{SP} + \phi$ for each analyzed sample by comparing the position of the C 1s peak from carbon soot overlayers deposited on purpose from a candle flame to the value of 283.8 eV, which was a previously reported BE for carbon prepared in a similar way. The difference was then assigned to $\phi_{SP} + \phi$ and the measured C 1s BE was corrected by the corresponding amount to serve as the absolute reference for aligning core-level lines from the sample. The procedure was applied under the assumption that charging in the C overlayer is the same as in the sample and was found to work very well for their analyzed samples: the reported deviation in peak positions was estimated to be only ± 0.2 eV.

3.3.3. Implanted noble gas atoms

Another attempt to solve the BE reference impasse is based on using core-level lines of implanted noble gas atoms [103,104]. With an incident energy in the range 1–5 keV, the implantation depth largely overlaps with the XPS probing depth making this approach especially interesting. In contrast to the technique based on noble metal deposition, there is no risk for attenuation of the specimen signals. The method, however, has shortcomings; Pelisson-Schecker et al. used XPS to analyze a series of Al-Si-N samples deposited by magnetron sputtering [134]. They found that the BE of the Ar $2p_{3/2}$ peak for implanted Ar atoms shifts with varying Si content with respect to that of Au $4f_{7/2}$ peaks from deposited Au clusters by as much as 1 eV, which is associated with a rapid increase in the concentration of trapped Ar atoms. This result was supported by the change in the Ar Auger parameter, calculated as the sum of the kinetic energy of the Ar(LMM) Auger line and the binding energy of the Ar $2p_{3/2}$ peak, and interpreted in terms of preferential Ar location at grain boundaries resulting in large chemical shifts. Strictly speaking, effects of this type do not qualify as chemical shifts as there is obviously no new bond formation involving Ar atoms, while the Au and Si peaks may be affected by their mutual phase solubility and tendency of Au to promote oxidation of Si. One should also consider that conductivity in the phase where Ar is being implanted may very well be a function of the Ar concentration. The actual implantation of Ar can also give rise to forward sputtering and Frenkel pair formation, where the resulting lattice point defects may affect the bonding signatures of the studied material. Nevertheless, this example shows that the noble character of implanted atoms does not guarantee constant binding energy of the associated core-level peaks, hence they cab not serve as a reliable BE reference.

3.3.4. Auger parameter

The method presented in this section is different from the other referencing techniques discussed in this review in that it does not involve BE scale calibration of any kind. It does, however, serve the purpose of chemical state identification, which is the ultimate goal of any XPS analyses.

With the aim of improving the accuracy of chemical-state determination, Wagner et al. advocated back in the 70s and 80s for the use of Auger transitions [105]. As a matter of fact chemical shifts for Auger lines are often greater than those of the equivalent photoelectron peaks [106]. Authors argued that due to different chemical shifts of Auger and photoelectron lines recorded from the same element, the difference between the Auger and the photoelectron kinetic energies of the most prominent lines $E_{kin}^A - E_{kin}^P$ constitutes a unique property of a given chemical state, denoted as the Auger parameter α. As the influence of surface charging tends to be the same for both Auger and photoelectron peaks, the Auger parameter is independent of the charging state of the sample, unlike either of the signals alone [107,108]. Later, to eliminate the dependency of α on the source energy as well as the possibility of negative α values, Wagner et al. introduced the modified Auger parameter α' by adding the kinetic energy of the Auger electron to the binding energy of the photoelectron [109]

$$\alpha' = E_{kin}^A + E_B^P \tag{11}$$

which can be rewritten by using Eq. (3) as

$$\alpha' = \alpha + h\nu. \tag{12}$$

The immunity of the Auger parameter from charging-induced spectral displacements may be very useful in systems where Auger transitions of significant intensity can be observed [110,111]. A disadvantage, however, is that the available data base is limited as compared to that for photoelectron lines alone [112], hence identification of the chemical state by referring to tabulated values is often not possible. A further complication is that the Auger lines often have complex envelopes and are characterized by greater linewidths (even more so for samples prone to charging), both making the resolution of multiple chemical states cumbersome, if not impossible. An additional problem arises for inhomogeneous samples, which exhibit differences either in charging state or in the chemical state as a function of depth. In such cases, different probing depths typically associated with Auger and photoelectron peaks prevent meaningful analyses. These are probably the reasons behind the relatively low popularity of this method; the overall trend in

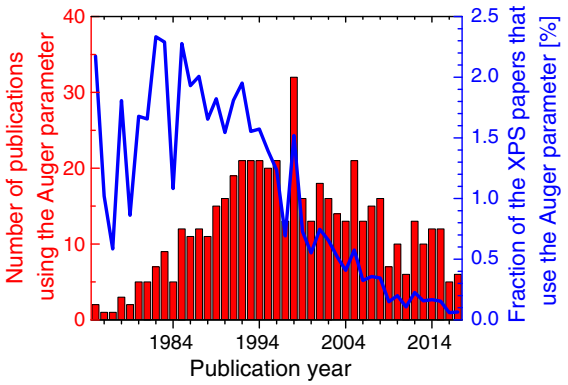

Fig. 20. Annual number of publications related to the Auger parameter (red bars) and its share in the total XPS publication volume (blue curve) since the invention of the technique. The search was performed in June 2018 with a Scopus data base and subject fields "XPS" and "Auger parameter".

the number of papers using the Auger parameter plotted in Fig. 20 indicates that the technique has shown an increasing recognition up to the mid-90s after which a clear decay is observed. Publications employing the Auger parameter technique never accounted for more than 2.5% of the total XPS annual publication volume (cf. blue curve in Fig. 20), and this number exhibits a continuous decay since 1990 to the present negligibly small value of 0.05%.

4. Referencing to the C 1s peak of AdC

It is difficult to overestimate the importance of the C 1s spectra in XPS. The C 1s core-level spectrum of a ethyl trifluoroacetate [59], better known to XPS experts as the "ESCA molecule" [62], is the most prominent example of chemical shifts. Not less important is the ability offered by the C 1s peak to distinguish a subtle difference between graphitic (sp^2-) and diamond (sp^3-hybridized) C atoms in diamond-like carbon (DLC) thin-film coatings widely used in industrial applications [113]. XPS of the C 1s peak is also a basic tool for polymer chemistry [114], and more recently in the blooming science of graphene [115–118]. Apart from these prominent examples, C 1s has made a spectacular career in BE referencing – mostly due to the fact that thin C contamination layers, in the form of so-called adventitious carbon are present on all surfaces analyzed in XPS that have been previously exposed to the atmosphere [4]. In this section, we review the method with emphasis on crucial issues like the origin of AdC and the BE of the C 1s peak from AdC. This is followed by a summary of the criticism directed towards this technique over the years. We end with a presentation of the *status quo*, which is based on an extensive literature survey.

4.1. A conventional method

The use of AdC for BE referencing is as old as XPS itself. The technique is described in the seminal book by Siegbahn et al. [4], which laid the basis for XPS applications in materials science and chemistry, and is by far the most common method for calibration of the BE scale. The common occurrence of AdC is a primary reason for the great popularity of this technique, which unlike essentially all other referencing methods summarized in Section 3.3, does not require any extra efforts in terms of sample preparation. The ISO 19318:2004 and ASTM E1523-15 guides recommend setting the C–C/C–H component of the measured C 1s spectrum of AdC at 284.6 to 285.0 eV and applying a corresponding shift to all other spectra [6,7]. It is, however, stated that: "*A significant disadvantage of this method lies in the uncertainty of the true nature of the carbon and the appropriate reference values which, as reported in the literature, have a wide range from 284.6 eV to 285.2 eV for the C 1s electrons from hydrocarbon and graphitic carbon.[…]*". Adding gravity to the situation, our literature survey revealed that to calibrate the BE scale the C–C/C–H peak of AdC is deliberately set in the BE range from 284.0 to 285.6 eV [1], which is significantly broader than that recommended by ISO and ASTM.

Both charge-referencing guides list important conditions upon which the specified BE range is valid: "*This reference energy is based on the assumption that the carbon is in the form of a hydrocarbon or graphite and that other carbon species either are not present or can be distinguished from this peak.*" [6,7], and "*With coverage of less than one monolayer of adventitious carbon, the C 1s binding energy sometimes decreases. The carbon binding energy may also shift as a consequence of ion sputtering*" [7]. It is recommended that: "… *the reference binding energy (and peak FWHM) should be determined on the user's own spectrometer for specimens with a similar carbon coverage. Ideally, this measurement should be carried out on a non-charging substrate similar in its chemical and physical properties to the material to be analyzed and covered by only a thin, uniform contamination layer (that is, of the order of a monolayer)*" [7].

Thus, there is an inherent degree of uncertainty and caution explicitly expressed in the description of the C 1s method. Moreover, it is implicitly assumed that the electrical potential in the AdC layer is the same as in the actual specimen it accumulates on, hence the fact that AdC is external to the analyzed sample is neglected. This motivates us to consider what constitutes AdC and its many possible varieties.

4.2. The origin of AdC

Adventitious carbon accompanied XPS essentially from the very beginning. In the ESCA book Siegbahn and co-workers stated: "[…] *we have found the carbon 1s line from the pump oil ideally suited for use as a calibration line. In fact, there is usually no difficulty in distinguishing this line from the rest of the spectrum since its relative intensity increases with time.*" [4]. Interestingly, this definitive and *ad hoc* assignment of AdC to diffusion pump oil was not backed up with any attempt of chemical identification, but rather based on the author's intuition. The possibility of AdC accumulating on samples during air exposure was not acknowledged at that time. Instead, the spectrometer itself was considered the main source of C contamination: another potential source, often mentioned by the Uppsala group, was O-ring grease [119]. This exclusive origin of AdC was questioned by Hnatowich et al. [92] and Dianis et al. [120]. Both groups pointed out that contamination introduced by sample handling may also contribute to the observed C 1s signal. The former group in fact went much further by pointing out that the use of substances of unknown and potentially varying composition for energy referencing is a highly questionable procedure, especially because the electrical equilibrium between adventitious carbon and specimen was not demonstrated. The possibility of carbon contamination originating from sources other than pump oil was also considered by Clark et al. [101], who suggested that the AdC may already be present on the samples prior to insertion into the spectrometer. This statement, today largely forgotten or little acknowledged, represents a major conceptual shift, as it had not previously been recognized that, in fact, AdC adsorbs on all air-exposed surfaces. In addition, the authors made a key observation that the majority of the hydrocarbon ending up on the samples in a vacuum system originates from the cap covering the Mg Kα source, which heated up during measurement leading to desorption of hydrocarbon species. Water-cooling of the cap significantly reduced the hydrocarbon buildup rate, which allowed for longer studies under continuous X-ray irradiation without the loss of signal intensity caused by attenuation in the adsorbed hydrocarbon layer. This evidence disproved diffusion pump oil as the dominant source of AdC contamination, at least in the instrument used by Clark et al.

In the early days of XPS, the high rate of hydrocarbon accumulation on the sample surface in vacuum was severely limiting signal intensities due to the short photoelectron mean free paths [32], often preventing analyses of samples that required longer spectra acquisition times. To visualize how serious a problem caused by AdC was, we compare in Fig. 21 C 1s spectra recorded from the third row transition metal (TM) carbides (HfC, TaC, and WC) by Ramqvist et al. [119] in 1969 and the corresponding spectra acquired on a state-of-the-art instrument of today [11]. For a fair comparison, all samples are in the as-received state. Apart from the evident

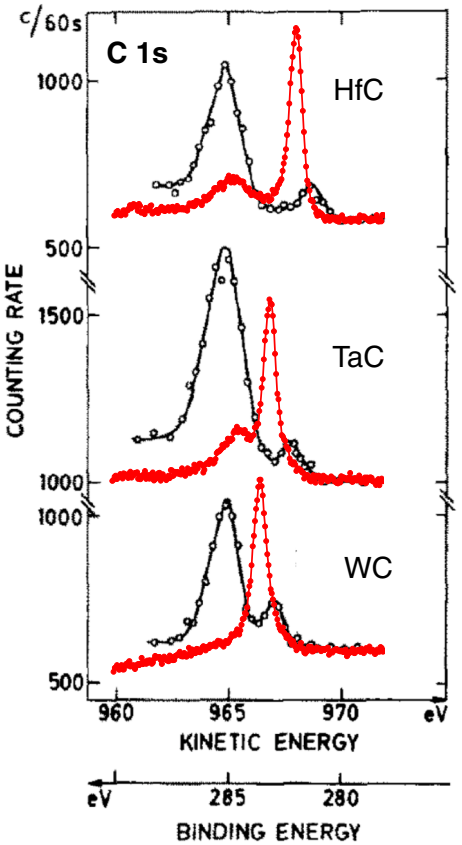

Fig. 21. Set of C 1s spectra recorded from the third-row transition metal carbides (HfC, TaC, and WC, shown as black curves) adapted from Ref. [119] plotted together with the corresponding spectra acquired on a state-of-the-art instrument of today (red curves) [Author's original work]. For a fair comparison, all samples are in the as-received state.

improvement in the energy resolution that took place over the last 50 years, evidenced by dramatically reduced FWHM of the carbide peaks, the early spectra are obscured by intense C 1s signals from the adventitious carbon that completely dominated the signal from carbide samples, making the correct BE determination of carbide lines rather difficult.

The problems associated with adventitious carbon built up on surfaces subjected to XPS analyses resulted in many papers studying the phenomenon. Brandt et al. [121] observed, while performing measurements in an instrument employing a Mg Kα source, that a one-hour acquisition time made the Au 4f and C 1s signals from a solid Au sample change only slightly while for MgO, a large decrease of the Mg 2s and O 1s peak intensities accompanied by an increase in the C 1s signal was noted. Similar results were obtained for other insulators including sodium halides, various polymers, and metal oxides which allowed the authors to conclude that AdC builds faster on insulating samples than on conductors. Two explanations were offered [121], where the first suggests that adsorbed hydrocarbons undergo pyrolyzation to carbonaceous material. Due to the higher heat conductivity of metals, their surfaces remain cooler for a longer time, which should explain the lower rate of AdC build up. The second, and more likely possibility is that difficulty to neutralize core holes on insulators makes such surfaces more chemically active resulting in higher sticking coefficient for all residual gas molecules. Hence, Brandt et al. [121] advised maintaining good vacuum and the use of low-energy electron sources. With prevailing adventitious carbon layer formation, associated problems with quantification of the XPS signals of the substrate, may be leveraged by applying a correction for signal loss due to AdC growth [122] or by using dedicated *in situ* techniques for removing hydrocarbons prior to XPS analyzes [123].

Rather amazingly, given the enormous popularity of BE referencing with AdC layers, the C 1s spectra itself is almost never reported. This situation prevents identification of the involved chemical species. There is only one study by Barr et al. that explicitly addresses the nature of AdC [124], and offers very relevant and original comments. First, authors pointed out that AdC species are typically not chemically reacting with the underlying substrates, hence the process of AdC deposition can be classified as physisorption. By comparing the recorded AdC C 1s spectra to the reference measurements performed on graphitic materials and hydrocarbon polymers such as polyethylene, they came to the conclusion that AdC consists predominantly of polymeric hydrocarbon species (C—C/C—H), together with a minor component (10–30%) due to carbon oxides containing C—O—C and O—C═O groups. The presence of graphitic units was excluded based on the lack of characteristic $\pi \rightarrow \pi$ transition in the region between 290 and 292 eV [125].

To summarize this section, it is worth emphasizing that the construction of the spectrometer including possible cooling systems, distance between the sample and the X-ray source, and the type of pumping system used, could directly impact on the type of accumulating AdC. Thus, it has to be recognized that the nature of carbon contamination is very likely a function of the technology development (e.g., introduction of oil-free pumps and/or overall transfer to UHV), which adds another dimension to this already complex subject. Nevertheless, it is quite embarrassing to the field that apart from the single study by Barr et al. which appeared in 1995, no other groups have addressed the issue of AdC chemical composition, despite the fact that thousands of publications have used the C 1s peak of AdC for BE referencing. We elaborate more on the issue of AdC chemical composition in Section 5.1 below.

4.3. Binding energy of the C 1s peak from AdC

Perhaps the largest confusion related to the use of the C 1s peak of AdC as the BE reference is caused by the lack of a unique BE value associated with this line. Evolution of the range of reported C 1s BEs of AdC over the years is plotted in Fig. 22, which is based on our literature survey. Due to the overwhelming number of XPS papers the data set used to create this plot is certainly not complete, hence the BE spread shown is likely underestimated. Nevertheless, even the limited data set shown in Fig. 22 indicates a disturbing trend over last 50 years. The originally introduced value of 285.0 eV used by the Uppsala group lasted for only a few years. Soon after,

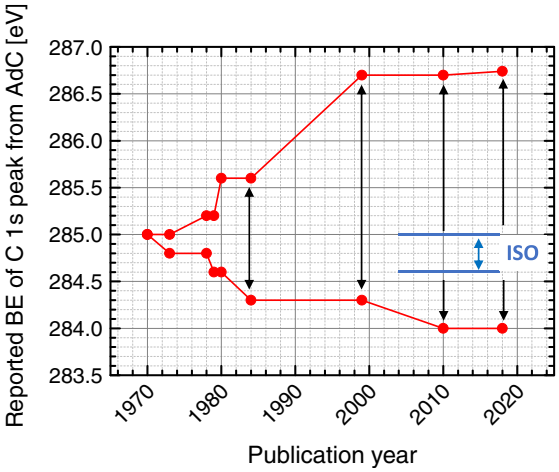

Fig. 22. Evolution of the reported C 1s peak position of AdC since the introduction of the referencing technique, except for extreme values. The values recommended in ISO 19318:2004 and ASTM E1523-15 guides are also indicated [6,7].

other laboratories reported certain deviations, which were all, however, within the error bars of what instruments available at that time could deliver. In the latest review on this subject published in 1982, Swift summarized that C1s has been set in the range from 284.6 to 285.2 eV [126]. This means that the uncertainty as to the C 1s peak position has increased 2.6 times during the last 3 decades. A contributing factor may be the strong increase in the popularity of XPS, reflected by a continued increase in the number of published papers (see Fig. 1), which along with obvious benefits brings also a risk for improper applications of the technique. Correspondingly, user communities settled around certain C 1s BE values, as can be seen from the here-cited references (see Section 4.5).

Interestingly, although AdC was used for calibration by the Uppsala group, no particular BE value was assigned to the C 1s peak which was presented, as all other spectra, as a function of kinetic energy. Historically, the first published value for the BE of the C 1s peak, although not in the context of BE referencing, was 283.8 eV obtained by Hagström et al. [127], from amorphous C layers prepared by sooting the Al backing in a candle flame. The same value is also given in the review paper by Bearden and Burr [128]. In Ref. [119], the C 1s spectra from transition metal carbide samples were aligned to the C 1s peak of adventitious carbon set at 285.0 eV. It was however, not clarified how this particular value was determined.

The first reported measurement of the C 1s BE from adventitious carbon was done by Malmsten et al. [129] who analyzed Pm specimens with Al, Cu, and Mo Kα X-rays using absolute calibration techniques. They obtained 285.0 ± 0.4 eV. About the same time, Gelius et al. performed extensive XPS studies of carbon-containing compounds to determine the C 1s BE of C atoms in various chemical environments [130], in which all core-level BEs were given to the reference hydrocarbon value of 285.0 eV. Hence, in these early days of XPS, the notion of a constant BE of C 1s peak from adventitious carbon seemed well proven leading to the common use of the related BE calibration method. The myth of the C 1s peak at 285.0 eV was born.

In many early works, the binding energy of C 1s electrons from hydrocarbons was believed to be constant irrespective of whether the species were adsorbates or an inherent part of the sample. This belief was reflected in the study by Lindberg et al. [131] who wrote "*The spectra were calibrated by reference to the C ls line from the sample. When carbon was part of the molecule it contributed the main part of the spectrum. When powder samples were studied a contribution from the hydrocarbon layer, which formed on the sample surface was also obtained*". This lack of clear distinction between the origin of hydrocarbons started a prevailing confusion with the BE referencing relying on the C 1s peak.

The first small deviations from the 285.0 eV value, e.g., 284.8 eV published by Schön et al. in 1973 [132], were all well within the experimental error of ±0.4 eV. In a rather extensive test of major referencing techniques available at that time, Dianis et al.[120] concluded that the C 1s peak of AdC accumulated on MoO_3 and Pt surfaces does not appear at 285.0 eV. One of the earliest values for the C 1s BE of AdC in the context of referencing which deviated significantly from 285.0 eV was 284.6 eV reported by Wagner et al. for residual hydrocarbon accumulated on abraded copper and gold [109]. In 1980, Bird et al. analyzed the C 1s peak for AdC accumulating on noble metals as well as on oxidized surfaces [133]. They concluded that, in the first group, the C 1s peak was present at 284.7 eV, while the second group exhibited significantly higher values extending to 285. 6 eV. This result put in doubt the supposed constancy of the C 1s BE and resulted in serious concerns for the use of this line for BE referencing, especially that it is the category of insulating samples (oxidized surfaces), where the C 1s BE referencing is needed due to problems with charging. In accordance, the same authors reported that the repeatability of the results was worse than for metallic substrates [133].

In the years leading into the 90s, the uncertainties related to the use of the C 1s peak of AdC for correcting the BE scale accumulated and numerous recent examples indicate that the problem remains unresolved [134,135]. Crist in his "Handbooks of Monochromatic XPS Spectra" published in 1999 summarized C 1s BEs for a range of samples with native oxides as well as after *in situ* Ar^+-ion etch [136]. He found that the position of the C 1s peak varies from 284.5 eV for Re to 286.7 eV for Y on the "as received" samples. For ion-etched specimens left in the UHV system for more than 14 h to allow the surfaces to accumulate a new layer of AdC contamination that originated from the residual gases, the C 1s peak varied from 284.2 eV for Pd and Te to 286.7 eV for Y. Hence, independently of the surface state, variation in the position of the C 1s peak which is supposed to serve the purpose of BE reference, exceeded 2 eV, which is significantly larger than typical chemical shifts. Again, similar to his predecessors, Crist warned for possible consequences in XPS data analysis: "*The various ranges in the hydrocarbon C 1s BE reported in this section are large enough that the XPS analyst can easily make a wrong assignment of chemical state to a chemical group or species that is part of a non-conductive material. The numerical data-banks that exist now most likely suffer from each of these fundamental problems and limitations*". Unfortunately, these alerts did not make the intended impact on the common practice, as revealed by our literature survey discussed above.

Detailed investigations performed in our laboratory for an extensive set of samples revealed that the BE of C 1s peak of AdC can vary by as much as 2.6 eV [137,138]. More importantly, we established that the BE of C 1s peak E_B^F is steered by the sample work function ϕ_{SA} in such a way that the sum $E_B^F + \phi_{SA}$ remains constant. This result implies that, contrary to the *ad hoc* assumption made back in the 60s, there is no common Fermi level at the interface between an AdC layer and the actual sample. Instead, the energy levels of the AdC layer align to the vacuum level, which is the natural reference level for gas-phase photoelectron spectroscopy. Such a situation is typically encountered for weakly-interacting systems, where charge transfer across the interface does not takes place. Hence, the conventional BE referencing method relying on the C 1s peak is not reliable, which remains in distinct contrast with its enormous popularity. These results are discussed in more detail in Section 5, before a remedy for BE referencing based on AdC for conducting samples is proposed.

4.4. Criticism

After the proposal by Siegbahn et al. [4] to use the C 1s peak of adventitious carbon as a charge reference, numerous studies have followed their advice for a number of years [129,131,139,140]. The authors of the present critical review also admit to having

published studies with insufficiently documented choice of the BE reference. The first criticism to the C 1s BE referencing method was raised in 1970 by Nordberg et al. [141] who suggested that the C 1s BE can be affected by the polarization of the thin layer and concluded that mixing two samples together to measure relative chemical shifts or mixing a sample with a reference such as graphite may give better results.

More serious doubts about the referencing of XPS spectra to the C 1s signal of AdC were expressed by Hnatowich et al. [92], who questioned the origin and chemical composition of the AdC layer. Other authors pointed out that such thin overlayers not necessarily need to be in electrical equilibrium with the specimen and, hence, their use for BE scale calibration is a precarious procedure. Correspondingly, Dianis et al. [120] concluded that the C 1s BE for AdC is highly uncertain and cannot be used for reference purposes. They also pointed out that C can react on catalytically active surfaces which adds to confusion as: "… *the interaction of the vapor with the active surface might shift the binding energy of the carbon. Therefore, one cannot be certain that one is looking at the same type of carbon every time.*"

As the result of criticism that followed in the early 70s in the review of XPS calibration methods, Johansson et al. wrote that "*Although different experiments have given the same C 1s binding energy, there have been objections to this procedure, since the contamination has not been fully identified*" [91].

Objections to the method did not stop at that. In 1976 the claim of constant BE of the C 1s peak was questioned by Kinoshita et al. [142] who studied adventitious carbon adsorbed on an *in situ* deposited Au surface and concluded that "[…] *the energy of the C 1s peak of contamination carbon adsorbed on metal surface can vary depending on the amount of adsorption, consequently its use as the reference of energy calibration seems to be dubious in some cases, especially for metallic samples*." Later it also became clear that it varies with the thickness of the hydrocarbon layer [143].

In the review of literature specifically devoted to the C 1s referencing method published in 1982, Swift indicated some doubts already in the title "*Adventitious Carbon-The Panacea for Energy Referencing?*", and concluded with more explicit concerns: "*although the use of C 1s electrons from adventitious carbon layers is often a convenient method of energy referencing, interpretation of binding energy data obtained should be treated with caution*" [126]. Clearly, this did not prevent the enormous popularity of the C 1s referencing and only occasionally related problems were reported. For example, referencing to the C 1s of AdC led to inconsistent results in studies of oxide growth on Al-Si alloys [144]. The authors concluded that specific experimental conditions (heat treatment, presence of the substrate) caused catalytic cracking and oxidation of the AdC layer. Similar conclusions as to the limited applicability of the C 1s BE referencing were drawn by Peplinski et al. who used XPS to study Cu-Zn-Al oxide catalysts [145]. To resolve the problem, referencing to the native O 1s signal was used instead. In another study, Gross et al. showed that the Au 4f signal from colloidal gold particles deliberately deposited on amorphous SiO_2 provides more reliable BE reference than C 1s [146]. A more recent example is the work of Jacquemin et al. [135], who showed that the BE of adventitious carbon accumulating on Pd/SiO_2-Al_2O_3 catalysts samples depends on the Si/Al ratios. The issue of correct referencing of XPS spectra thus remains largely unresolved.

One of the top-cited papers employing the XPS technique to study iron oxides reports on problems associated with the C 1s referencing method [147]. The authors found the C 1s peak of AdC to be shifting between 284.6 and 285.3 eV depending on the sample and concluded that the C 1s peak is not a suitable reference for unknown reasons. In a similar manner, Biesinger et al. admit in their highly-cited paper devoted to XPS analysis of the first row transition metals, oxides, and hydroxides that "*Experience with numerous conducting samples and a routinely calibrated instrument has shown that the non-charge corrected C 1s signal generally ranges from 284.7 eV to as high as 285.2 eV*" [148].

Doubts with the AdC referencing method are also reflected in the description of this technique provided in the ISO and ASTM reference guides for charge control and correction (see Section 4.1) [6,7]. The main disadvantage mentioned in both documents is the wide range of reported C 1s BE values and the uncertainty as to the true nature of the AdC species.

In view of the XPS publications from over 50 years, it is highly disturbing that the C 1s method has remained so popular. While it can be to some extent understood that the poor energy resolution in the early XPS days (see e.g., data by Ramqvist et al. included in Fig. 21) potentially prevented realization that the BE of AdC C 1s peak is not constant, it is beyond comprehension why this fact, once reported, did not disprove the applicability of this approach among peers and journal editors alike. A poor explanation for this *status quo* is that no good alternatives exist. This, however, should not be used as an excuse to continue with a method that is highly questionable. We hope it stops at this juncture.

4.5. Status Quo Ante

Our survey of the XPS literature covering the last 20 years reveals that the majority of XPS-related papers used C 1s of AdC as the BE reference, while, *as alarmingly, the remaining papers lack information about any referencing method used at all.* This situation is disturbing since doubts to the C 1s referencing have been pointed out as early as 1970. The origin and the chemical nature of AdC are rarely considered, and essentially never reported in connection with use of the C 1s peak as the reference. In addition, it is unclear what a "correct" BE of the C 1s peak would be.

Perhaps even more worrying is the fact that among papers that use the C 1s referencing, the applied procedure differs greatly between labs to an extent that calls into question any meaningful comparison of the obtained results. This is illustrated in Table 1, where selected quotations from experimental sections of XPS papers are presented [149–165], including the relevant passage from the article written by the authors of this review back in 2012 [149]. There are three apparent inconsistencies, which are color-coded to facilitate comparison: (green) contamination species used for referencing, (red) how the method is applied, and (blue) which BE is used for the C 1s peak.

First of all, that there is no apparent consensus as to the nature of the carbon species that are used for referencing. Apart from the

Table 1
Selection of quotations from experimental sections of XPS papers revealing the apparent inconsistencies, which are color-coded to facilitate comparison: (green) contamination species used for referencing, (red) how the method is applied, and (blue) which BE is used for the C 1s peak.

Description of how the adventitious carbon was used for BE calibration	Ref.
" The C(1s) core level signal at **284.5** eV, corresponding to **aliphatic carbon from the surface contamination layer**, was used for the binding energy (BE) scale **calibration**. "	A. Khatibi et al. 2012 [149]
"the binding energy scale was **normalized** to the **C1s adventitious carbon peak** at **285** eV."	R. França et al. 2014 [151]
" The XPS binding energy (BE) values were **charge-corrected** to that of **uncharged adventitious carbon** at **285.0** eV."	M. Chen et al. 2000 [152]
" The **position of the C1s peak** was **taken as a standard** (binding energy is **285.0** eV)."	W.J. Gammon et al. 2003 [153]
"To **compensate** for sample charging, all binding energies were **referenced** to the **low binding energy component of the C(1s) spectrum**, which was assigned a value of **284.6** eV."	B. Liu et al. 2005 [154]
" All the spectra were **calibrated** with **C1s**, which was **assumed** to have the binding energy of **284.6** eV."	R.J.J. Jansen et al. 1995 [160]
"All binding energies (BEs) were **corrected** for charging of the sample by **calibration** on the **graphitic carbon C1s peak** at BE **284.50** e V."	T. Yamashita et al. 2008 [147]
"The binding energy scale was **set by fixing** the **C 1s component due to carbon only bound to carbon and hydrogen [C-(C,H)]** at **284.8** eV."	J. Landoulsi et al. 2016 [155]
"The position of the core level spectra on the binding energy scale was **determined** before sputtering process relative to the **lines of carbon C 1s** (**285.6** eV)"	B. Psiuk et al. 2016 [156]
" **The C–C/C–H component of the C1s peak** was **adjusted** to **285.0** eV."	B. Finke et al. 2011 [157]
"The spectra were **calibrated** with **C 1s**, which exhibits the binding energy of **284.0** eV."	S-H. Lee et al. 2010 [158]
"The binding energies of the photoelectron lines of the sample as received are **charge-referenced** to **the C 1s line of adventitious hydrocarbon** at **284.8** eV."	D. Schild et al. 2010 [159]
" All XPS spectra were **calibrated** according to **universal C 1s** binding energy at **284.8** eV"	A. Kohandehghan et al. 2013 [164]
" The binding energies were **referenced** to **neutral adventitious C 1s peak** at **285.0** eV"	M.J. Chuang et al. 2010 [163]
" In order to take into account the charging effect on the measured binding energies (BEs), the spectra were **calibrated** using the C1s line (BE=**284.8** eV, **C-C (CH)n bonding) of the adsorbed hydrocarbon** on the sample surface."	A. Marin et al. 2017 [162]
" spectra were further **corrected** with reference to **adventitious aliphatic carbon** at **285.0** eV,"	F. Spadaro et al. 2017 [161]
" To correct the sample charging during XPS, **the peak maximum for the C(1s) feature** was **set** at binding energy **285.0** eV."	S. Gaddam et al. 2015 [165]
"The XPS binding energy (BE) values were **charge-corrected** to that of **uncharged adventitious carbon** at **285.0** eV."	R. França et al. 2014 [151]

general term “adventitious carbon”, some groups are more specific and call the contamination graphitic or aliphatic carbon [147,161], while others write about hydrocarbons [155,157,162]. These statements are, however, not grounded by means of proper chemical analysis of surface species, but rather assumptions based on earlier literature claims by others. The task of chemical identification is certainly not easy due to the small chemical shift between sp^2 and sp^3-bonded carbon [166,167], nevertheless this effort is essentially never undertaken. The C 1s spectra are published only if they contain contributions from the primary material to be analyzed. Hence, in general, *referencing is performed using the C 1s signal from an unknown compound*, indicating that nothing has changed since the original criticism by Johansson et al. in 1973 [91]. There is also a large group of authors who do not name the carbon contamination at all. Instead, terms “C 1s peak” or “C 1s spectrum” are used quite interchangeably, which is not correct as

there are typically many components present in the AdC spectrum. No less disturbing are numerous adjectives like “uncharged AdC” [152] or “neutral AdC” [163] which are completely unjustified, as the charging state of the sample cannot be known *a priori*.

Secondly, based on the summary presented in Table 1, there is no common agreement upon how the C 1s peak of AdC is actually employed (see the red-marked text). Terms like “calibration”, “referencing” and “correcting” are used quite frequently in the context of the linear rigid shift applied to the binding energy scale after the measurement, in order to account for the surface charging potential. In some cases, however, there is a serious doubt as to what was actually done. For example, the BE can be “*normalized* to the C 1s” [151], or “*set by fixing* the C 1s component” [155]. Similarly confusing are also C 1s peak statements such as “taken as a standard” [153], “adjusted” [157], or “set” [165]. Presumably, all authors mean the same procedure, nevertheless improper or inadequate description further undermines the already ill-defined method. In general, terms like “calibration” and “referencing” have been used interchangeably while discussing the C 1s method based on AdC since the early days. Strictly speaking, the former should only be applied when dealing with a procedure employing well-defined standard samples such as sputter-cleaned Au, Ag, or Cu foils to measure characteristic lines and, based on comparison to recommended values [5], to adjust the instrument parameters resulting in correct representation of binding energies (see Section 3.2). In contrast, “referencing” or “charge referencing” means that an unknown sample is measured and a rigid shift is applied to all acquired spectra with the magnitude determined by comparison of recorded peak positions to literature values. Hence, the aim of “calibration” is to confirm that a spectrometer works correctly and such procedure should be performed on regular bases, while “referencing” serves the purpose of chemical-state identification of the unknown samples.

The third, and perhaps most striking issue, is the large spread in the BE values assigned to the C 1s peak (see blue-coded text in Table 1). Among the examples listed in the table, the C 1s peak is set anywhere between 284.0 and 285.6 eV (here we excluded the two extreme values of 283.0 (Ref. [168]) and unthinkable 298.8 eV (Ref. [169]), which appeared in the literature survey). Hence, the initial confusion as to the correct BE of the C 1s peak of AdC that was triggered back in the early days of XPS, as described in the previous section, has not only persisted throughout all these years, but developed to the point which puts in question the whole method. The trend is definitely negative: uncertainty as to the BE of the C 1s of AdC BE has grown significantly since 1982, when the last review was published [126], as indicated in Fig. 22. This serious inconsistency contradicts the notion of a BE reference, which per definition should be based on one unique value (as was originally intended in Ref. [4]). The arbitrary character of the method easily accounts for the large spread of reported BE values for the same chemical species (see examples above).

In addition, numerous papers use referencing to the C 1s signal of AdC although they are dealing with materials that are well-conducting, which calls for more reliable methods like referring to metal peaks or to the FL cut-off.

5. Critique: C 1s referencing revisited

Faced by ambiguities of the BE referencing based on the C 1s peak of AdC outlined in the previous section, we set out to test the basic assumptions behind this method by performing consistent studies involving a wide range of metal, nitride, carbide, boride, oxide, and oxynitride thin film samples [137,138]. Measurements were conducted in the same instrument under similar experimental conditions on samples that were exposed to the atmosphere for time periods ranging from just a few minutes to several years.

Adhering to the virtue of reporting the employed analysis conditions such that others may repeat or challenge the study, we state the experimental details here. An Axis Ultra DLD instrument from Kratos Analytical with a base pressure during operation better than 1.1×10^{-9} Torr (1.5×10^{-7} Pa) achieved by a combination of turbomolecular and ion pumps, was used to acquire core-level XPS spectra from samples in the as-received state, unless otherwise stated. Residual gas analysis revealed that the main background gases were: H_2O (46%), CO_2 (30%), and CO/N_2 (24%). The excitation source was monochromatized Al Kα radiation ($h\nu = 1486.60$ eV) from the water-cooled anode operated at 150 W. Work function ϕ_{SA} measurements by ultraviolet photoelectron spectroscopy (UPS) were performed in the same instrument with unmonochromatized He I radiation ($h\nu = 21.22$ eV), immediately after XPS analyses, employing the standard procedure in which ϕ_{SA} is assessed from the secondary-electron cutoff energy in the He I UPS spectra [170,171], with an accuracy of ±0.05 eV. The calibration of the binding energy scale was confirmed by examining sputter-cleaned Au, Ag, and Cu samples according to the recommended ISO standards for monochromatic Al Kα sources that place Au $4f_{7/2}$, Ag $3d_{5/2}$, and Cu $2p_{3/2}$ peaks at 83.96, 368.21, and 932.62 eV, respectively [172,5]. The charge neutralizer was not used in any of the reported experiments. The results from our experiments are presented in the following sections.

5.1. Expressions of AdC

The Merriam-Webster dictionary defines “adventitious” as: “*(1) coming from another source and not inherent or innate, or (2) arising or occurring sporadically or in other than the usual location.*” That brings us to the problem at hand. As revealed in Section 4, the C 1s peak of adventitious carbon has been widely adopted for charge referencing despite the fact that the chemical identity of the carbon contamination is not routinely known or studied. The general practice is to assign – without supporting evidence – the main peak of the C 1s spectra recorded from samples in the as-received state to hydrocarbons or aliphatic carbon. As a consequence, the majority of published XPS spectra are aligned to a signal originating from an unknown species. Actually, the situation is much worse than that, in that during the 50-years-long XPS history only one paper [124] specifically addressed the nature of adventitious carbon.

Below, we review the findings from our recent experiments specifically intended to study the origin of AdC as well as its chemical nature as a function of the environment (laboratory air, high- or ultra-high vacuum), the substrate type, and the exposure time (varying from minutes to years).

As summarized in Section 4.2, during the early years of the technique AdC was believed to originate from the vacuum system

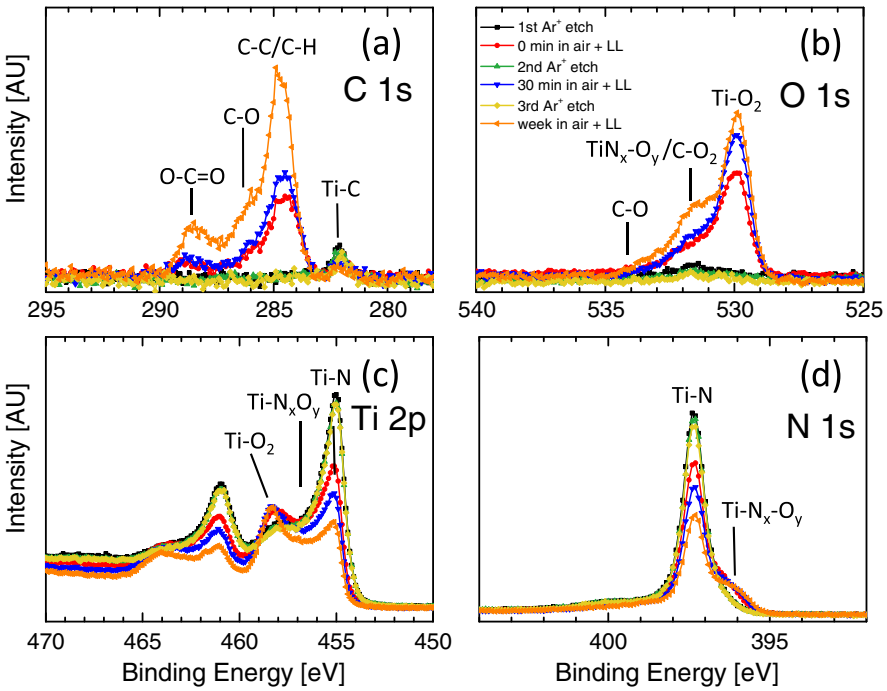

Fig. 23. C 1s, O 1s, Ti 2p, and N 1s core-level spectra recorded from a TiN thin film sample after: ("0 min in air + LL") 1-h-long pumping from the atmosphere pressure in the fast-entry load-lock chamber of the XPS instrument, ("30 min in air + LL") the 30-min-long exposure to the laboratory air (23 °C, 40% RH) followed by the pumping step in the load lock chamber, and ("week in air + LL") the-1-week-long air exposure followed by the pumping step in the load lock chamber [Author's original work]. The reference spectra after each Ar^+ sputter etch step used to reset the sample history are also shown.

itself, while other possible sources like sample handling or air exposure were mentioned at a later stage. In order to address the controversy regarding the origin of AdC, we performed a series of experiments while carefully tracking the sample history. In Fig. 23(a)–(d) are shown C 1s, O 1s, Ti 2p, and N 1s spectra recorded from a TiN sample after: (a) one-hour-long pumping from atmospheric pressure in the fast-entry load-lock chamber of the XPS instrument during which the high vacuum (HV) conditions were reached (low 10^{-7} mbar range) with the help of a pumping line consisting of diaphragm and turbomolecular pumps (denoted as "LL" in the legend of Fig. 23(b)), (b) 30-min-long exposure to the laboratory air (23 °C, 40% RH) followed by the pumping step as in (a), and (c) one-week-long air exposure followed by the pumping step as in (a). Prior to each exposure, the sample history was reset by means of Ar^+ sputter etching consisting of two steps: 3 min. with 4 keV Ar^+ ions after which the incident ion energy was reduced to 0.5 keV for another 10 min. to minimize the extent of damage in the surface region (see Section 2.7.1). The core-level spectra after each cleaning step are included in Fig. 23 for reference. To exclude the potential effect of sample handling, which was mentioned as one possible reason for AdC build up [92,120], all specimens were left in the sample holders during air exposures such that nothing except the ambient could come in contact with the analyzed surface.

The C 1s spectra in Fig. 23(a) indicate that both types of exposure, the one in the fast-entry load lock chamber as well as storage in air, contribute to AdC build up on the TiN surface: all AdC components including C—C/C—H (285.0 eV), C—O (286.5 eV), and O═C—O (288.5 eV) are observed in both cases. The pronounced difference in the C 1s peak intensity between one week and 30 min ambient exposures indicates that AdC accumulation in air does not saturate on this time scale. The small peak at around 282.0 eV is due to TiC known to form as a result of Ar^+ ion etch [173]. The process of AdC adsorption is accompanied by oxidation of the TiN surface, as evidenced by the evolution of Ti 2p, N 1s, and O 1s spectra (Fig. 23(b)–(d)) [174], which show oxide and oxynitride components that become dominant after longer air-exposures. Based on these results, one may conclude that AdC layers present on samples stored in air for longer periods of time (>1 week) originate mostly from the air exposure. The contribution of species accumulated inside the vacuum system is minor, for the typical pumping down routines implying the HV exposure times of the order of one hour. Should the sample be exposed to HV environment for longer periods of time (e.g., over-night pumping), one has to take into account also that AdC accumulates during that time, and that it may possess a different chemical nature. We consider the case of prolonged HV exposures below.

To address the effect of the XPS measurement itself (the combined effect of exposure to X-rays and UHV environment), additional tests during spectra acquisition were performed on the TiN specimen previously exposed to air for a period of one month to ensure significant thickness of the adsorbed AdC layer. C 1s, O 1s, Ti 2p, and N 1s core-level spectra from the TiN sample were repeatedly recorded over a time period of nearly 3 h. The time for each acquisition step consisting of three scans of all core-level peaks was 10 min. Results shown in Fig. 24 reveal a slight drop in the C 1s intensity with time which is accompanied by an increase in the Ti 2p and N 1s signals, while O 1s remains constant. This evolution indicates that a small fraction of the AdC species desorbs from the

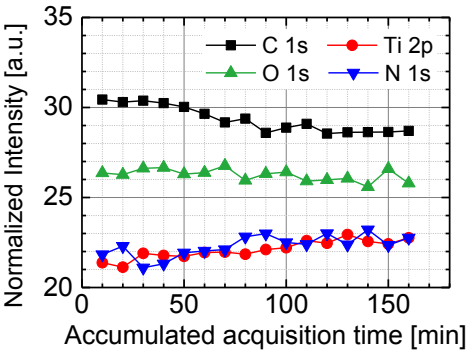

Fig. 24. Evolution of normalized C 1s, O 1s, Ti 2p, and N 1s peak intensities recorded from several-months-old TiN specimen as a function of acquisition time. Each data point is an average of three sweeps. Trends reflect a combined effect of exposure to X-rays and ultra-high vacuum environment. [Author's original work]

oxidized TiN surface upon prolonged acquisition, which may be caused by sample heating due to X-ray exposure. Hence, the trend is rather opposite to that observed in the early days of XPS where carbon contamination building up with time was a serious concern (see Section 4.2). The implications for our analyses are straightforward: AdC detected at the surface is determined by the sample history prior to the XPS measurement itself, from synthesis, through storage in air to HV exposure during the pump-down procedure. On top of these unavoidable factors comes also the potential contribution of sample handling where the surfaces to be analyzed come in physical contact with other objects (e.g., storage/transport sample boxes or packing material).

After concluding that both air and HV exposures result in the AdC build up, we turn attention to the nature of the chemical species that adsorb in various environments. For completeness, we also include prolonged exposure to UHV (unlike in the experiment described above, X-ray irradiation is off). Fig. 25 shows three sets of C 1s, O 1s, N 1s, and F 1s spectra recorded from native Au surfaces after prolonged (1 day) exposures to (i) ambient air (23 °C, 40% RH), (ii) high vacuum (low 10^{-7} mbar range), and (iii) UHV (mid 10^{-10} mbar range) conditions [175]. To facilitate comparison, all spectra are recorded from one sample that was sputter-cleaned in between XPS measurements to reset history. The results reveal distinctly different chemical natures of the carbon contamination layer accumulating on the Au surface. Air-exposure results in a strong C−C/C−H peak and an enhanced intensity of the higher-BE components in the C 1s spectra, assigned to C−O and O−C═O bonds, likely due to CO and CO_2 adsorption. Detailed peak modelling shown in Fig. 26 for the air-exposed Au sample, employing a Shirley type background [45] and Voigt functions, reveals that a

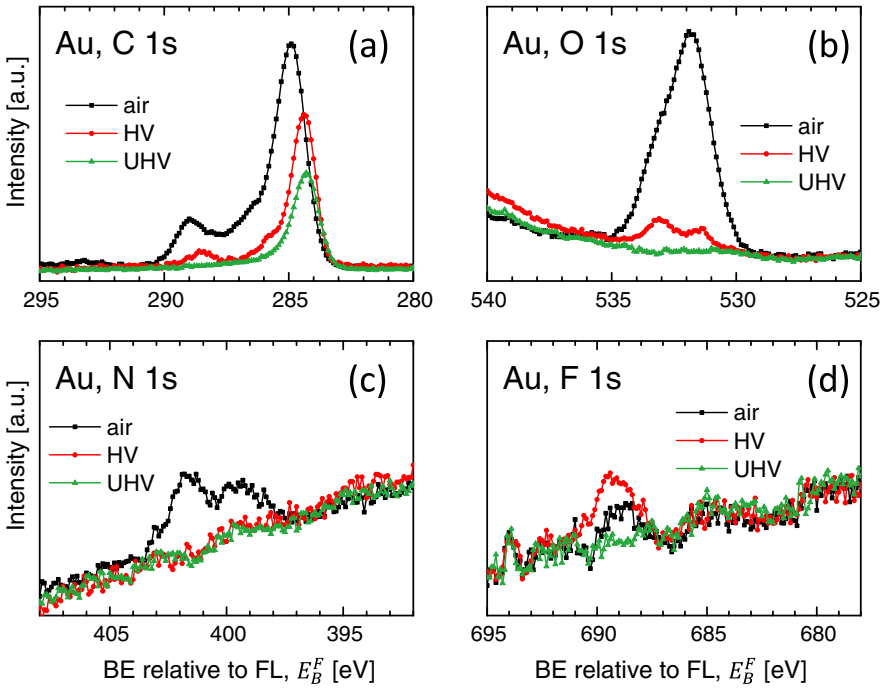

Fig. 25. Three sets of C 1s, O 1s, N 1s, and F 1s spectra recorded from native Au surfaces after one-day-long exposures to (i) ambient air (23 °C, 40% RH), (ii) high vacuum (low 10^{-7} mbar range), and (iii) ultra-high vacuum (UHV, mid 10^{-10} mbar range) conditions. [Author's original work.]

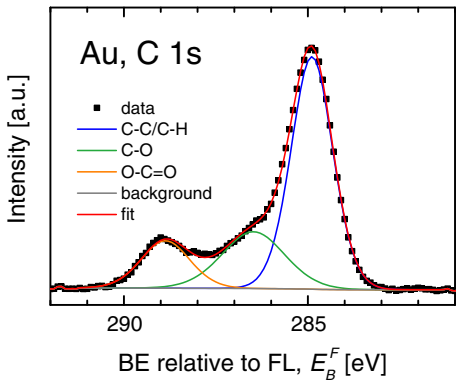

Fig. 26. XPS peak model of the C 1s spectrum acquired from an Au specimen exposed to ambient air for several months. [Author's original work.]

satisfactory fit can be obtained with these three components. This result is consistent with an intense multi-component O 1s peak (cf. Fig. 25(b)). In addition, some N is also present at the surface (see N 1s spectra in Fig. 25(c)), hence carbo-nitride formation cannot be excluded.

In contrast, exposure to HV shows significantly reduced CO and CO_2 components in the corresponding C 1s spectrum, consistent with the observed lowering of the O 1s signal intensity, as compared to the air exposure. The F 1s spectrum (see Fig. 25(d)) shows an increased intensity, likely indicating that carbon fluorides are forming on the sample surface.

In the case of the Au surface exposed to residual gases in the UHV chamber, the signal due to carbon oxides is minimized and the C 1s spectrum indicates only a C−C/C−H peak with no N, F or O contaminants, within XPS detection limits. Hence, in contrast to the conditions encountered during the measurements discussed above (see Fig. 24) where sample heating due to X-ray exposure leads to a small loss of the AdC signal intensity, prolonged exposure to UHV clearly contributes to the buildup of carbon contamination and, as such, ought to be included in the determination of the chemical nature of AdC.

One can also notice that the BE of the C 1s peak due to C−C/C−H depends on the environment the Au sample has been exposed to. This effect is treated in more detail in Section 5.2.

From the results shown in Figs. 23–26 and the discussion above, we conclude that the type of environment the sample has been exposed to prior to XPS measurement, i.e., the sample history, determines what type of species are present on the surface. Because of this, the first prerequisite for meaningful BE referencing employing the C 1s peak is that the chemical identity of AdC should be assessed. Hence, all related core-level signals have to be acquired and analyzed, taking into account also the cross-peak correlations. The latter should be considered in two steps (cf. Section 2.6). First, the requirement of *qualitative self-consistency* implies that in the constructed peak model of the compound with the chemical formula A_mB_n, for the component peak *A1* in the spectrum of element *A* there is a corresponding peak *B1* in the core-level signal of element *B*. Secondly, *quantitative self-consistency* requires that the elemental concentrations extracted based upon the *A1* and *B1* peak areas (assuming sample homogeneity within the probed volume) correspond to the compound stoichiometry *m/n* [13]. Only this type of careful analysis gives an opportunity to identify the chemical nature of the AdC layer, which is a crucial part of meaningful BE referencing.

Another experiment designed to resolve further details of AdC adsorption, complementary to the ones described above, involves exposure of various types of surfaces to the same environment. Fig. 27(a) and (b) contain C 1s and O 1s spectra recorded from Ti, Mn, Mo, Y, and Zr surfaces exposed to laboratory air for one day [175]. These are the most representative cases, selected from a much wider set to illustrate observed differences. To facilitate comparison, all spectra are referenced to the vacuum level (instead of the commonly used Fermi level), for reasons that are treated in Section 5.2. C 1s spectra are normalized to the intensity of the lowest BE peak, while O 1s spectra are normalized to the intensities of corresponding C 1s peaks. The results obtained from Au substrates exposed to UHV are added as a reference to show that lack of O results in the C 1s spectrum which exhibits only hydrocarbon peak.

Our results reveal that carbon is present in several chemical states on every surface analyzed, as evident from the multipeak nature of both C 1s and O 1s spectra. More importantly, the appearance of both core-level signals differs greatly between the substrates, revealing that the chemical nature of adsorbing AdC to a large extent depends on the type of substrate. There are four clearly-defined contributions in the C 1s spectra assigned, in the order of increasing BE, to C−C/C−H, C−O, O−C═O, and C bonded to three O atoms [176]. The shifts relative to the hydrocarbon peak are 1.51, 3.83, and 4.85 eV for C−O, O−C═O, and CO_3 components, respectively. The observed variations in the relative peak intensities between spectra recorded from AdC depositing on various substrates, show spectacular changes in the concentrations of carbonaceous species [175]. For example, in the case of the Mo sample only C−C/C−H and C−O species are present, with a relatively high population of the latter ones.

In contrast, no C−O component is detected in the C 1s spectrum obtained from AdC adsorbed on the Y surface, in which case the carbon contamination layer is entirely composed of C−C/C−H, O−C═O, and CO_3 fragments. Three types of carbon species are present for the air-exposed Ti sample: C−C/C−H, C−O, and O−C═O, while Mn is the only surface on which all four carbonaceous compounds are found. Also spectacular is the appearance of the C 1s spectra of AdC detected on the Zr surface, which, in contrast to all other spectra in Fig. 27(a), is dominated by the intense O−C═O peak.

All changes in the C 1s spectra are consistent with corresponding evolution of the O 1s signals (see Fig. 27(b)). However, due to

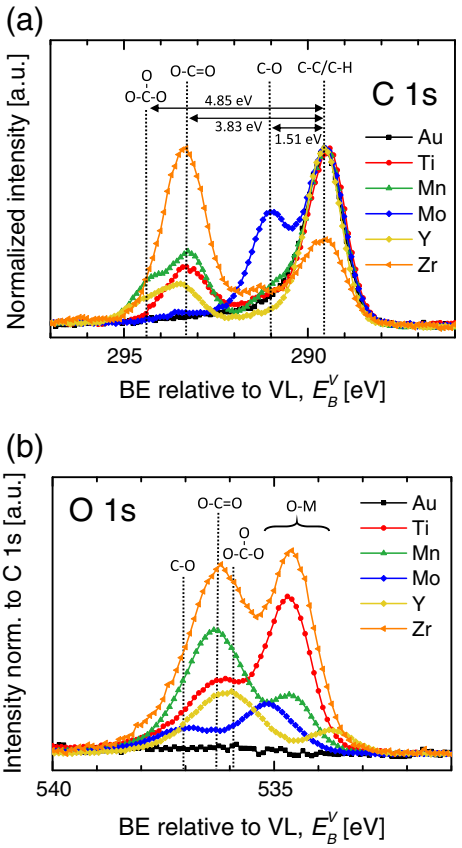

Fig. 27. (a) C 1s, and (b) O 1s spectra recorded from Ti, Mn, Mo, Y, and Zr surfaces exposed to laboratory air for the time period of one day. The results obtained from Au substrates exposed to the UHV environment are added for reference to show that lack of O results in the C 1s spectrum with only hydrocarbon peak. All spectra are referenced to the vacuum level to compensate for the shifts in C 1s peak positions due to differences in sample work function. [Author's original work.]

the significantly higher FWHM of the O 1s peaks, relative to that of C 1s, not all contributions related to various carbon oxides can be identified in the O 1s spectra. Nevertheless, in each case the lowest BE contributions are due to metal oxides. The BE of the latter components follows the trend in the metal electronegativity, which is lowest for Y (1.22 on the Pauling scale) [177] resulting in the largest charge transfer from metal to O atoms and, in consequence, the lowest BE of the related O 1s peak. This is followed by Zr, Ti, Mn and finally Mo, which possesses the highest electronegativity of all metals included in this comparison (2.16) [177]. As for the carbo-oxide portion of the O 1s spectra, C—O is the only peak from the Mo sample, which allows us to identify the O 1s peak at 537 eV as being due exclusively to the C—O bonds. The highest BE of this component is intuitively expected as the largest charge transfer per atom (compared to all other carbo-oxide species, which involve more than one O atom and, hence, have to share the charge). Also, the relatively low intensity of the O—C peak as compared to that obtained from the other surfaces is consistent with the lowest O:C ratio (1:1). In a similar manner, the O 1s spectrum recorded from the Zr surface can be used to determine the position of the O—C═O peak, which appears to be 536.2 eV, hence 0.8 eV lower than that of C—O. C bonded to three O atoms gives rise to extra intensity on the lower BE side of the O—C═O component (~535.8 eV), which is clearly visible in the O 1s spectra of Mn and Y, as these are the only surfaces that exhibit significant CO_2 concentrations based on the C 1s spectra.

More insight into the nature of involved carbon oxides can be gained from angle-dependent XPS studies. One example of such work is included in Fig. 28, which shows the C 1s spectra of AdC accumulating on the Zr substrate recorded at the tilt angle ψ with respect to sample normal of 0 and 60° [175]. A very pronounced decrease in the intensity of the O—C═O peak relative to that of C—C/C—H contribution at $\psi = 60°$, indicates that the former species are located closer to the Zr-oxide interface.

Hence, we can conclude that the type of AdC accumulating on the specimen, in addition to the environment the sample has been exposed to, depends strongly on the underlying substrate. Whether this is due to different absorption rates or the result of different reactivity towards the surface oxides is beyond the scope of this review. Importantly, the data included in Fig. 27 corroborate that the nature of AdC varies greatly between specimens. *Efforts thus have to be undertaken to analyze the layer composition prior to using this signal for BE referencing.*

In addition to the environment and the substrate type, another variable that we considered in our experiments is the exposure time. This aspect was analyzed for a series of metal samples exposed to ambient air. Fig. 29 shows the concentration of AdC c_{AdC} on sputter-cleaned samples, as well as after 10 min, 1 week, and 7 months of exposure to laboratory air (23 °C, 40% RH) [175,178]. The

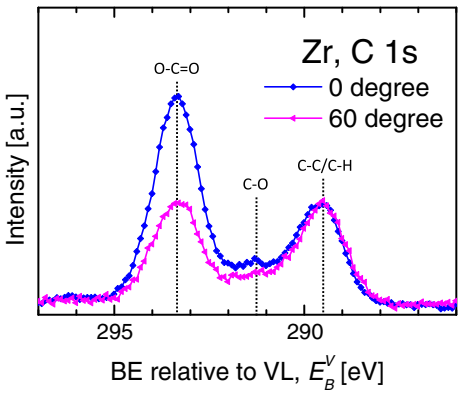

Fig. 28. The C 1s spectra of AdC accumulating on the Zr substrate recorded at the sample tilt angle with respect to the surface normal of 0 and 60°. Spectra are referenced to the vacuum level to compensate for the shifts in C 1s peak positions due to differences in sample work function. [Author's original work.]

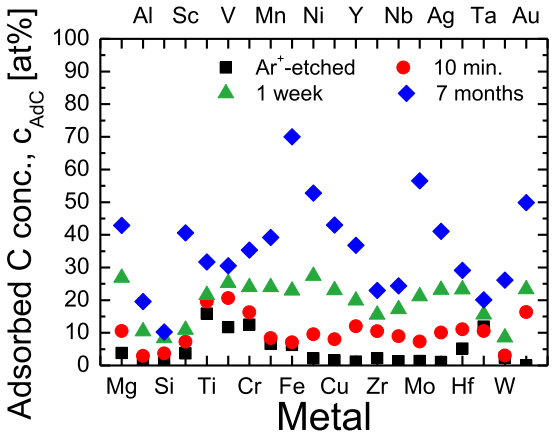

Fig. 29. Concentration of AdC c_{AdC} on sputter-cleaned samples, as well as after 10 min, 1 week, and 7 months of exposure to laboratory air (23 °C, 40% RH). The non-zero c_{AdC} values recorded for some metals (e.g., Ti, V, Cr, Hf, and Ta) are due to carbides that form upon Ar^+ ion etch. [Author's original work.]

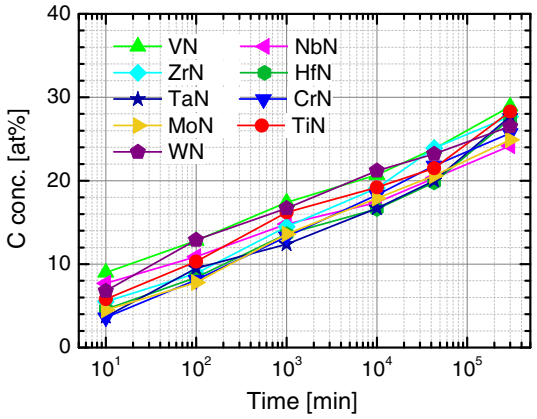

Fig. 30. AdC accumulation rate for a series of transition metal nitride samples exposed to ambient air for the time span from 10 min. to 7 months [adapted from Ref. [137]].

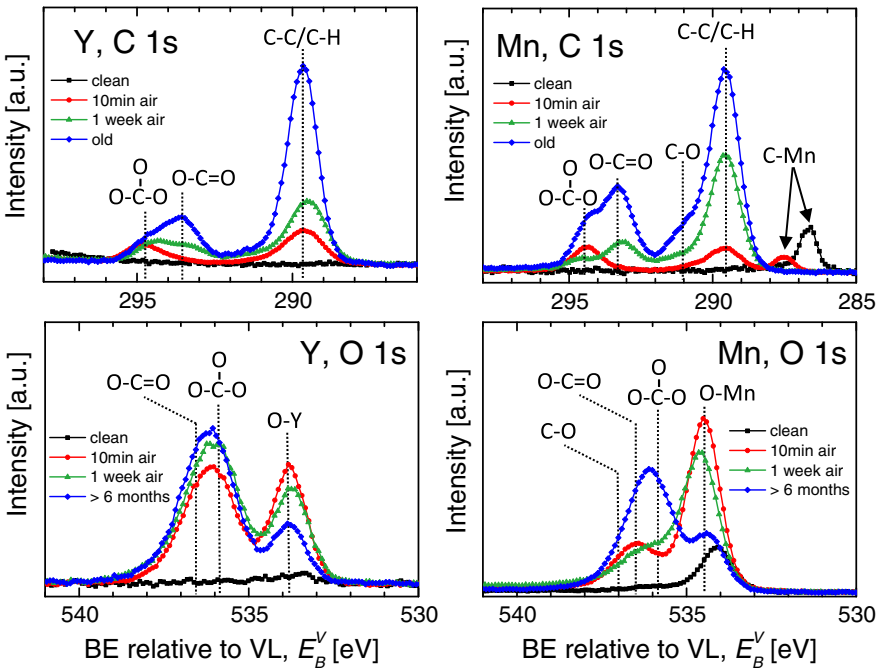

Fig. 31. C 1s (top) and O 1s (bottom) core-level spectra acquired from Y and Mn surfaces as a function of air exposure time. All spectra are referenced to the vacuum level to compensate for the shifts in C 1s peak positions due to differences in sample work function. [Author's original work]

non-zero c_{AdC} values recorded for some metals (e.g., Ti, V, Cr, Hf, and Ta) are due to carbides that form upon Ar^+ ion etch. Remarkably, for any exposure time there is a tremendous difference between the substrates as to the amount of adsorbed carbon. For example, after 7 months-long air exposure c_{AdC} varies from 10% for Si to 70% for Fe. Other metal surfaces that exhibit lower adsorption rates for AdC are Al (c_{AdC} = 20%), Zr (c_{AdC} = 23%), Nb (c_{AdC} = 24%), Ta (c_{AdC} = 20%), and W (c_{AdC} = 26%). Apart from Fe, AdC adsorbs fairly quickly on Ni (c_{AdC} = 53%), Mo (c_{AdC} = 57%), and Au (c_{AdC} = 50%). The process of AdC adsorption is continuous and there are no indications from our data that it would saturate beyond the longest tested exposure times of a few years. More supporting evidence is presented in Fig. 30, where the rate of AdC accumulation during air exposure is found rather constant for a series of TM nitride samples. For time spans from 10 min to 7 months, independent of sample type, the amount of adsorbed C shows a steady increase with air exposure time of ca. 5 at.% for each decade [137].

As could be intuitively expected, exposure time not only affects the amount of carbon at the surface, but has also a profound influence on the chemical composition of AdC accumulating on one and the same surface. Fig. 31 shows examples from C 1s and O 1s core-level spectra acquired from Y and Mn surfaces as a function of air exposure time. In both cases, the CO_3 component is the one that forms first (see the 10 min exposure). The formation of O−C═O requires longer exposure times (ca. 1 week), independent of the substrate. It seems also that the prolonged exposure leads to faster growth of the O−C═O and C−C/C−H peaks. The changes in the C 1s spectra are mirrored in the corresponding O 1s signals, thus confirming the effect.

The strong time dependence of the AdC concentration and composition illustrated by the data in Figs. 29–31 calls for precise control over the air exposure time. This aspect is not recognized in the XPS literature. The sample state in synthesis-oriented papers is often characterized “as-deposited”, while in the spectroscopy literature “as-received” dominates. In both cases, the crucial aspects of (a) exposure time and (b) the environment the samples were exposed to, are missed.

To summarize this section, it is emphasized that *there is no such defined compound as adventitious carbon*. The chemical nature of AdC depends rather on the substrate it accumulates on, the type of environment it has been exposed to, as well as the exposure time. In the vast majority of cases, samples experience several environments before the actual XPS measurement is performed (e.g., air exposure followed by HV in the fast-entry lock chamber and finally UHV), which certainly adds to the complexity of AdC layer. For meaningful referencing, *all* variables should be considered and the nature of contaminating carbon should be identified. Our results put a new perspective on studies like the one by Barr et al. [124] as the substrate dependence together with the sample history are decisive factors, which, if neglected, prevent general conclusions regarding the nature of AdC.

5.2. The myth of constant C 1s binding energy

As pointed out in Section 4, throughout the history of XPS there has been confusion regarding the BE that was assigned to the C−C/C−H peak of adventitious carbon. The uncertainty has even grown over the years and led to the C 1s peak being set almost anywhere between 284.0 and 285.6 eV. Typically, this is done *ad hoc*, with or without reference or motivation.

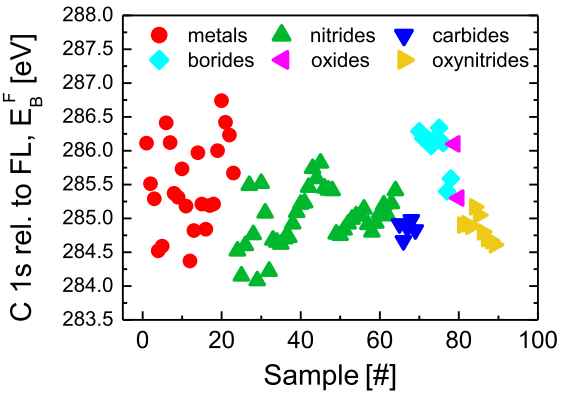

Fig. 32. Binding energy of the C−C/C−H peak E_B^F for AdC layers accumulating during air exposure on metals, nitrides, carbides, oxides, borides, and oxynitrides. The exposure time ranges between several weeks and a few years. [Author's original work.]

To address this issue, we measured the BE of the C−C/C−H peak E_B^F for AdC layers accumulating during air exposure on a whole range of substrates including metals, nitrides, carbides, oxides, borides, and oxynitrides. The exposure time ranged between several weeks and a few years. Results for all samples are shown in Fig. 32 [138]. Surprisingly, and contrary to common practice that assigns one single BE value to the C 1s peak, it turns out that E_B^F varies over a wide range, from 284.08 to 286.74 eV, depending on the type of surface AdC adsorbs on. The spread of 2.66 eV is disturbingly large as it reflects the magnitude of the error made while aligning XPS spectra to the C 1s peak if set at an arbitrarily chosen value. This practice corrupts spectral interpretation and assignment of the chemical bonds, as the chemical shifts are most often less than 2.66 eV. These results prove that *the BE of the C 1s peak is not an inherent property of the carbon layer alone* and that the substrate influence is decisive, which may explain the 50-year-long confusion over the C 1s position.

It is instructive to compare BE values for the C−C/C−H peak of AdC accumulating on metal samples after prolonged air exposure [138] with numbers reported by Crist [136]. This is shown in Fig. 33 where the BE differences between our data and those recorded by Crist ΔC are plotted for metals in the "as-received" state as well as after sputter-cleaning. Interestingly, despite the fact that the experiments were conducted in different labs and with instruments of a different type, there is a quite good agreement. With few exceptions, ΔC does not exceed ±0.5 eV for most metals. This agreement indicates that some correlation exists between the substrate material and the BE of the C 1s peak from the corresponding AdC layer. We discuss this matter in more detail in Section 5.5.

5.3. Can charging account for shifts in the C 1s peak position?

One of the immediate concerns while observing large shifts in the C 1s peak position of adventitious carbon (see Fig. 32) is the role of sample charging. The latter can potentially occur in samples being analyzed as well as in the AdC layer. We consider these two cases separately.

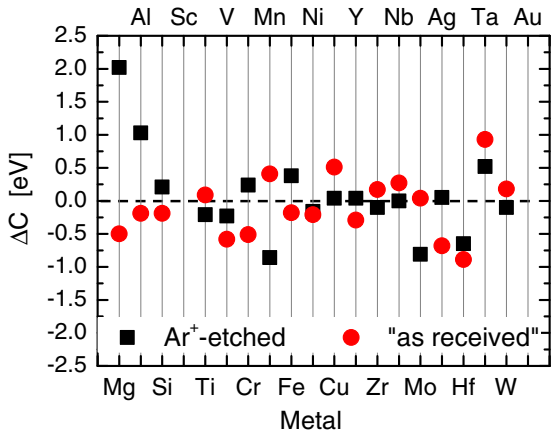

Fig. 33. Binding energy difference ΔC between values for the C−C/C−H peak of AdC reported by two different laboratories (see Ref. [136,138]). AdC layers were adsorbed on metal samples after prolonged air exposure. ΔC is plotted for samples in the "as-received" state as well as after Ar^+ ion etch.

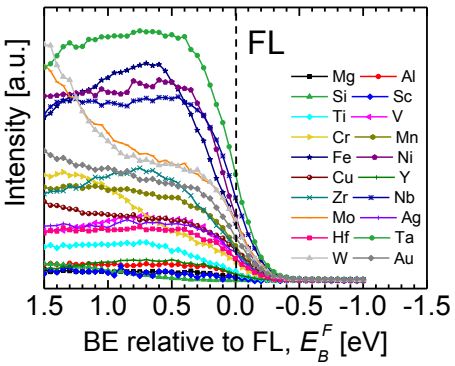

Fig. 34. Valence band spectra in the vicinity of the Fermi level (FL) for the subset of metallic samples. In all cases FL cut-off coincides with "0" eV on the BE scale, indicative of that FL is aligned between sample and the spectrometer and proving that a good electrical contact is established to the instrument. [Author's original work]

To evaluate the potential influence of charging effects on the signals from the substrates, we recorded DOS in the vicinity of the Fermi energy (the Fermi level cut-off) from all metallic samples. Electrons originating from FL possess the highest kinetic energy of all photoelectrons (essentially equal to $h\nu - \phi_{SA}$), resulting in relatively long inelastic mean free paths λ, from to 18 to 24 Å.[32] As a consequence, the XPS probing depth, given by $3 \times \lambda$, substantially exceeds the likely AdC layer thickness (assuming reasonable sample storage conditions). This situation, together with the fact that all saturated hydrocarbons, being wide-band-gap materials, do not possess DOS near the FL [114,124], implies that the spectral intensity in this region is solely determined by the underlying substrate. Fig. 34 shows the valence band (VB) spectra in the vicinity of the Fermi level for the subset of metallic samples [175]. The DOS at the FL varies to a large extent, in accordance with the changes in the electronic structure. Nevertheless, in all cases the FL cut-off coincides with "0 eV" on the BE scale, which indicates that the Fermi level is aligned between sample and the spectrometer and proves that good electrical contact is established to the instrument. Hence, charging of the substrate can definitely be excluded and cannot account for the observed 2.37 eV shift in the position of the C 1s peak from AdC accumulated on metallic samples (see Fig. 32).

Due to poor electrical conductivity, hydrocarbons and carbon oxides constituting AdC can potentially acquire positive charge during experiments leading to apparent C 1s shifts towards higher BE, quite independent of the substrate. However, there are arguments that speak against the charging of the AdC layer being responsible for the observed C 1s shifts.

First of all, shifts are noted even for very short air exposure times, i.e., for fractional (< 1 ML) carbon coverage (see Section 5.5). With the involved electron inelastic mean free paths being of the order of 10–20 Å [32], the photo-induced conductivity in the surface region is certainly sufficient to compensate electron loss due to the photoelectric effect and, hence, to prevent charging.

A second condition which speaks against charging, is that the C 1s shifts persist for air exposure times of up to several months, indicating that the effect is independent of the AdC thickness (see Fig. 30). Should charging in the AdC layer occur, a gradual shift towards higher BE with air exposure time would be expected as the carbon layer grows thicker.

Thirdly, the BE of the C 1s peak on metals with low reactivity such as Au and Ag (E_B^F = 284.92 and 284.82 eV, respectively) is higher than that measured for numerous metallic, nitride, carbide, and oxynitride samples, which developed pronounced native oxide layers during the air exposure, as evident from the data shown in Fig. 32. The latter group of samples is certainly more prone to

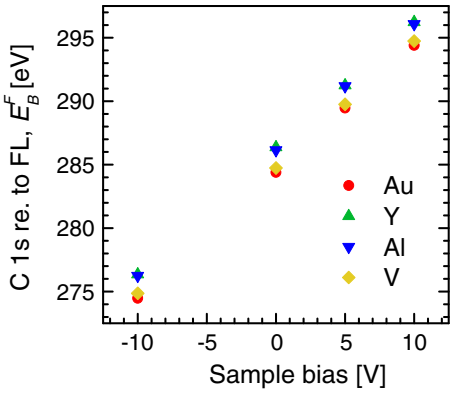

Fig. 35. Binding energy of the C 1s peak of AdC plotted as a function of the applied substrate bias for selected Au, Y, Al, and V substrates representing large E_B^F spread and varying reactivity towards oxygen. [Author's original work.]

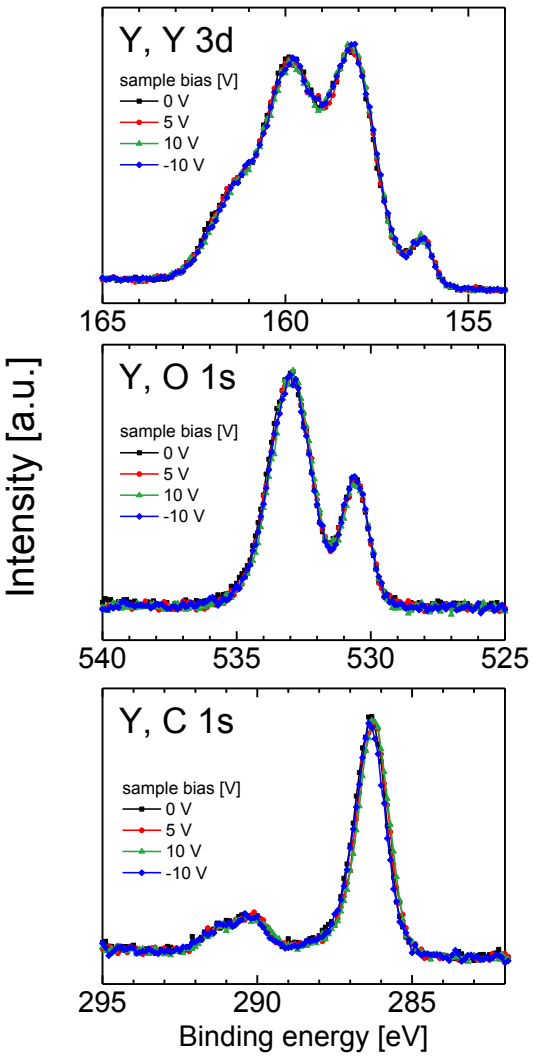

Fig. 36. Y 3d, O 1s, and C 1s core-level signals acquired from a Y sample with native oxide and adsorbed AdC layer. All spectra recorded at the substrate bias different from zero are shifted by the corresponding amount to allow direct comparison to the non-biased data. [Author's original work.]

charging, hence AdC depositing on top of a native oxide with limited conductivity should shift more to the higher BE than AdC growing on a non-reactive metal surfaces, which is not observed.

Fourth, and perhaps the strongest argument, is the excellent correlation between the C 1s BE and the sample work function (see Section 5.5), which cannot in any way be accounted for by charging.

To definitely exclude the possibility of charging in the AdC layer as a source of the observed C 1s peak shifts between different substrates, we measured E_B^F as a function of applied sample bias V_s. In Fig. 35, the BE of the C 1s peak is plotted as a function of V_s for AdC layers accumulated on selected Au, Y, Al, and V substrates representing a large E_B^F spread and varying reactivity towards oxygen. Clearly, independent of the substrate type, the C 1s peak of AdC closely follows the substrate potential, in accordance with the core-levels of the substrate, such that the original separation between the C 1s peak positions recorded with $V_s = 0$ V is reproduced for any V_s value tested to within 0.1 eV. The slopes dE_B^F/dV_s vary from 0.993 for Y to 0.997 for Au. The core-level spectra recorded as a function of V_s are essentially identical. This result is illustrated in Fig. 36 with the Y 3d, O 1s, and C 1s core-level signals acquired from the Y sample with native oxide and adsorbed AdC layer. All spectra recorded at $V_s \neq 0$ V are shifted by the corresponding amount to allow direct comparison to the non-biased data. Clearly, signals from the Y metal, Y oxide, as well as all C-containing species in the AdC layer (including, apart from C−C/C−H, also C−O and O═C−O components) immediately acquire the applied bias voltage, and no evidence for peak smearing indicative of voltage drop in the surface oxide and AdC layers is found. Hence, sample charging can be definitely ruled out as an explanation for large changes in E_B^F of the C 1s peak between different substrates in our model experiments.

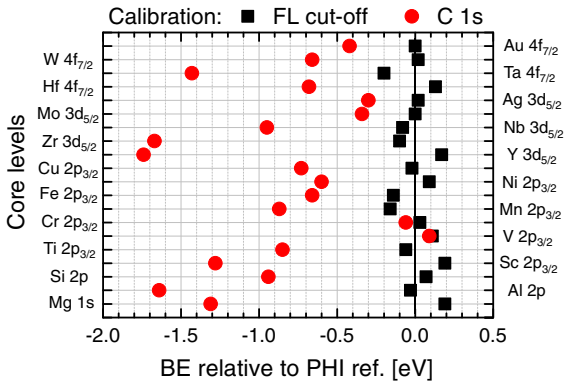

Fig. 37. Binding energy difference between measured positions of primary core-level peaks from a set of metallic samples [Author's original work] and the handbook values (taken from Ref. [180]) calculated using two referencing methods: (black squares) the Fermi level cut-off and (red circles) the AdC technique with the C 1s peak set at 284.5 eV.

5.4. Consequences of C 1s shifts for BE referencing

The fact that C 1s shifts (cf. Fig. 32), while the underlying substrate remains in good electrical contact to the spectrometer (Fig. 34), clearly indicates *decoupling* of the measured energy levels of adventitious carbon from the FL of the substrate and, hence, from that of the spectrometer. The implications for BE referencing based on the C 1s peak are severe. For example, let us consider the outcome of the BE scale correction based on the C 1s peak position of AdC accumulated on metallic substrates. Although the C 1s method is usually not used in studies of metallic samples as they exhibit core-level peaks with rather well-defined energies (cf. Fig. 2) [179], there are no explicit reasons as to why it should *not* be used to correct BE scale for this particular class of materials. In Fig. 37 the binding energy difference between measured peak positions of primary metal core-levels and the handbook values [180] are plotted using two referencing methods, namely the Fermi level cut-off or the C 1s peak at 284.5 eV. Using the former reference gives a fair agreement to values in the XPS handbook, and the largest deviation does not exceed 0.2 eV. In contrast, correction of the BE scale obtained by setting the corresponding C 1s peak of AdC at 284.5 eV results in very significant differences. In nearly all cases, with the exception of the Cr $2p_{3/2}$ and V $2p_{3/2}$ peaks, the BEs of the core-levels are severely underestimated with respect to the tabulated values. For Zr $3d_{5/2}$, Y $3d_{5/2}$, and Al 2p, this deviation exceeds 1.5 eV. Clearly, in this comparison the C 1s referencing method fails spectacularly.

To demonstrate that problems caused by C 1s referencing are not limited to metallic samples, we consider in the next example a series of air-exposed transition metal nitrides (TM)Ns (TM = Mo, V, W, Ti, Cr, Nb, Ta, Zr, and Hf) which are the subset of all specimens discussed in the previous section (see Fig. 32) [137]. Within this group, the BE of the C 1s peak varies by 1.44 eV from 283.78 eV for MoN to 285.22 eV for HfN. Fig. 38(a) shows the VB spectra in the vicinity of the Fermi level recorded from all (TM)Ns. In all cases, the Fermi level cut-off coincides with "0 eV" on the BE scale, indicating Fermi level alignment between the sample and the spectrometer. If we disregard for a while this result and, as commonly practiced, acquire the C 1s spectrum from corresponding AdC layers and correct the BE scale by setting the C−C/C−H peak at 284.5 eV (cf. Fig. 38(b)), some specimens (TiN, VN) exhibit no

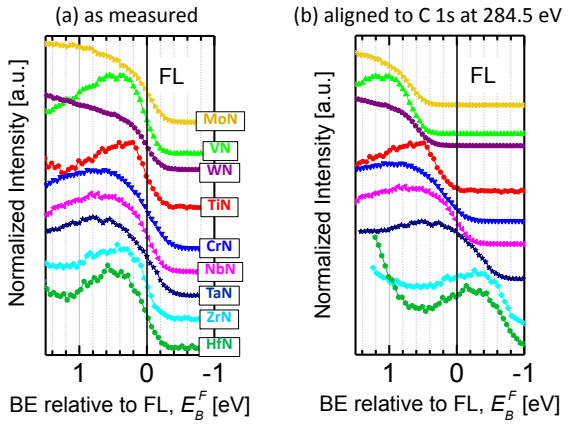

Fig. 38. Portion of the valence band spectra in the close vicinity of the Fermi level (FL) recorded from a set of transition metal nitride thin films: (a) as-measured (referencing to FL), and (b) aligned by using the common procedure of referencing to C1s peak of AdC set at 284.5 eV [adapted from Ref. [137]].

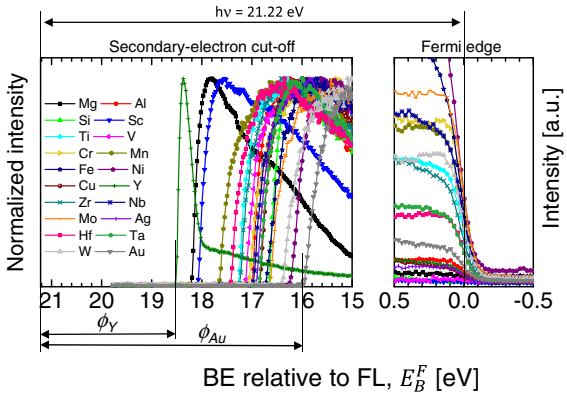

Fig. 39. He I UPS spectra from a set of metal samples: (left) the secondary electron cut-off region, and (right) the vicinity of Fermi level. The alignment of Fermi edge with the "0" eV confirms good electrical contact between sample and the spectrometer, while large variation in the cut-off position reveals substantial difference in work function between analyzed samples. [Author's original work.]

DOS at the FL despite their metallic character, while for other films (HfN, ZrN, and TaN) such a referencing procedure results in a non-zero DOS above the Fermi level. These examples demonstrate clearly that the common procedure of *referencing to the C 1s peak of AdC, besides chemical ambiguity, leads to unphysical results*. The latter situation is not obvious in everyday XPS practice as BE scale correction is regularly applied to core-level spectra, in which case changes in peak positions by ± 1 eV do not lead to such obvious contradictions, although these shifts have direct (and unnoticed) impact on the interpretations of chemical bonding.

5.5. The role of sample work function and vacuum level alignment

One of the essential parameters in the energy-level diagram is the sample work function ϕ_{SA} which determines the contact potential difference between sample and spectrometer (see Fig. 19(a)). To investigate possible effects of ϕ_{SA} on the BE of the C 1s peak E_B^F, we used ultraviolet photoelectron spectroscopy to estimate the sample work function from the secondary-electron cut-off in the He I ($h\nu = 21.22$ eV) UPS spectra, according to the standard procedure described elsewhere [171]. The cut-off spectra for all metal samples are shown in Fig. 39 together with the corresponding narrow-range UPS spectra, which reveal the DOS in the vicinity of the Fermi level. The latter spectra confirm FL alignment between sample and the spectrometer (cf. Section 5.3). Large differences between the cut-off positions reveal that there is substantial difference in work functions among the samples.

To address possible influence of sample work function on the apparent position of the C 1s peak of AdC, we plotted E_B^F as a function of ϕ_{SA} for all specimens in Fig. 40. Interestingly, there is a very close correlation between the BE of the C 1s peak and the sample work function. Thus, the position of the C 1s peak measured with respect to the FL is steered by ϕ_{SA}, which disqualifies this core-level as a reliable reference. Moreover, the linear fit of all data points has a slope of -0.994, implying that the sum $E_B^F + \phi_{SA}$ is essentially constant at 289.58 ± 0.14 eV. The latter quantity corresponds to a BE referenced to the vacuum level E_B^V (cf. Fig. 19(a)).

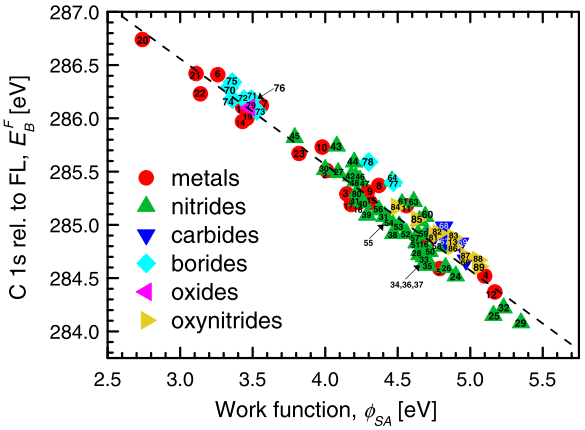

Fig. 40. Binding energy of the C 1s peak of AdC E_B^F plotted *vs.* sample work function ϕ_{SA} for the carefully selected set of nearly one hundred predominantly thin film samples spanning wide range of material systems representing metals, nitrides, carbides, borides, oxides, and oxynitrides [adapted from Ref. [138] which also contains a detailed list of all samples].

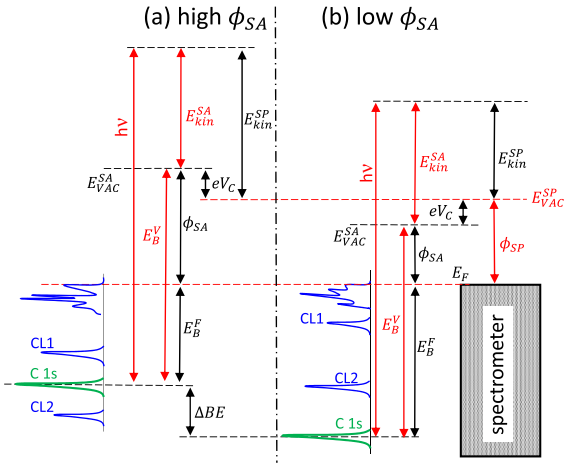

Fig. 41. Energy level diagrams showing critical parameters for (a) a high- and (b) a low-work-function sample in contact with the spectrometer. All parameters sketched in red are constant, i.e., independent of the sample being measured.

Thus, we conclude that the BE of the C 1s peak due to AdC is essentially constant with respect to the VL, rather than the FL as commonly assumed. This result can be explained by the fact that the adventitious carbon does not constitute an integral part of the specimen, which makes this case analogous to organic layers deposited on metals by *ex-situ* techniques such as spin-coating [181]. Contacts for these samples often remain within the Schottky-Mott limit, with the electronic levels of the adsorbate being determined by the substrate work function [182]. The position of the C 1s C—C/C—H peak referenced to E_{VAC}, 289.58 ± 0.14 eV, corresponds very well with the gas-phase values of 290.76 to 290.15 eV measured for alkanes by Pireaux et al. [183], compensated for the intermolecular relaxation energy due to electronic and atomic polarization of the neighboring molecules surrounding the core hole, which is typically of the order of 1–3 eV [184,185].

Our findings are schematically summarized in Fig. 41, where the relevant energy levels and critical parameters are indicated for (a) a high- and (b) a low-work-function sample. All parameters sketched in red are considered constant, i.e., independent of the sample being measured. Irrespective of ϕ_{SA} the Fermi level cut-off aligns with that of the spectrometer (which is established during the calibration procedure, see Section 3.2), while the BE of the C 1s peak of AdC, E_B^F, closely follows the changes in sample work function. The position of the C 1s peak with respect to the vacuum levelE_B^V remains constant at 289.58 ± 0.14 eV [89,186]. Depending upon the relation between ϕ_{SA} and ϕ_{SP}, the contact potential difference V_c may be positive or negative. The error one makes by forcing the C 1s peak to be at 285.0 eV (or any other constant value) and shifting all core-levels peaks of the sample accordingly (denoted in the figure as CL1 and CL2) is schematically shown for high and low ϕ_{SA} specimens in panels (a) and (b), respectively. For a low-work-function sample, the BE of the C 1s peak is higher than 285.0 eV, hence "correction" implies a tangible shift towards lower BE. If the sample possesses a DOS at the Fermi level, this procedure results in spectral features appearing above the Fermi energy, which should dismay a careful user. In other cases, where no FL cut-off exists, the unphysical nature of such "correction" may go unnoticed. In either situation, the conventional procedure leads to a severe error in the BE assigned to the CL1 and CL2 signals. An analogous situation takes place for high work function samples, with the difference being that the BE of the C 1s peak is lower than 285.0 eV, thus BEs of all peaks are "corrected" by shifting all spectra towards higher BE.

It is worth emphasizing that ϕ_{SA} accounts for the work function of the sample (i.e., together with the adsorbed AdC layer) and not

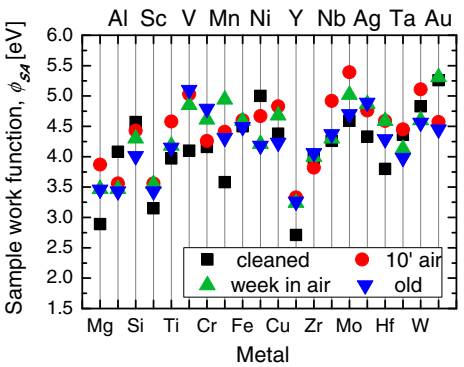

Fig. 42. Sample work function assessed by ultraviolet photoelectron spectroscopy (UPS) plotted for a whole range of metal samples after various conditions of AdC accumulation, starting from sputter-cleaned surface, to the one exposed to ambient air for several months or longer. [Author's original work.]

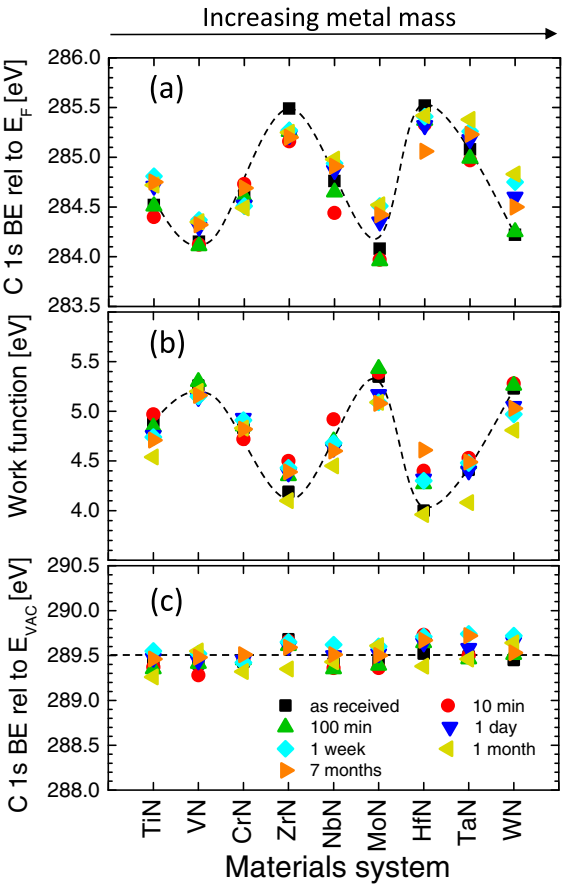

Fig. 43. (a) Binding energy of the C–C/C–H peak in the C 1s spectra of AdC referenced to Fermi level E_B^F, (b) sample work function ϕ_{SA}, and (c) C 1s BE referenced to Vacuum level E_{VAC}^F for a set of transition metal nitride thin films grown by magnetron sputtering. The dashed curves in (a) and (b) are only for eye guiding to emphasize the symmetry between the plots [adapted from Ref. [137]].

that of the bare substrate. This is a very important distinction as illustrated in Fig. 42, where measured work functions are plotted for a wide range of metal samples and for various conditions of AdC accumulation, starting from a sputter-cleaned surface to one exposed to air for several months or longer. Clearly, for each sample, ϕ_{SA} varies with exposure time, which is due to the different thickness (and possibly also type) of AdC species. The typical variation is ~1 eV, and is lowest for Fe (0.21 eV) and highest for Mn (1.36 eV). Hence, these large changes in ϕ_{SA} imply that sample work function has to be measured for a given sample condition and one cannot simply refer to *ad hoc* literature reference values.

We have shown in the previous sections that the exposure time has a determining effect on the chemical composition of AdC (see Fig. 31). Therefore, it is also highly relevant to test whether the peculiar correlation observed between the BE of the C 1s peak and the sample work function varies with the exposure time. In Fig. 43 are shown (a) the binding energy of the C–C/C–H peak in the C 1s spectra of adventitious C referenced to the Fermi level E_B^F, (b) the work function, and (c) the C 1s BE referenced to the vacuum level E_B^V for a set of polycrystalline (TM)N thin film samples exposed to atmosphere for a time period ranging from 10 min to 7 months [137]. Clearly, although for each sample both E_B^F and ϕ_{SA} vary slightly with exposure time by 0.3–0.5 eV, the sum $E_B^F + \phi_{SA}$ is constant at 289.50 ± 0.15 eV, indicating that the VL is a useful reference for any exposure time to ambient air.

5.6. A remedy for binding energy referencing based on AdC for conducting samples

Although C 1s referencing is the least bad option and correspondingly the most commonly used method for samples that are prone to charging, our literature survey reveals that it is often used also for electrically conducting specimens (see Section 4). Whether this practice is justified by scientific reasons (e.g., no reliable core-level signals from the sample due to peak overlaps) or is simply a matter of poor experimental judgement and/or lack of basic knowledge is not of our concern. It is, however, important to emphasize that the constant BE of the C 1s peak with respect to the vacuum level, offers in fact a possibility of reliable energy referencing for well-conducting samples. The method cannot be applied to samples prone to charging as XPS and UPS measurements in general lead to different surface potentials for such specimens, hence, the relationship $E_B^F + \phi_{SA} = 289.58$ eV is not expected to hold. For conducting samples, a complementary measurement of ϕ_{SA}, which as we have shown above, is closely correlated to the C 1s peak position, should be performed in direct connection to the XPS analyses (without breaking the vacuum to avoid potential changes to

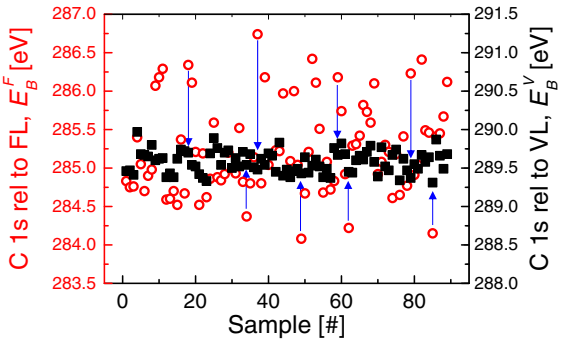

Fig. 44. Binding energy of the C 1s peak corresponding to C–C/C–H bonds of AdC referenced to (left axis) the Fermi level E_B^F, and (right axis) the vacuum level E_{VAC}^F. To facilitate direct comparison the range of vertical axes is kept constant. Arrows indicate the overall trend observed for E_{VAC}^F values to accumulate at 289.58 ± 0.14 eV [adapted from Ref. [138]].

the AdC layer, see Section 5.1). Then the C–C/C–H component of the C 1s spectrum of adventitious C is set at 289.58 – ϕ_{SA} eV and all other core-levels are shifted accordingly.

To illustrate the advantage of using the BE of the C 1s peak of AdC referred to VL (E_B^V) rather than to the FL (E_B^F) for BE-scale referencing, we directly compare in Fig. 44 the magnitude of energy spreads in the C 1s peak position, while using these two reference levels, for a range of substrates including metals, nitrides, carbides, oxides, and borides [138]. To facilitate comparison, the same energy range is used on both vertical axes (3.5 eV in each case). Clearly, the standard deviation in the C 1s peak position is reduced by a factor of 4.1 if referencing to vacuum level rather than to Fermi level is used. E_B^F ranges from 284.08 eV for MoN to 286.74 eV for Y sample, while variation in E_B^V is much smaller, from 289.31 eV for VN to 289.97 eV for TiB_2. The latter result agrees with a common-sense notion of a constant energy levels associated with C atoms present in the same chemical environment and provides grounds for more reliable referencing of XPS spectra.

Even though no straightforward way exists to exploit VL referencing for poorly conducting samples due to different charging conditions experienced during XPS and UPS analyses, there is no apparent reason to question the conceptualization that the C 1s peak of AdC accumulating on non-conducting samples also would exhibit vacuum level alignment, just as for all conducting specimens included in the present study for which experimental verification is possible. Thus, XPS referencing guides for charge control during analyses of poorly conducting specimens, that explicitly rely on the use of AdC layers [6,7], have to be revisited.

The relationship $E_B^F + \phi_{SA} = 289.58$ eV may in fact serve as a criterion for determining the charging state of the specimen, which is not known *a priori*. If $E_B^F + \phi_{SA} > 289.58$ eV, it is likely that the sample has a tendency to acquire positive potential during XPS and/or UPS measurements.

Interestingly, the possibility of referencing XPS spectra to the VL (instead of the FL) was suggested as early as 1973 by Evans et al. [170], who pointed out that such referenced BEs can be directly compared to gas-phase data or calculations. The method has not been widely adopted and there are only few examples of works where VL referencing was considered after the conventional method failed. For example, Legare et al. studied Ni, Pd, and Pt on an α-alumina single-crystal and showed that the binding energies of the substrate core-levels peaks with respect to the metal Fermi level depend on the metal work function. The authors assigned this effect to vacuum level alignment between the metal and the insulating substrate [187]. We thus end this review on a positive note. The next 50 years will surely show intensified interest in XPS accompanied with novel analysis opportunities and enhanced accuracy resulting from improved binding energy referencing as outlined in this paper.

6. Conclusions

During the five decades long history of XPS, the BE referencing technique involving the C 1s peak of adventitious carbon has been, and certainly still is today, the most commonly employed method. This status quo contrasts with the striking inconsistencies revealed by a literature survey, concerning: (i) the unclear chemical nature of contamination species used for referencing, (ii) the lack of a well-defined single energy value associated with the C 1s peak of AdC, (iii) differences in the methodology of BE scale referencing, and (iv) the lack of understanding when referencing employing AdC is indeed unavoidable.

To address these alarming issues, which undermine the reliability of chemical-state identification in modern XPS, we performed extensive studies of all essential aspects of the problem. Our work involved a carefully selected set of nearly one hundred predominantly thin-film samples spanning a wide range of material systems representing metals, nitrides, carbides, borides, oxides, and oxynitrides. The most important conclusions from this work are:

(1) For samples that have been stored in air for relatively long periods of time (one week or longer), most of the AdC found on the surface during XPS analysis originates from air exposure. For shorter storage times, the effect of carbon contamination adsorbing inside the vacuum system has to be taken into account.
(2) The chemical nature of AdC depends on the substrate, the type of environment it has been exposed to, and the exposure time. Prior to meaningful referencing, the nature of the contaminating carbon species should be verified. For the latter, not only C 1s,

but also related core-level spectra (O 1s, F 1s, N 1s) should be evaluated to obtain a consistent picture of the chemical composition of the AdC layer.

(3) The BE of the C−C/C−H peak of AdC depends on the substrate it accumulates on and may vary by as much as 2.66 eV for the range of tested materials systems. This shift in the C 1s peak is not caused by charging.

(4) Due to (3), calibrating the BE scale to the C 1s peak set at 284.5 eV is not justified and may lead to unphysical results, like a non-zero density of states above the Fermi level. This situation occurs even for well-conducting samples like metals, where charging effects can definitely be excluded.

(5) The BE of the C 1s peak is not an inherent property of the AdC layer alone and the substrate influence is decisive, which may explain the prevailing confusion as to the "correct" C 1s peak position.

(6) The magnitude of C 1s shifts caused by the substrate is larger than typical chemical shifts, which definitely prevents any meaningful bonding assignments.

(7) Since a large number of authors use C 1s referencing, the substrate dependence of the C 1s BE significantly contributes to the noticed and unacceptably large spread of reported BEs found in XPS data bases.

(8) The BE of the C−C/C−H peak of AdC E_B^F correlates with the sample work function ϕ_{SA}, in such a way that the sum $E_B^F + \phi_{SA}$ is constant within the measurement accuracy.

(9) For nearly a hundred analyzed samples, representing a wide range of material classes and for air exposure times varying from 10 min to 7 months, we determined that $E_B^F + \phi_{SA} = 289.58 \pm 0.14$ eV.

(10) $E_B^F + \phi_{SA}$=constant, indicates invariant binding energy of the C 1s peak with respect to the vacuum level. This VL, rather than the commonly assumed FL alignment, results from the fact that AdC is not an inherent part of the analyzed sample and as such may not remain in a proper electrical contact with the substrate (and spectrometer) in the sense of establishing a common FL.

(11) In the context of an energy reference, the case of adsorbed carbonaceous species weakly interacting with the underlying substrate is analogous to the gas phase measurements, where the VL is a natural energy reference.

(12) Since the position of the C 1s peak is steered by the sample work function, it cannot serve as a reliable reference for calibrating the BE scale. This conclusion applies irrespective of whether the samples are conducting or not. Hence, conventional procedures for charge control, like the XPS referencing guides developed by both ASTM and ISO have to be revisited.

(13) A possible remedy for samples that are not prone to charging is a complementary measurement of the sample work function. The C−C/C−H component of the C 1s spectrum is then set at 289.58 – ϕ_{SA} eV and all other core-levels are shifted accordingly. This solution allows a user to maintain the concept of a single specific BE value associated with the C 1s peak of AdC, as originally intended by Siegbahn et al. [4]. It is, however, limited to conducting samples.

(14) The above method is not expected to work for insulators as ϕ_{SA} cannot be easily assessed. Thus, in view of all the evidence, *there is no reliable referencing method involving AdC for non-conducting samples. No method is, however, better than an incorrect method.*

(15) *Last, but not least*, referencing to AdC which is always external to the analyzed sample, should only be used if no internal reference levels, such as the Fermi level cut-off in density of states, are available. This point is often blindly overlooked in the literature.

6.1. Suggestion of an experimental protocol for future XPS studies

In the spirit of improving accuracy and reliability of the information extracted from XPS analyses employing C 1s referencing, authors are encouraged to record and report more information that would help to understand the type of AdC species present at the surface of their samples and how this information was used for BE referencing. Such practice would also facilitate inter-laboratory comparisons of chemical-state information.

Below is a suggested template which includes the necessary experimental details. Apart from a number of instrumental parameters that are rarely reported, it puts an emphasis on the precise description of the sample history prior to XPS analyses, which as discussed in Section 5, may have deleterious effects on the state of the surface, and AdC in particular. This protocol goes beyond the notion of frequently used "as-deposited" *vs*. "as-received" sample state by specifying explicitly the synthesis method, storage time from preparation to loading into the spectrometer, and the type of environment the samples have been exposed to:

"XPS was used in this study with the aim of analyzing [state chemical bonding/ elemental composition/ lateral and depth distribution of elements or compounds]. The spectrometer was [model and manufacturer]. The base pressure during spectra acquisition was better than [state value with the X-rays ON] achieved by [details of the pumping system]. Residual gas analysis revealed that the main background gases in the analysis chamber were [……]. The excitation source was [state anode type / excitation energy / and whether or not a monochromator was used] operated at [source power]. The recorded spectra include [core-levels / valence band,….] and the total acquisition time was [….]. The spectra were acquired [sequentially or in parallel mode]. The calibration and linearity of the binding energy scale was confirmed by [method]. With the selected scan parameters, the energy resolution was [value for direct compared to other instruments, e.g., FWHM of the Ag $3d_{5/2}$ or Au $4f_{7/2}$ peak, and how it was determined]. The size of the analyzed sample area was [….]. Complementary work function measurements were performed by UPS with [state excitation source and energy, and whether or not a monochromator was used]. The samples were prepared by [synthesis method] and stored for [time] in [environment details: pressure, temperature, humidity, etc.] prior to loading into the spectrometer. The transfer procedure within the spectrometer includes exposure to [vacuum level, pumping system] for [time] prior to XPS analyses. [additional details (if applicable): the charge neutralizer (what type), sputter cleaning (ion type, energy, incidence angle, size of the cleaned area, exposure time), and/or the use of capping layers [state which]. The charge referencing method used was [….]. [(if AdC) show the C 1s spectra and describe how the BE scale was corrected]".

7. Outlook

Based on the evidence summarized in this article, one may only wish that the problems with the referencing to the C 1s peak of AdC should be widely recognized by the fast-growing XPS community. Our historical review reveals that criticism with using the essentially unknown compound which is external to the analyzed sample for BE referencing has been reiterated over the last five decades. The warning signals appearing from various laboratories were largely neglected in the "main stream" or bulk of XPS research activities. It is in fact hard to understand the wide spread of the AdC referencing method, which relies on the constant BE of the C 1s peak, given the fact that many groups reported contradictory evidence. The fact that no good alternatives exists cannot serve as an excuse.

To change the *status quo,* more attention is required from peers and journal editors, who should challenge the provided description of the experimental XPS procedures, and demand complete tracking of the sample history and publication of the C 1s spectra used for charge referencing (e.g., as a supplementary material, see our suggestion in Section 6.1). Not less important is the role of instrument manufacturers, who are often responsible for customer training and consultation. Furthermore, XPS data bases should be critically reviewed with the intention of removing results that lack sufficient description of the referencing technique used.

Out of all methods used for chemical state determination (see Section 3.3), measurements of the Auger parameter appear to be based on the most solid physical and chemical grounds, although the technique carries practical problems of operation and inherent limitations. More efforts are required to build a database for compounds where suitable Auger lines are observed with commonly employed X-ray sources. An improved energy resolution of modern spectrometers should favor precise measurements of Auger parameters and allow for detection of relatively small chemical shifts.

The charge referencing guidelines published by both ASTM and ISO, have to be revisited promptly with proper disclaimers, recognizing the external nature of AdC layers, which typically exhibit weak interaction to the underlying specimen and, in consequence, do not align to the Fermi level of the spectrometer. Thus, we look forward to the building of better spectrum databases for elements and compounds.

Acknowledgements

The authors most gratefully acknowledge the financial support of the Knut and Alice Wallenberg Foundation Scholar Grant KAW2016.0358, the VINN Excellence Center Functional Nanoscale Materials (FunMat-2) Grant 2016-05156, the Swedish Research Council VR Grant 2018-03957, the Åforsk Foundation Grant 16-359, and Carl Tryggers Stiftelse contract CTS 17:166.

References

[1] Source: Scopus, as of 2018-06-22.
[2] Sokolowski E, Nordling C, Siegbahn K. Chemical shift effect in inner electronic levels of Cu due to oxidation. Phys Rev 1958;110:776.
[3] Crist BV. XPS in industry – problems with binding energies in journals and binding energy databases. J Electron Spectrosc Relat Phenom 2019;231:75.
[4] Siegbahn K, Nordling C. ESCA, atomic, molecular and solid state structure studied by means of electron spectroscopy. Nov. Act. Uppsaliensis; 1967.
[5] ISO 15472:2010. Surface chemical analysis – X-ray photoelectron spectrometers – Calibration of energy scales (ISO, Geneva, 2010).
[6] ASTM E1523-15. Standard guide to charge control and charge referencing techniques in X-ray photoelectron spectroscopy. West Conshohocken (PA): ASTM International; 2015, www.astm.org.
[7] ISO 19318:2004. Surface chemical analysis – reporting of methods used for charge control and charge correction.
[8] According to the Scopus Data base search for "XPS" and "magnetron sputtering" articles published during 2010-2016, as of 2016-11-24.
[9] NIST X-ray Photoelectron Spectroscopy Database, Version 4.1 (National Institute of Standards and Technology, Gaithersburg, 2012); http://srdata.nist.gov/xps/ [accessed: 2018-03-02].
[10] Here we considered only material systems with at least 5 independent entries [accessed: 2018-03-02].
[11] Greczynski G, Primetzhofer D, Hultman L. Reference binding energies of transition metal carbides by core-level X-ray photoelectron spectroscopy free from Ar^+ etching artefacts. Appl Surf Sci 2018;436:102–10.
[12] Greczynski G, Primetzhofer D, Lu J, Hultman L. Core-level spectra and binding energies of transition metal nitrides by non-destructive x-ray photoelectron spectroscopy through capping layers. Appl Surf Sci 2017;396:347–58.
[13] Greczynski G, Hultman L. Self-consistent modelling of X-ray photoelectron spectra from air-exposed polycrystalline TiN thin films. Appl Surf Sci 2016;387:294–300.
[14] Hofmann S. Auger- and X-ray photoelectron spectroscopy in materials science. Springer-Verlag; 2013.
[15] Hűfner S. Photoelectron spectroscopy: principles and applications. Springer-Verlag; 2003.
[16] Briggs D, Grant JT, editors. Surface analysis by Auger and X-ray photoelectron spectroscopy. Chichester (UK): IM Publications; 2003.
[17] Fadley CS. X-ray photoelectron spectroscopy: progress and perspectives. J Electron Spectrosc Rel Phenom 2010;178–179:2.
[18] Bagus P, Eugene S, Ilton S, Nelin CJ. The interpretation of XPS spectra: Insights into materials properties. Surf Sci Rep 2013;68:273–304.
[19] Powell CJ. Improvements in the reliability of X-ray photoelectron spectroscopy for surface analysis. J Chem Educ 2004;81:1734.
[20] Hertz H. Ann Phys U Chem (Wied. Ann) 1887;31:421.
[21] Lenard P. Ueber die lichtelektrische Wirkung. Ann Phys 1902;313:149–98.
[22] Einstein A. On a heuristic point of view about the creation and conversion of light. Ann Phys 1905;17:132–48.
[23] Rutherford E. Philos Mag 1914;28:305.
[24] Rutherford E, Robinson H, Rawlinson WF. Philos Mag 1914;18:281.
[25] Reed SJB. Electron probe microanalysis. 2nd ed. Cambridge, UK: Cambridge University Press; 1993.
[26] Potts AW. X-ray science and technology. Bristol, UK: Institute of Physics Publications; 1993. p. 48.
[27] see for example: Briggs D. XPS. Basic principles, spectral features and qualitative analysis. In: Briggs D, Grant JT, editors. Surface Analysis by Auger and X-ray Photoelectron Spectroscopy. Chichester (UK): IM Publications; 2003.
[28] Siegbahn K, Hammond D, Fellner-Feldegg H, Barnett EF. Electron spectroscopy with monochromatized X-rays. Science 1972;176:245.
[29] Seah MP. In: Walls JM, editor. Methods of surface analysis. Cambridge (UK): Cambridge University Press; 1989. p.57.
[30] Roy D, Tremblay D. Design of electron spectrometers. Rep Prog Phys 1990;53:1621.
[31] Tompkins HG. The fundamentals of vacuum technology. 2nd ed.. AVS monograph Series M-6. New York: American Vacuum Society; 1991.

[32] Tanuma S, Powell CJ, Penn DR. Calculations of electron inelastic mean free paths. IX. Data for 41 elemental solids over the 50 eV to 30 keV range. Surf Interface Anal 2011;43:689–713.
[33] Powell CJ, Jablonski A. Surface sensitivity of X-ray photoelectron spectroscopy. Nucl Instrum Methods Phys Res, Sect A 2009;601:54–65.
[34] Shard AG. Detection limits in XPS for more than 6000 binary systems using Al and Mg Kα X-rays. Surf Interface Anal 2014;46:175–85.
[35] Palmberg W. Quantitative analysis of solid surfaces by Auger electron spectroscopy. Anal. Chem. 1973;45:549A.
[36] Seah MP. Data compilations: their use to improve measurement certainty in surface analysis by AES and XPS. Surf Interface Anal 1986;9:85.
[37] Wagner CD, Riggs WM, Davis LE, Moulder JF, Muilenberg GE. Handbook of X-ray photoelectron spectroscopy. Eden Prairie: Perkin-Elmer Corporation, Physical Electronics Division; 1979.
[38] Ikeo N, Iijima Y, Niimura N, Sigematsu M, Tazawa T, Matsumoto S, et al. Handbook of X-ray photoelectron spectroscopy. Tokyo: JEOL; 1991.
[39] Castle JE, Chapman-Kpodo H, Proctor A, Salvi AM. Curve-fitting in XPS using extrinsic and intrinsic background structure. J Electron Spectrosc Relat Phenom 2000;106:65–80.
[40] Jo M. Direct, simultaneous determination of XPS background and inelastic differential cross section using Tougaard's algorithm. Surf Sci 1994;320:191–200.
[41] Seah MP. Background subtraction: I. General behaviour of Tougaard-style backgrounds in AES and XPS. Surf Sci 1999;420:285–94.
[42] Végh J. The Shirley background revised. J Electron Spectrosc Relat Phenom 2006;151:159–64.
[43] See for example: Seah MP. Quantification in AES and XPS. In: Briggs D, Grant JT, editors. Surface analysis by Auger and X-ray photoelectron spectroscopy. Chichester: IM Publications; 2003. p. 345–76, or Tougaard S. Quantification of nano-structures by electron spectroscopy. In: D. Briggs, J.T. Grant Surface analysis by Auger and X-ray photoelectron spectroscopy. Chichester: IM Publications; 2003. p. 295–344.
[44] Beamson G, Briggs D. High resolution XPS of organic polymers, the Scienta ESCA 300 database. Chichester, UK: John Wiley & Sons; 1992.
[45] Shirley DA. High-resolution X-ray photoemission spectrum of the valence bands of gold. Phys Rev B 1972;5:4709.
[46] Tougaard S. Quantitative analysis of the inelastic background in surface electron spectroscopy. Surf Interface Anal 1988;11:453–72.
[47] Tougaard S. Practical algorithm for background subtraction. Surf Sci 1989;216:343–60.
[48] Tougaard S, Jansson C. Comparison of validity and consistency of methods for quantitative XPS peak analysis. Surf Interface Anal 1993;20:1013–46.
[49] Tougaard S. Formalism for quantitative surface analysis by electron spectroscopy. J Vac Sci Technol A 1990;8:2197–203.
[50] Tougaard S. Inelastic background correction and quantitative surface analysis. J El Spec Rel Phenom 1990;52:243–71.
[51] Tougaard S. Surface nanostructure determination by x-ray photoemission spectroscopy peak shape analysis. J Vac Sci Technol A 1996;14:1415–23.
[52] Tougaard S. Inelastic background removal in x-ray excited photoelectron spectra from homogeneous and inhomogeneous solids. J Vac Sci Technol, A 1987;5:1230–4.
[53] Tougaard S. Accuracy of the non-destructive surface nanostructure quantification technique based on analysis of the XPS or AES peak shape. Surf Interface Anal 1998;26:249–69.
[54] Carlson TA. Basic assumptions and recent developments in quantitative XPS. Surf Interface Anal 1982;4:125–34.
[55] Strohmeier BR. An ESCA method for determining the oxide thickness on aluminum alloys. Surf Interface Anal 1990;15:51–6.
[56] Mårtensson N, Sokolowski E, Svensson S. 50 years anniversary of the discovery of the core level chemical shifts. The early years of photoelectron spectroscopy. J Electron Spectrosc Relat Phenom 2014;193:27–33.
[57] Hagström S, Nordling C, Siegbahn K. Electron spectroscopic determination of the chemical valence state. Zeitschrift für Physik 1964;178:439–44.
[58] Hagström S, Nordling C, Siegbahn K. Electron spectroscopy for chemical analyses. Phys Lett 1964;9:235–6.
[59] Axelson G, Ericson U, Fahlman A, Hamrin K, Hedman J, Nordberg R, et al. New approach to structure studies in organic chemistry. Nature 1967;213:70.
[60] Nordberg R, Albridge RG, Bergmark T, Ericson U, Fahlman A, Hamrin K, et al. Shifts in electron spectra of nitrogen in organic molecules. Nature 1967;214:481.
[61] Fahlman A, Hamrin K, Hedman J, Nordberg R, Nordling C, Siegbahn K. Electron spectroscopy and chemical binding. Nature 1966;210:4–8.
[62] Travnikova O, Børve KJ, Patanen M, Söderström J, Miron C, Sæthre LJ, et al. The ESCA molecule—historical remarks and new results. J Electron Spectrosc Relat Phenom 2012;185:191–7.
[63] Gelius U, Basilier E, Svensson S, Bergmark T, Siegbahn K. A high resolution ESCA instrument with X-ray monochromator for gases and solids. J Electron Spectrosc Relat Phenom 1973;2:405–34.
[64] Sherwood PM. The use and misuse of curve fitting in the analysis of core X-ray photoelectron spectroscopic data. Surf Interface Anal 2019. https://doi.org/10.1002/sia.6629.
[65] Porte L, Roux L, Hanus J. Vacancy effects in the x-ray photoelectron spectra of TiN_x. Phys Rev B 1983;28:3214.
[66] Strydom I, Hofmann S. The contribution of characteristic energy losses in the core-level X-ray photoelectron spectroscopy peaks of TiN and (Ti, Al) N studied by electron energy loss spectroscopy and X-ray photoelectron spectroscopy. J Electron Spectrosc Relat Phenom 1991;56:85.
[67] Arranz A, Palacio C. Screening effects in the Ti 2p core level spectra of Ti-based ternary nitrides. Surf Sci 2006;600:2510.
[68] Gall D, Haasch R, Finnegan N, Lee T-Y, Shin C-S, Sammann E, et al. Surf Sci Spectra 2000;7:167.
[69] Lewin E, Gorgoi M, Schäfers F, Svensson S, Jansson U. Influence of sputter damage on the XPS analysis of metastable nanocomposite coatings. Surf Coat Technol 2009;204:455–62.
[70] Oswald S, Reiche R. Binding state information from XPS depth profiling: capabilities and limits. Appl Surf Sci 2001;179:307–15.
[71] Panzner G, Egert B, Schmidt HP. The stability of CuO and Cu2O surfaces during argon sputtering studied by XPS and AES. Surf Sci 1985;151:400–8.
[72] Ziegler JF, Biersack JP, Littmark U. The stopping and range of ions in solids. Vol. 1 of series “Stopping and Ranges of Ions in Matter”. New York: Pergamon Press; 1984.
[73] www.srim.org [accessed on 2013-06-28].
[74] Greczynski G, Petrov I, Greene JE, Hultman L. Al capping layers for non-destructive x-ray photoelectron spectroscopy analyses of transition-metal nitride thin films. J Vac Sci Technol A 2015;33:05E101.
[75] Haasch RT, Lee T-Y, Gall D, Greene JE, Petrov I. Epitaxial TiN(001) grown and analyzed in situ by XPS and UPS. II. Analysis of Ar+ sputter etched layers. Surf Sci Spectra 2000;7:204.
[76] Kramer B, Tomasch G, Ray M, Greene JE, Salvati L, Barr TL. J. Vac Sci Technol A 1988;6:1572.
[77] Kramer B, Tomasch G, Greene JE, Salvati L, Barr TL, Ray M. Phys Rev B, Condens Matter 1992;46:1372.
[78] Gan L, Gomez RD, Powell CJ, McMichael RD, Chen PJ, Egelhoff Jr. WF. J Appl Phys 2003;93:8731.
[79] Greczynski G, Hultman L. In-situ observation of self-cleansing phenomena during ultra-high vacuum anneal of transition metal nitride thin films: prospects for non-destructive photoelectron spectroscopy. Appl Phys Lett 2016;109:211602.
[80] Sanada N, Yamamoto A, Oiwa R, Ohashi Y. Extremely low sputtering degradation of polytetrafluoroethylene by C60 ion beam applied in XPS analysis. Surf Interface Anal 2004;36:280–2.
[81] Miyayama T, Sanada N, Bryan SR, Hammond JS, Suzuki M. Removal of Ar^+ beam-induced damaged layers from polyimide surfaces with argon gas cluster ion beams. Surf Interface Anal 2010;42:1453–7.
[82] Steinberger R, Walter J, Greunz T, Duchoslav J, Arndt M, Molodtsov S, et al. XPS study of the effects of long-term Ar^+ ion and Ar cluster sputtering on the chemical degradation of hydrozincite and iron oxide. Corros Sci 2015;99:66–75.
[83] Vereecke GR, Rouxhet PG. Surface charging of insulating samples in x-ray photoelectron spectroscopy. Surf Interface Anal 1998;26:490–7.
[84] Wagner CD. Studies of the charging of insulators in ESCA. J Electron Spectrosc Relat Phenom 1980;18:345–9.
[85] Clark DT, Dilks A, Thomas HR. ESCA applied to polymers. XXI. Investigation of sample-charging phenomena. J Polym Sci, Part A: Polym Chem 1978;16:1461–74.
[86] Metson JB. Charge compensation and binding energy referencing in XPS analysis. Surf Interface Anal 1999;27:1069–72.
[87] Baer DR, Engelhard MH, Gaspar DJ, Lea AS, Windisch CF. Use and limitations of electron flood gun control of surface potential during XPS: two non-homogeneous sample types. Surf Interface Anal 2002;33:781–90.
[88] See for example: Ashcroft NW, Mermin ND. Solid state physics. Saunders College Publishing; 1976.

[89] Ishii H, Sugiyama K, Ito E, Seki K. Energy level alignment and interfacial electronic structures at organic/metal and organic/organic interfaces. Adv Mater 1999;11:605–25.
[90] Seah MP. Instrument calibration for AES and XPS. In: Briggs D, Grant JT, editors. Surface analysis by Auger and X-ray photoelectron spectroscopy. Chichester: IM Publications; 2003. p. 167–89.
[91] Johansson GG, Johansson J, Hedman A, Berndtsson M, Klasson R, Nilsson. J Electron Spectrosc Relat Phenom 1973;2:295.
[92] Hnatowich DJ, Hudis J, Perlman ML, Ragaini RC. Determination of charging effect in photoelectron spectroscopy of nonconducting solids. J Appl Phys 1971;42:4883–6.
[93] Windawi H. Definitive XPS binding energies for heterogeneous materials. J Electron Spectrosc Relat Phenom 1981;22:373–7.
[94] Ebel MF, Ebel H. About the charging effect in X-ray photoelectron spectrometry. J Electron Spectrosc Relat Phenom 1974;3:169–80.
[95] Ascarelli P, Missoni G. Secondary electron emission and the detection of the vacuum level in ESCA. J Electron Spectrosc Relat Phenom 1974;5:417–35.
[96] Lewis RT, Kelly MA. Binding-energy reference in X-ray photoelectron spectroscopy of insulators. J Electron Spectrosc Relat Phenom 1980;20:105–15.
[97] DiCenzo SB, Berry SD, Hartford Jr EH. Photoelectron spectroscopy of single-size Au clusters collected on a substrate. Phys Rev B 1988;38:8465.
[98] Wertheim GK, DiCenzo SB, Youngquist SE. Unit charge on supported gold clusters in photoemission final state. Phys Rev Lett 1983;51:2310.
[99] Stephenson DA, Binkowski NJ. X-ray photoelectron spectroscopy of silica in theory and experiment. J Non-Cryst Solids 1976;22:399–421.
[100] Edgell MJ, Baer DR, Castle JE. Biased referencing experiments for the XPS analysis of non-conducting materials. Appl Surf Sci 1986;26:129–49.
[101] Clark DT, Thomas HR, Dilks A, Shuttleworth D. A method to reduce the hydrocarbon contamination of samples in X-ray photoelectron spectroscopy. J Electron Spectrosc Relat Phenom 1977;10:455–60.
[102] Vesely CJ, Langer DW. Electronic core levels of the II B− VI A compounds. Phys Rev B 1971;4:451.
[103] Citrin PH, Hamann DR. Measurement and calculation of polarization and potential-energy effects on core-electron binding energies in solids: X-ray photoemission of rare gases implanted in noble metals. Phys Rev B 1974;10:4948.
[104] Bertoti I. Characterization of nitride coatings by XPS. Surf Coat Technol 2002;151:194–203.
[105] Wagner CD. Chemical shifts of Auger lines, and the Auger parameter. Faraday Discuss Chem Soc 1975;60:291–300.
[106] Wagner CD, Biloen P. X-ray excited Auger and photoelectron spectra of partially oxidized magnesium surfaces: the observation of abnormal chemical shifts. Surf Sci 1973;35:82–95.
[107] Wagner CD. Auger parameter in electron spectroscopy for the identification of chemical species. Anal Chem 1975;47:1201–3.
[108] Wagner CD, Six HA, Jansen WT, Taylor JA. Improving the accuracy of determination of line energies by ESCA: chemical state plots for silicon-aluminum compounds. Appl Surf Sci 1981;9:203.
[109] Wagner CD, Gale LH, Raymond RH. Two-dimensional chemical state plots: a standardized data set for use in identifying chemical states by X-ray photoelectron spectroscopy. Anal Chem 1979;51:466–82.
[110] Moretti G. Auger parameter and Wagner plot in the characterization of chemical states by X-ray photoelectron spectroscopy: a review. J Electron Spectrosc Relat Phenom 1998;95:95–144.
[111] Wagner CD, Joshi A. The auger parameter, its utility and advantages: a review. J Electron Spectrosc Relat Phenom 1988;47:283–313.
[112] Powell CJ. Recommended Auger parameters for 42 elemental solids. J Electron Spectrosc Relat Phenom 2012;185:1–3.
[113] Leung TY, Man WF, Lim PK, Chan WC, Gaspari F, Zukotynski S. Determination of the sp3/sp2 ratio of a-C: H by XPS and XAES. J Non-Cryst Solids 1999;254:156–60.
[114] Crist BV. Handbook of monochromatic XPS spectra—polymers and polymers damaged by X-rays. John Wiley & Sons; 2000.
[115] Riedl C, Coletti C, Iwasaki T, Zakharov AA, Starke U. Quasi-free-standing epitaxial graphene on SiC obtained by hydrogen intercalation. Phys Rev Lett 2009;103:246804.
[116] Li X, Wang H, Robinson JT, Sanchez H, Diankov G, Dai H. Simultaneous nitrogen doping and reduction of graphene oxide. J Am Chem Soc 2009;131:15939–44.
[117] Tang L, Wang Y, Li Y, Feng H, Lu J, Li J. Preparation, structure, and electrochemical properties of reduced graphene sheet films. Adv Funct Mater 2009;19:2782–9.
[118] Park S, An J, Potts JR, Velamakanni A, Murali S, Ruoff RS. Hydrazine-reduction of graphite-and graphene oxide. Carbon 2011;49:3019–23.
[119] Ramqvist L, Hamrin K, Johansson G, Fahlman A, Nordling C. Charge transfer in transition metal carbides and related compounds studied by ESCA. J Phys Chem Solids 1969;30:1835–47.
[120] Dianis WP, Lester JE. External standards in X-ray photoelectron spectroscopy. Comparison of gold, carbon, and molybdenum trioxide. Anal Chem 1973;45:1416–20.
[121] Brandt ES, Untereker DF, Reilley CN, Murray RW. A comparison of carbon contaminant buildup on conductors and insulators in X-ray photoelectron spectroscopy. J Electron Spectrosc Relat Phenom 1978;14:113–20.
[122] Evans S. Correction for the effects of adventitious carbon overlayers in quantitative XPS analysis. Surf Interface Anal 1997;25:924–30.
[123] Dukes CA, Baragiola RA. Compact plasma source for removal of hydrocarbons for surface analysis. Surf Interface Anal 2010;42:40–4.
[124] Barr TL, Seal S. Nature of the use of adventitious carbon as a binding energy standard. J Vacuum Sci Technol A: Vacuum Surf Films 1995;13:1239–46.
[125] Barr TL. Advances in the application of X-ray photoelectron spectroscopy (ESCA) Part II. New methods. Crit Rev Anal Chem 1991;22:229–325.
[126] Swift P. Adventitious carbon—the panacea for energy referencing? Surf Interface Anal 1982;4:47–51.
[127] Hagström S, Karlsson S-E. Extension of the photo electron method to elements of low atomic number. Ark Fysik 1964;31:451–76.
[128] Bearden JA, Burr AF. Reevaluation of X-ray atomic energy levels. Rev Mod Phys 1967;39:125.
[129] Malmsen G, Nilsson O, Thorén I, Bergmark JE. Electron binding energy determinations on the 2.6 year promethium isotope. Phys Scr 1970;1:37.
[130] Gelius U, Heden PF, Hedman J, Lindberg BJ, Manne R, Nordberg R, et al. Molecular spectroscopy by means of ESCA. III. Carbon compounds. Phys Scripta 1970;2:70.
[131] Lindberg B, Hamrin K, Johansson G, Gelius U, Fahlman A, Nordling C, Siegbahn K. Molecular spectroscopy by means of ESCA II. Sulfur compounds. Correlation of electron binding energy with structure. Phys Scr 1970;1:286.
[132] Schön G. High resolution Auger electron spectroscopy of metallic copper. J Electron Spectrosc Relat Phenom 1972;1:377–87.
[133] Bird RJ, Swift P. Energy calibration in electron spectroscopy and the re-determination of some reference electron binding energies. J Electron Spectrosc Relat Phenom 1980;21:227–40.
[134] Pélisson-Schecker A, Hug HJ, Patscheider J. Charge referencing issues in XPS of insulators as evidenced in the case of Al-Si-N thin films. Surf Interface Anal 2012;44:29–36.
[135] Jacquemin M, Genet MJ, Gaigneaux EM, Debecker DP. Calibration of the X-ray photoelectron spectroscopy binding energy scale for the characterization of heterogeneous catalysts: is everything really under control? ChemPhysChem 2013;14:3618–26.
[136] Crist BV. Handbooks of monochromatic XPS spectra – the elements and native oxides. Volume 1. Mountain View (CA, USA): XPS Inter-national LLC; 1999.
[137] Greczynski G, Hultman L. C 1s peak of adventitious carbon aligns to the vacuum level: dire consequences for material's bonding assignment by photoelectron spectroscopy. ChemPhysChem 2017;18:1507–12.
[138] Greczynski G, Hultman L. Reliable determination of chemical state in x-ray photoelectron spectroscopy based on sample-work-function referencing to adventitious carbon: resolving the myth of apparent constant binding energy of the C 1s peak. Appl Surf Sci 2018;451:99–103.
[139] Malmsten G, Thorén I, Högberg S, Bergmark JE, Karlsson SE, Rebane E. Selenium compounds studied by means of ESCA. Phys Scr 1971;3:96.
[140] Prins R, Novakov T. X-ray photoelectron spectra and molecular orbital interpretation of the valence region of ClO_4^- and SO_4^{2-}. Chem Phys Lett 1971;9:593–6.
[141] Nordberg R, Brecht H, Albridge RG, Fahlman A, Van Wazer JR. Binding energy of the“ 2p” electrons of silicon in various compounds. Inorg Chem 1970;9:2469–74.
[142] Kinoshita S, Ohta T, Kuroda H. Comments on the energy calibration in X-ray photoelectron spectroscopy. Bull Chem Soc Jpn 1976;49:1149–50.
[143] Kohiki S, Oki K. Problems of adventitious carbon as an energy reference. J Electron Spectrosc Relat Phenom 1984;33:375–80.
[144] Werrett CR, Bhattacharya AK, Pyke DR. The validity of Cls charge referencing in the XPS of oxidised Al-Si alloys. Appl Surf Sci 1996;103:403–7.

[145] Peplinski B, Unger WE, Grohmann I. Characterization of Cu-Zn-Al oxide catalysts in the precipitaed, calcined and reduced state by means of XPS with the help of a finger-print data base. Appl Surf Sci 1992;62:115–29.
[146] Gross T, Ramm M, Sonntag H, Unger W, Weijers HM, Adem EH. An XPS analysis of different SiO_2 modifications employing a C 1s as well as an Au $4f_{7/2}$ static charge reference. Surf Interface Anal 1992;18:59–64.
[147] Yamashita T, Hayes P. Analysis of XPS spectra of Fe^{2+} and Fe^{3+} ions in oxide materials. Appl Surf Sci 2008;254:2441–9.
[148] Biesinger MC, Payne BP, Grosvenor AP, Lau LW, Gerson AR, Smart RS. Resolving surface chemical states in XPS analysis of first row transition metals, oxides and hydroxides: Cr, Mn, Fe, Co and Ni. Appl Surf Sci 2011;257:2717–30.
[149] Khatibi A, Sjölen J, Greczynski G, Jensen J, Eklund P, Hultman L. Structural and mechanical properties of Cr–Al–O–N thin films grown by cathodic arc deposition. Acta Mater 2012;60:6494–507.
[150] Gong V, Franca R. Nanoscale chemical surface characterization of four different types of dental pulp-capping materials. J Dent 2017;58:11–8.
[151] França R, Samani TD, Bayade G, Yahia LH, Sacher E. Nanoscale surface characterization of biphasic calcium phosphate, with comparisons to calcium hydroxyapatite and β-tricalcium phosphate bioceramics. J Colloid Interface Sci 2014;420:182–8.
[152] Chen M, Pei ZL, Sun C, Wen LS, Wang X. Surface characterization of transparent conductive oxide Al-doped ZnO films. J Cryst Growth 2000;220:254–62.
[153] Gammon WJ, Kraft O, Reilly AC, Holloway BC. Experimental comparison of N (1s) X-ray photoelectron spectroscopy binding energies of hard and elastic amorphous carbon nitride films with reference organic compounds. Carbon 2003;41:1917–23.
[154] Liu B, Zhao X, Zhang N, Zhao Q, He X, Feng J. Photocatalytic mechanism of TiO_2–CeO_2 films prepared by magnetron sputtering under UV and visible light. Surf Sci 2005;595:203–11.
[155] Landoulsi J, Genet MJ, Fleith S, Toure Y, Liascukiene I, Methivier C, et al. Organic adlayer on inorganic materials: XPS analysis selectivity to cope with adventitious contamination. Appl Surf Sci 2016;383:71–83.
[156] Psiuk B, Szade J, Szot K. SrTiO3 surface modification upon low energy Ar^+ bombardment studied by XPS. Vacuum 2016;131:14–21.
[157] Finke B, Hempel F, Testrich H, Artemenko A, Rebl H, Kylián O, et al. Plasma processes for cell-adhesive titanium surfaces based on nitrogen-containing coatings. Surf Coat Technol 2011;205:S520–4.
[158] Lee SH, Yamasue E, Ishihara KN, Okumura H. Photocatalysis and surface doping states of N-doped TiOx films prepared by reactive sputtering with dry air. Appl Catal B 2010;93:217–26.
[159] Schild D, Ulrich S, Ye J, Stüber M. XPS investigations of thick, oxygen-containing cubic boron nitride coatings. Solid State Sci 2010;12:1903–6.
[160] Jansen RJ, Van Bekkum H. XPS of nitrogen-containing functional groups on activated carbon. Carbon 1995;33:1021–7.
[161] Spadaro F, Rossi A, Lainé E, Woodward P, Spencer ND. Elucidating the resistance to failure under tribological tests of various boron-based films by XPS and ToF-SIMS. Appl Surf Sci 2017;425:948–64.
[162] Marin A, Lungu CP, Porosnicu C. Influence of gaseous inclusions on aluminum-tungsten coatings investigated by XPS. J Vacuum Sci Technol A: Vacuum Surf Films 2017;35:061304.
[163] Chuang MJ, Huang HF, Wen CH, Chu AK. On the structure and surface chemical composition of indium–tin oxide films prepared by long-throw magnetron sputtering. Thin Solid Films 2010;518:2290–4.
[164] Kohandehghan A, Kalisvaart P, Cui K, Kupsta M, Memarzadeh E, Mitlin D. Silicon nanowire lithium-ion battery anodes with ALD deposited TiN coatings demonstrate a major improvement in cycling performance. J Mater Chem A 2013;1:12850–61.
[165] Gaddam S, Kazi H, Dong B, Driver M, Kelber J. Surface cleaning for enhanced adhesion to packaging surfaces: effect of oxygen and ammonia plasma. J Vacuum Sci Technol A: Vacuum Surf Films 2015;33:021301.
[166] Merel P, Tabbal M, Chaker M, Moisa S, Margot J. Direct evaluation of the sp^3 content in diamond-like-carbon films by XPS. Appl Surf Sci 1998;136:105–10.
[167] Kaciulis S. Spectroscopy of carbon: from diamond to nitride films. Surf Interface Anal 2012;44:1155–61.
[168] Nirupama V, Gunasekhar KR, Sreedhar B, Uthanna S. Effect of oxygen partial pressure on the structural and optical properties of dc reactive magnetron sputtered molybdenum oxide films. Curr Appl Phys 2010;10:272–8.
[169] Senthilkumar V, Jayachandran M, Sanjeeviraja C. Preparation of anatase TiO_2 thin films for dye-sensitized solar cells by DC reactive magnetron sputtering technique. Thin Solid Films 2010;519:991–4.
[170] Evans S. Work function measurements by X-Pe spectroscopy, and their relevance to the calibration of X-Pe spectra. Chem Phys Lett 1973;23:134–8.
[171] see for example: Chapter 1 in S. Hűfner Photoelectron spectroscopy: principles and applications. 3rd ed. Springer; 2003. ISSN 1439-2674.
[172] Seah MP. Summary of ISO/TC 201 Standard: VII ISO 15472: 2001—surface chemical analysis—X-ray photoelectron spectrometers—calibration of energy scales. Surf Interface Anal 2001;31:721–3.
[173] Greczynski G, Mráz S, Hultman L, Schneider JM. Unintentional carbide formation evidenced during high-vacuum magnetron sputtering of transition metal nitride thin films. Appl Surf Sci 2016;385:356–9.
[174] Greczynski G, Mráz S, Hultman L, Schneider JM. Venting temperature determines surface chemistry of magnetron sputtered TiN films. Appl Phys Lett 2016;108:041603.
[175] Our unpublished results.
[176] See Appendix E in Briggs D, Grant JT, editors. Surface analysis by auger and X-ray photoelectron spectroscopy. Manchester: IM Publications, 2003.
[177] Huheey JE, Keiter EA, Keiter RL. Inorganic chemistry: principles of structure and reactivity. 4th ed. New York, USA: HarperCollins; 1993.
[178] In this example we assumed that carbon is distributed uniformly within the probed volume. While this is not necessarily true for thinner AdC coverage, it does not affect the main conclusions from the experiment.
[179] Powell CJ. Elemental binding energies for X-ray photoelectron spectroscopy. Appl Surf Sci 1995;89:141–9.
[180] Moulder JF, Stickle WF, Sobol PE, Bomben KD. Handbook of X-ray photoelectron spectroscopy. Eden Prairie, USA: Perkin-Elmer Corporation; 1992.
[181] Braun S, Salaneck WR, Fahlman M. Energy-level alignment at organic/metal and organic/organic interfaces. Adv Mater 2009;21:1450–72.
[182] Rhoderick EH, Williams RH. Metal-semiconductor contacts. Oxford: Clarendon Press; 1988.
[183] Pireaux JJ, Svensson S, Basilier E, Malmqvist PÅ, Gelius U, Caudano R, et al. Core-electron relaxation energies and valence-band formation of linear alkanes studied in the gas phase by means of electron spectroscopy. Phys Rev A 1976;14:2133.
[184] Pireaux JJ, Caudano R. X-ray photoemission study of core-electron relaxation energies and valence-band formation of the linear alkanes II. Solid-phase measurements. Phys Rev B 1977;15:2242.
[185] Lögdlund M, Greczynski G, Crispin A, Kugler T, Fahlman M, Salaneck WR. Photoelectron spectroscopy of interfaces for polymer-based electronic devices. In: Salaneck WR, Seki K, Kahn A, Pireaux JJ, editors. Conjugated polymer and molecular interfaces: science and technology for photonic and optoelectronic application. New York: Marcel Dekker; 2001.
[186] Hagstrum HD. The determination of energy-level shifts which accompany chemisorption. Surf Sci 1976;54:197–209.
[187] Legare P, Fritsch A. XPS study of transition metal/alumina model catalysts: equilibrium and energy referencing. Surf Interface Anal 1990;15:698–700.

Grzegorz Greczynski is an Associate Professor in the Department of Physics, Linköping University (LiU). He is a Fellow of the American Vacuum Society. Dr. Greczynski received his PhD degree in Materials Physics from Linköping University in 2001 and has an eight-year industrial track record. He heads the Fundamental Science of Thin Films Group of the Thin Film Physics Division and acts as a Director of the Surface Analysis Laboratory. Greczynski has more than 20 years hands on experience in photoelectron spectroscopy and is one of the pioneers in high-power pulsed magnetron sputtering (HiPIMS) research through his present position at LiU and his previous employment at Chemfilt Ionsputtering, the original HiPIMS company. His research interests are presently focused on low-energy ion/surface interactions for nanostructure control during low-temperature growth of thin films by physical vapor deposition. He has coauthored more than 100 papers with >3400 citations.

Prof. Lars Hultman, Born 1960 in Linköping, Sweden. He is Chief Executive Officer of The Swedish Foundation for Strategic Research (SSF), since 2013. He is leave of absence with time for research from Linköping University, Sweden. He is an elected member of the Royal Swedish Academy of Science (KVA) and Engineering Sciences (IVA), as well as Fellow of the American Vacuum Society and the Forschungszentrum Dresden-Rossendorf. He received his PhD 1988 and became Professor/Head of Division in Thin Film Physics at IFM, Linköping University in 1998 after being a visiting scientist to Northwestern University, USA. He made a sabbatical at University of Illinois at Urbana-Champaign during 2004-2006. His research interest is in materials science and nanotechnology of functional thin film materials. He has procured and managed the electron microscopy laboratory at Linköping, including the FEI Analytical Monochromated Double-aberration-corrected 60-300 kV Titan^3 high-resolution instrument and its dedicated vibration-free building. Recognitions include the European ERC Advanced Grant, a Wallenberg Scholar Grant, the Akzo Nobel Sweden Science Award, and Fellow of the American Vacuum Society. He has served as Director for several Centers of Excellence in Materials Research. He has authored 800 papers for a Web-of-Science h-index of 72, and holds 25 patents from active collaboration with industry for wear-resistant cutting tools, low-friction coatings for components, thin film neutron detectors, and diffusion barriers in microelectronics.